

Ultra-High Performance Concrete Shear Walls in Tall Buildings

Thomas Christian Dacanay

Thesis submitted to the faculty of the Virginia Polytechnic Institute and State University in
partial fulfillment of the requirements for the degree of

Master of Science

In

Civil Engineering

Cristopher D. Moen, Chair
Carin L. Roberts-Wollmann
David W. Mokarem

January 19, 2016
Blacksburg, VA

Keywords: Ultra-high performance concrete, shear wall, Lattice Discrete Particle Model, sustainability

Ultra-High Performance Concrete Shear Wall in Tall Buildings

Thomas Christian Dacanay

ABSTRACT (ACADEMIC)

This thesis presents the results of an effort to quantify the implications of using ultra-high performance concrete (UHPC) for shear walls in tall buildings considering structural efficiency and environmental sustainability. The Lattice Discrete Particle Model (LDPM) was used to simulate the response to failure of concrete shear walls without web steel bar reinforcement under lateral loading and constant axial compressive loading. The structural efficiency of UHPC with simulated compressive strength of $f'_c = 231$ MPa was compared to that of a high-performance concrete (HPC) with $f'_c = 51.7$ MPa simulated compressive strength. UHPC shear walls were found to have equal uncracked stiffness and superior post-cracking capacity at a thickness 58% of the HPC shear wall thickness, and at 59% of the HPC shear wall weight. Next, the environmental sustainability of UHPC with compressive strength $f'_c = 220$ - 240 MPa was compared to that of an HPC with compressive strength $f'_c = 49$ MPa with a life-cycle assessment (LCA) approach, using SimaPro sustainability software. At a thickness 58% of the HPC shear wall thickness, UHPC shear walls with 0% fiber by volume were found to have an environmental impact 6% to 10% worse than that of HPC shear walls, and UHPC shear walls with 2% fiber by volume were found to have an environmental impact 47% to 58% worse than that of HPC shear walls. The results detailed herein will allow for design guidelines to be developed which take advantage of UHPC response in shear. Additionally, this work may be implemented into topology optimization frameworks that incorporate the potential improvements in structural efficiency and sustainability through using UHPC.

ABSTRACT (PUBLIC)

This thesis presents the results of a study aiming to quantify the structural and environmental implications of using an innovative type of concrete, called ultra-high performance concrete (UHPC), for shear walls in tall buildings and compare to that of ordinary concrete. The structural aspects of UHPC shear walls were quantified using a novel modeling approach, the Lattice Discrete Particle Model (LDPM). The framework for testing UHPC structural solutions developed here can be used in future studies to rapidly ascertain other ways in which UHPC might be used to improve the design of structures. Possible improvements include lighter structural components, faster speed of construction, and lessened environmental impact. Such improvements would result in expansion of the possibilities of structural design, and would allow the construction industry to take advantage of the advanced properties of UHPC.

Acknowledgements

I would first like to acknowledge that this research project would not have been possible or successful without the support of the Qatar National Research Fund (QNRF) and the National Science Foundation (NSF).

I would like to thank my advisor, Dr. Cristopher Moen, for his support, guidance, and knowledge throughout the course of this project. I would also like to thank my committee members, Dr. Carin Roberts-Wollmann and Dr. David Mokarem, for their knowledge and guidance that helped this study to be successful. I would like to express my gratitude to Dr. Gianluca Cusatis at Northwestern University for his knowledge of the LDPM model, and to Dr. Sean McGinnis at Virginia Tech for his knowledge of LCA, SimaPro, and for helping me set up my sustainability model.

I would also like to thank my friends, including Rafic El Helou, Valerie Black, Rachel Gordon, Evan May, Fannie Tao, and many others, for providing help with this project, or a good laugh during a long day – or night.

Lastly, I would like to thank my family, Allan, Linda, and Katie Dacanay, for supporting me, helping me throughout graduate school, and for their guidance and love throughout my life.

Funding Support

This material is based upon work supported by the Qatar National Research Fund under NPRP No.: 7-1518-2-547 to Virginia Tech, and the National Science Foundation under Grant No. 1201087 to Virginia Tech with Subcontract to Northwestern University. Any opinions, findings, and conclusions or recommendations expressed in this material are those of the authors and do not necessarily reflect the views of the Qatar National Research Fund or the National Science Foundation.

Table of Contents

ABSTRACT	ii
Acknowledgements	iv
Table of Contents	v
List of Figures	vii
List of Tables.....	ix
CHAPTER 1. Introduction.....	1
1.1 Tall Concrete Buildings	3
1.2 Lateral Load-Resisting Systems in Tall Buildings.....	4
1.3 High-Strength and High-Performance Concrete.....	7
1.3 Ultra-High Performance Concrete	10
CHAPTER 2. Lattice Discrete Particle Model and MARS	14
2.1 Introduction to the LDPM.....	14
2.2 LDPM Material Parameters	18
2.3 MARS.....	21
2.4 Benefits of the LDPM and MARS	22
2.5 LDPM Simulation Procedure with Example.....	22
2.5.1 “Gen” File: <i>GenUhcpWall.mrs</i>	23
2.5.2 “Run” File: <i>RunUhcpWall.mrs</i>	26
2.5.3 “Submission” file: <i>Nrun.sh</i>	41
CHAPTER 3. Ultra-High Performance Concrete Shear Wall Parameter Study	44
3.1 Varied Axial Stress.....	50
3.2 Edge Vertical Reinforcing Bars	53
3.3 Fiber Reinforcement.....	57
3.4 Comparison of the Shear Response of Cement-Based Composites.....	60
3.5 UHPC Shear Wall Thickness Study Without Transverse Reinforcement	66
CHAPTER 4. SimaPro and Life-Cycle Assessment	73
4.1 Life-Cycle Assessment with SimaPro.....	74
4.2 Life-Cycle Assessment Methods.....	76
4.2.1 Structure of LCA Methods.....	76
4.2.2 ReCiPe 2008	80

4.2.3 Cumulative Energy Demand.....	81
CHAPTER 5. Sustainability of Ultra-High Performance Concrete Shear Walls	83
5.1 LCA Results by Constituent.....	84
5.2 LCA Results for Cementitious-Based Composites	85
5.3 LCA Results for Shear Walls	87
CHAPTER 6. Conclusions.....	89
6.1 Summary of Conclusions	89
6.2 Future Work	89
REFERENCES	91
APPENDIX A. Sample of MARS Files	93
A.1 GenUhpcWall.mrs	93
A.2 RunUhpcWall.mrs	94
A.3 Nrun.sh	100
APPENDIX B. Effect of Further Coarse Graining.....	101
APPENDIX C. Effect of Rebar Size.....	102

List of Figures

Figure 1.1: Tall buildings under construction in Doha, Qatar (QNRf 2015)	3
Figure 1.2: Chicago’s Willis Tower is an example of a bundled tube (Gerometta)	5
Figure 1.3: Chicago’s John Hancock Center employs a trussed tube design (Gerometta)	6
Figure 2.1: a) Tetrahedral between particle centers formed by the LDPM tessellation algorithm, b) Polyhedral cells containing two adjacent particles (Cusatis et al. 2011)	15
Figure 2.2: a) Distribution of particles within a specimen, b) Fully-constructed LDPM specimen showing external surface facets (Cusatis et al. 2011)	16
Figure 2.3: a) Debonding of a steel fiber with embedment length L_e and load P , b) load-slip curve showing the portions the fiber response corresponding to fracture energy, and slip-friction, with slip hardening-softening parameter β (Schauffert and Cusatis et al. 2012)	18
Figure 2.4: Distribution of particles in a shear wall specimen, 2 mm to 4 mm aggregate size	26
Figure 2.5: Distribution of fibers in the concrete matrix with random orientation and $V_f = 2\%$ (1/4 of the fibers are shown)	31
Figure 2.6: Simulated reinforcing bars for a shear wall specimen	34
Figure 2.7: Paraview software interface	40
Figure 3.1: Simulated shear wall specimen	46
Figure 3.2: LDPM-simulated component dimensions	46
Figure 3.3: Top and bottom elastic concrete block dimensions	47
Figure 3.4: Elevation view of the simulated specimen, showing a) the applied location of the velocity curve on the side of the top elastic concrete block; b) the distributed axial load on the top surface of the top elastic concrete block; and c) the fixed displacement and rotation conditions applied to the bottom face of the bottom elastic concrete block	47
Figure 3.5: Base shear vs. drift ratio for Cor-Tuf UHPC with $t = 60$ mm, with different applied axial stresses	51
Figure 3.6: Crack widths at 1.2%, 4.4%, and 8.0% drift for Cor-Tuf UHPC specimen with $t = 60$ mm and 20 MPa axial stress	52
Figure 3.7: Crack widths at 1.2% drift, 4.4% drift, and post-failure for Cor-Tuf UHPC specimen with $t = 60$ mm and 100 MPa axial stress	52
Figure 3.8: Elevation view of wall specimen with 12.5 mm diameter steel reinforcing bars	54
Figure 3.9: Cross-sectional view of shear wall, showing the layout of the 12.5 mm diameter steel reinforcing bars	54
Figure 3.10: Base shear vs. drift ratio for Cor-Tuf UHPC with $t = 60$ mm, with and without rebar at wall edges	55
Figure 3.11: Crack widths at 1.2%, 4.4%, and 8.0% drift for Cor-Tuf UHPC specimen with $t = 60$ mm, vertical reinforcing bars at the wall edges and 20 MPa axial stress	56
Figure 3.12: Crack widths at 1.2%, 4.4%, and 8.0% drift for Cor-Tuf UHPC specimen with $t = 60$ mm, vertical reinforcing bars at the wall edges, and 100 MPa axial stress	56

Figure 3.13: Base shear vs. drift ratio for Cor-Tuf UHPC with $t = 60$ mm, with and without fibers	58
Figure 3.14: Crack widths at 1.2%, 4.4%, and 8.0% drift for Cor-Tuf UHPC specimen with $t = 60$ mm, without fiber reinforcement, and with 50 MPa axial stress	59
Figure 3.15: Crack widths at 1.2%, 4.4%, and 8.0% drift for Cor-Tuf UHPC specimen with $t = 60$ mm, fiber reinforcement, and 50 MPa axial stress	59
Figure 3.16: Base shear vs. drift ratio for “Section 9” HPC with $t = 60$ mm	61
Figure 3.17: Base shear vs. drift ratio for “Section 9” HPC and Cor-Tuf UHPC with $t = 60$ mm and 11 MPa axial stress	62
Figure 3.18: Base shear vs. drift ratio for “Section 9” HPC and Cor-Tuf UHPC with $t = 60$ mm and 20 MPa axial stress	63
Figure 3.19: Crack widths at 0.4%, 0.8%, and 1.5% drift for “Section 9” HPC specimen with 11 MPa axial stress	64
Figure 3.20: Crack widths at 0.4%, 0.8%, and 1.5% drift for Cor-Tuf UHPC specimen with 11 MPa axial stress and without fiber reinforcement	64
Figure 3.21: Crack widths at 0.4%, 0.8%, and 1.5% drift for Cor-Tuf UHPC specimen with 11 MPa axial stress and with fiber reinforcement	65
Figure 3.22: Base shear vs. drift ratio for “Section 9” HPC with $t = 60$ mm and 198 kN axial load, and Cor-Tuf UHPC with $t = 35$ mm	68
Figure 3.23: Base shear vs. drift ratio for “Section 9” HPC with $t = 60$ mm and 360 kN axial load, and Cor-Tuf UHPC with $t = 35$ mm	69
Figure 3.24: Crack widths at 0.4%, 0.8%, and 1.5% drift for “Section 9” HPC specimen with $t = 60$ mm and 198 kN axial load	70
Figure 3.25: Crack widths at 0.4%, 0.8%, and 1.5% drift for Cor-Tuf UHPC specimen with $t = 35$ mm, 198 kN axial load, and without fiber reinforcement	70
Figure 3.26: Crack widths at 0.4%, 0.8%, and 1.5% drift for Cor-Tuf UHPC specimen with $t = 35$ mm, 198 kN axial load, and fiber reinforcement	71
Figure 3.27: Crack widths at 0.4%, 0.8%, and 1.5% drift for “Section 9” HPC specimen with $t = 60$ mm and 360 kN axial load	71
Figure 3.28: Crack widths at 0.4%, 0.8%, and 1.5% drift for Cor-Tuf UHPC specimen with $t = 35$ mm, 360 kN axial load, and without fiber reinforcement	72
Figure 3.29: Crack widths at 0.4%, 0.8%, and 1.5% drift for Cor-Tuf UHPC specimen with $t = 35$ mm, 360 kN axial load, and fiber reinforcement	72
Figure 4.1: Excerpt of a SimaPro network diagram for a UHPC, showing constituents and the top level processes	75
Figure 4.2: Flowchart of ReCiPe 2008 methodology (Goedkoop et al. 2013)	77
Figure B.1: Base shear vs. drift ratio for aggregate size 2 to 4 mm and 8 to 16 mm	101
Figure C.1: Base shear vs. drift ratio for Cor-Tuf UHPC shear wall specimen with $d = 12.5$ mm and $d = 15$ mm rebar at wall edges	102

List of Tables

Table 1.1 Range of typical HPC material characteristics	9
Table 1.2 Examples of HPC mix designs (Kosmatka and Panarese 2002).....	9
Table 1.3: Typical UHPC material composition (Graybeal 2006).....	10
Table 1.4: Ductal UHPC material characteristics (Graybeal 2006).....	11
Table 1.5: Range of UHPC material properties (Graybeal 2013).....	11
Table 2.1: LDPM Parameters.....	20
Table 3.1 Cor-Tuf material proportion by weight (Smith et al. 2014).....	44
Table 3.2 Cor-Tuf material composition (Smith et al. 2014).....	44
Table 3.3 “Section 9” HPC material composition (Cusatis et al. 2011)	45
Table 3.4: LDPM parameters for shear wall simulations	49
Table 3.5: Energy dissipation with and without fiber reinforcement from 0 to 2% drift.....	57
Table 3.6: Energy dissipation of HPC, t = 60 mm and UHPC, t = 35 mm from 0 to 1% drift.....	67
Table 4.1 SimaPro normalized percentage of total environmental impact for Cor-Tuf UHPC using ReCiPe 2008 midpoint method	79
Table 5.1 Electricity mixes for the United States and Qatar.....	83
Table 5.2 Constituent single score results per kg of material	84
Table 5.3 Constituent amount per m ³ for “Type C” UHPC and “HP2” HPC	85
Table 5.4 Single score per m ³ for “Type C” UHPC and “HP2” HPC, ReCiPe 2008	86
Table 5.5 Single score per m ³ for “Type C” UHPC and “HP2” HPC, Cumulative Energy Demand	86
Table 5.6 LCA results for UHPC and HPC shear wall specimens	88
Table 5.7 Comparison of Dissipated Energy and Embodied Energy.....	88

CHAPTER 1. Introduction

In this research, the viability and benefits of using ultra-high performance concrete (UHPC) for shear walls in tall buildings in Qatar is assessed, considering the metrics of both structural efficiency and environmental sustainability. The performance and capacity of shear walls using this material is characterized using a validated computational model, the Lattice Discrete Particle Model (LDPM), which can capture the structural behavior of cement-based composites throughout loading to failure. With the LDPM, a study is performed to determine the reduced thickness at which UHPC shear walls have equal or superior structural response to high performance concrete (HPC) shear walls. The environmental impact of UHPC shear walls is ascertained with a life cycle assessment (LCA) approach.

The goal of this research is to explore and quantify the multi-objective benefits, in terms of structural efficiency and improved sustainability, of incorporating UHPC into the lateral force-resisting system of tall buildings. In this process a basis is formed for how to design using this relatively new material, and in determining situations where its use is appropriate. Structural efficiency generally refers to the ratio of strength to weight – the load a system can carry divided by the weight of the system itself. In tall buildings, improved structural efficiency results in advantages like less material used and more floor space available for use. With regard to materials and structural engineering, sustainability refers to the degree to which practices like resource use and pollution emissions can be continued without consequences to the environment. Concrete sustainability is of chief importance as its production is energy- and resource-intensive, and thus has significant impacts on the environment (Mehta 2001).

UHPC is characterized by compressive strength in excess of 150 MPa, post-peak tensile capacity resulting from micro steel fibers embedded in the concrete matrix, and excellent durability due to the dense concrete matrix (Graybeal 2013). High material cost and significant environmental impact per unit volume of material, due to the large amount of Portland cement and inclusion of micro steel fibers in the UHPC mix design, drive the need to be selective in the way it is used in structures (Stengel and Schießl 2014). With this in mind, successful multi-objective design which balances UHPC benefits and drawbacks will convey enhanced structural performance and safety, improved sustainability, and expansion of the physical boundaries of what is possible and practical to be built.

Advancements in tall building design and construction in Qatar and the United States can be realized from the results detailed herein. Smaller cross-sections of structural members can allow for taller buildings through the overall reduction of weight. Given the material properties of UHPC, this is achieved with while maintaining the necessary stiffness and performance under lateral and vertical loading. In buildings incorporating this new material, increased architectural freedom and use of space will be permitted as the footprints of structural components are reduced. From this and other work, the basis for the development of UHPC design guidelines for tall buildings and other applications will be formed, facilitating wider adaptation of the material in practice.

With the aid of software, sustainability metrics like embodied energy are used in this research to compare the environmental performance of cement-based composites. The embodied energy of, for example, a beam, is the total amount of energy needed to construct the member from raw materials to finished product, including all relevant aspects like the extraction of material, grinding and processing aggregate, and transportation it to where it will be used. This body of



Figure 1.1: Tall buildings under construction in Doha, Qatar (QNRF 2015)

information, once constructed, gives the ability to perform an overall quantitative comparison on the sustainability of different solutions for a given case, and accounts for all processes in the manufacture of materials which contribute to environmental impact.

Through this work, a framework is developed for comparing UHPC structural solutions to other materials considering the aforementioned objectives of structural efficiency and environmental sustainability. Though the present research is performed for tall building shear walls in Qatar and the United States, the completed framework applies to any structural component in whichever geographical region a user desires to analyze, with minimal additional effort. Future research may use the results detailed here as a springboard to more quickly explore the viability of UHPC for other uses.

1.1 Tall Concrete Buildings

Concrete is the most widely used construction material in the world (Crow 2008). It is versatile, being able to be applied in many different ways, and its ability to take on multiple geometric forms meshes well with the up-and-coming field of topology optimization. As

populations in Qatari cities and elsewhere grow and demand more space in confined regions, the need for tall buildings increases (Blanco-Carrasco et al. 2010). Innovations with concrete have gone hand-in-hand with advances in the ability to meet these demands.

The work detailed here aims to perform structural and environmental comparisons of cementitious-based composite shear walls for the rapidly growing and changing country of Qatar in the Middle East, as well as the United States. Doha, Qatar's capital city, is ranked 33rd in the world and 3rd in the Middle East by number of 150 meter or taller buildings, with 78% of these buildings employing concrete as the primary building material (CTBUH 2015). A significant number of additional tall buildings are planned or under construction in the city – 26 are completed, while 12 are currently under construction as of late 2015, some of which are visible in Figure 1.1 (CTBUH 2015).

1.2 Lateral Load-Resisting Systems in Tall Buildings

The first reinforced concrete skyscraper worldwide was the 16-story Ingalls Building in Cincinnati, built in 1903 (Ali 2001). It is a frame structure, consisting of beams, joists, columns, and slabs. The Ingalls Building was an important step in the use of concrete as it dispelled widespread notions that concrete's low tensile strength would cause buildings of a significant height to crumble as soon as the formwork was removed (Ali 2001). Buildings following this simple framed form do, however, have a limited height; as the system is applied to buildings of increasing heights, the lateral and vertical loads the structure must resist become larger, from wind, earthquakes, structural members, equipment, and so on. The members and member connections become prohibitively expensive and unwieldy, and past a certain building height, can no longer be designed with adequate capacity and stiffness to handle these loads and meet serviceability requirements (Ali 2001).



Figure 1.2: Chicago’s Willis Tower is an example of a bundled tube (Gerometta)

In response to these limitations, the 1940s saw reinforced concrete shear walls begin to be used in general practice (Ali 2001). Shear walls provide the structure with stiffness and strength in the lateral direction, and allowed taller buildings to be constructed. Also referred to as structural walls, ACI 318-14 provides a definition as a “wall proportioned to resist combinations of shears, moments, and axial forces in the plane of the wall” (ACI 2014). Lateral loads, from wind or seismic effects, are transmitted from floor diaphragms to the shear walls, which provide stiffness and strength in the direction of loading. They may be visualized as vertical, cantilevered deep beams, and can be either concentrated at one location (e.g. centrally and containing building services like elevator shafts), or dispersed throughout the floor plan. In tall buildings utilizing concrete, the lateral load-resisting system is often referred to as the shear core of the building (Ali 2001).



Figure 1.3: Chicago's John Hancock Center employs a trussed tube design (Gerometta)

Larger-scale structural systems were pioneered by engineer and designer Fazlur Khan in the 1960s, many of which form part of the tallest buildings today (Ali 2001). The basic system of shear walls and frames was taken a step further by Khan into cohesive overall designs – framed tubes. In a framed tube, like the one in Figure 1.2, multi-floor groupings of structural elements are designed to be relatively stiff and to handle more load. These elements act together to resist lateral loading, allowing the other portions of the building to have more widely-spaced structural elements, since they only have to resist gravity loads. In skyscrapers, the space occupied by structural elements and building services (like elevator shafts) is critical to the ability of the building's space to be utilized, and is a chief concern of building designers. Interior space freed by using framed tube systems results in buildings being more profitable to builders (Ali 2001).

The concept of tubular structures has been developed further into multiple forms, like bundled tubes (Willis Tower, formerly known as the Sears Tower, Figure 1.2) and trussed tubes (John Hancock Center, Figure 1.3). Shear walls are often used as a part of the lateral load-resisting

system in these tubular structures. For example, the Burj Khalifa, currently the tallest building in the world, uses a bundled tube system and shear walls to reach its height and meet performance requirements (CTBUH 2015).

Additional advances in building technology have strongly impacted the field. New types of formwork significantly sped up construction times and, with reusable forms, lowered costs. Improved concrete pumping technology gave the ability to successfully pump material to new heights (Ali 2001). An important area of advancement that this research relates to is the creation and development of new types of concrete. Improvement in concrete material properties and behavior unlocks new possibilities in structural design.

1.3 High-Strength and High-Performance Concrete

Around the time period that Khan was developing large structural systems for skyscrapers, a major advancement for the building construction field came into play: high-strength concrete (HSC). Its development has occurred gradually, and improvements are still being made today. ACI Committee 363 on High-Strength Concrete refers to the material as having “specified compressive strengths for design of 6000 psi (41 MPa) or greater” (ACI 1997). Concrete meeting this specific definition was not commercially available until the 1960s, when compressive strengths between 6000 and 7500 psi (41 MPa and 52 MPa) were developed (ACI 1997). It is important to note that this designation is the result of the need for a quantitative measure to define HSC, and does not signify that there is any abrupt or significant physical occurrence or change when concrete reaches a compressive strength of 41 MPa (ACI 1997). High-strength concretes are wide ranging in their materials and properties, given the very general requirements defining the term.

Though the term high-strength concrete is sometimes used to refer to any concrete with compressive strength significantly higher than that of ordinary Portland cement concrete, there is no clear consensus on what to call these materials, and definitions differ from author to author. Today, high-strength concrete is often perceived to be an inadequate description of many of the types of concrete available (Kosmatka and Panarese 2002). The term gives the impression that the only advantage of this class of materials is increased compressive strength. In reality, many commercially-available products demonstrate additional characteristics, like high early-age strength, high modulus of elasticity, enhanced durability, self-consolidating nature, and enhanced impact resistance (Kosmatka and Panarese 2002).

High-performance concrete (HPC) is a term which more accurately describes the characteristics of this group of materials. In modern skyscraper construction, high-strength concrete will often also exhibit high early-age strength and a self-consolidating nature for ease of placing. Looking at the issue from the opposite direction, it is noted by Kosmatka and Panarese (2002) that “high-performance concrete almost always has a higher strength than normal concrete.” Taking all this into account, this paper will refer to high compressive strength concrete for tall buildings exhibiting additional high performance characteristics as HPC.

As previously discussed, HPC material properties can differ significantly with varying material composition and compressive strengths. Table 1.1 gives a general range for material characteristics, with data from Kosmatka and Panarese (2002) and the ACI 363 State-of-the-Art Report on High-Strength Concrete (ACI 1997).

Table 1.1 Range of typical HPC material characteristics

Material Characteristic	Range
Compressive Strength (MPa)	41 – 138
Modulus of Elasticity (GPa)	31 – 45
Density (kg/m ³)	2400 – 2500
Poisson's Ratio	0.20 – 0.30

HPC is often characterized by a low water-to-cement ratio, which is related to the material's increased compressive strength and durability. Depending on the specific application of the concrete, the potential requirements for high early-age strength, temperature and conditions during curing, and other factors, the mix proportions of HPC vary significantly. Some facts regarding HPC do remain constant: to achieve a low water-to-cement ratio without compromising workability, superplasticizers or high-range water reducers are used; and HPC will often contain supplementary cementitious materials like silica fume, fly ash, and slag (Kosmatka and Panarese 2002). Examples of mix designs are given in Table 1.2.

Table 1.2 Examples of HPC mix designs (Kosmatka and Panarese 2002)

Material	Mix 1	Mix 2	Mix 3	Mix 4
Water (kg/m ³)	145	135	145	130
Cement (kg/m ³)	398	500	335	513
Fly ash (kg/m ³)	45	-	-	-
Slag (kg/m ³)	-	-	125	-
Silica fume (kg/m ³)	32	30	40	43
Coarse aggregate (kg/m ³)	1030	1100	1130	1080
Fine aggregate (kg/m ³)	705	700	695	685
Water reducer (L/m ³)	1.7	-	1.0	-
Retarder (L/m ³)	-	1.8	-	-
HRWR (L/m ³)	3.0	14	6.5	15.7
Water to cementitious ratio	0.30	0.27	0.29	0.25
91-day comp. strength (MPa)	60	107	104	145

1.3 Ultra-High Performance Concrete

Ultra-high performance concrete (UHPC), a relatively new material which has been developed in the past few decades, takes the advantages offered by HPC much further. In the UHPC State-of-the-Art Report (Graybeal 2013), it is defined as a cementitious-based composite material with discontinuous fiber reinforcement, compressive strength greater than 150 MPa, and pre- and post-cracking tensile strength greater than 5 MPa. Another defining feature common to all types of UHPC is its dense concrete matrix, with only fines being used for aggregate, which results in enhanced durability due to the discontinuous pore structure (Graybeal 2013).

UHPC contains Portland cement and additional cementitious materials – silica fume and ground quartz. It utilizes superplasticizer or high-range water-reducing admixture (HRWR) to achieve a low water-to-cement ratio while retaining workability, and fine sand as aggregate (no coarse aggregate is used). Short fibers, usually consisting of steel, are added to the mixture commonly between 2 and 6 percent by volume (Graybeal 2013). A typical material composition, in this case a commercially-available UHPC mix called Ductal, is given in Table 1.3 below.

Table 1.3: Typical UHPC material composition (Graybeal 2006)

Material	Amount (kg/m³)	Percent by Weight
Portland cement	712	28.5
Fine sand	1020	40.8
Silica fume	231	9.3
Ground quartz	211	8.4
Superplasticizer / HRWR	30.7	1.2
Accelerator	30.0	1.2
Steel fibers	156	6.2
Water	109	4.4

UHPC has a very high compressive strength which can exceed 200 MPa, and a tensile strength that can reach 10 MPa depending on the mix and the curing regimen used (Graybeal 2013). The fibers embedded in the concrete matrix aid in reaching this tensile strength and also

give the material post-peak tensile capacity and ductile response. UHPC has a density that, like HPC, is slightly higher than conventional concrete. A general sense of UHPC material characteristics may be ascertained from the following examples: for Ductal UHPC, shown in Table 1.4, and for UHPC in general, given in ranges, provided in Table 1.5.

Table 1.4: Ductal UHPC material characteristics (Graybeal 2006)

Material Characteristic	Range
Compressive Strength (MPa)	180 – 225
Modulus of Elasticity (GPa)	55 – 58.5
Flexural Strength (MPa)	40 – 50
Entrapped Air Content (%)	2 – 4
Post-Cure Shrinkage (microstrain)	0
Density (kg/m ³)	2440 – 2550

Table 1.5: Range of UHPC material properties (Graybeal 2013)

Material Characteristic	Range
Compressive Strength (MPa)	140 – 200
Tensile Cracking Strength (MPa)	6 – 10
Modulus of Elasticity (GPa)	40 – 70
Poisson's Ratio	0.2

The micro steel fibers in the matrix bridge cracks and prevent localized failures from propagating and resulting in a brittle and sudden global failure. The failure mechanism for a single fiber can be represented by the pullout without rupture of the fiber from the matrix (Wille et al. 2012). Energy is required to overcome the initial bond of the fiber to the matrix, and the frictional effects as the fiber is pulled out (Wille et al. 2012). These actions cause multiple cracking to develop within the fiber-reinforced members and result in the high energy absorption capacity of UHPC during loading (Wille et al. 2012). Limiting crack propagation and crack widths also has a positive effect on UHPC durability throughout its design life, as deleterious agents are less able to enter the matrix and cause degradation (Graybeal 2013).

The increased tensile strength and improved ductile behavior of UHPC as a result of the inclusion of fiber reinforcement allows designs which could potentially reduce or eliminate steel bar reinforcement, simplifying both the design and construction of structures. Enhanced flexural capacity and ductility gives UHPC the ability to be used in designs with reduced member thickness as compared to those sized for conventional concrete. Designing to fully utilize UHPC's advantages is instrumental to determine the benefits of using UHPC in various applications. This research aims to further efforts towards that need by quantifying the aspects of using UHPC for shear walls in tall buildings.

Novel materials like UHPC require exploration through research in order to find how to use them most effectively and mesh their use with current technology. Experimentation can be costly, difficult, and time-consuming; having a computational model capable of simulating experiments instead allows this exploration to take place much more rapidly and increase the rate at which new technologies can be utilized by industry.

The structural behavior of the shear walls which is discussed in the following chapters is determined using a computational modeling protocol, the Lattice Discrete Particle Model (LDPM). Following calibration and validation of the LDPM parameters for each material tested in this research, performed in Smith et al. (2014) and Cusatis et al. (2011), the model is capable of simulating structural members to collapse. It captures the heterogeneity of concrete, resulting in realistic representations of cracking and thin-walled behavior. The simulation of concrete cracking in turn allows for the accurate prediction of failure modes for the member being modeled, a unique feature of the LDPM. The model has also been extended to include the effects of discrete fibers embedded within the matrix. The LDPM is embedded in a commercial software platform, called

Modeling and Analysis of the Response of Structures (MARS), to provide an interface for users to interact with the model and simulations.

When applied to shear walls, UHPC presents the opportunity to improve both structural efficiency and environmental sustainability. In conjunction with the lateral load-resisting systems discussed previously, UHPC shear walls would allow buildings to reach new heights and new forms. The work and conclusions discussed herein describe the structural and environmental quantification of the benefits of UHPC shear walls. In the following chapter, the LDPM is described in more detail, and an example is presented which describes how simulations of cement-based composite structural members are defined and performed using MARS and supercomputing resources. Next, Chapter 3 shows the results of the parameter studies for UHPC shear walls, which utilize LDPM simulation to determine by how much the thickness of the walls can be reduced and to determine the effects of other parameters. Thereafter, Chapter 4 gives an overview of life cycle assessment (LCA) and the methodologies used here to perform LCA. Using LCA, the environmental impact of materials can be quantified and directly compared to other materials. Chapter 5 presents the results of a sustainability study which compares UHPC to HPC. Finally, Chapter 6 draws the conclusions which resulted from this research endeavor.

CHAPTER 2. Lattice Discrete Particle Model and MARS

The Lattice Discrete Particle Model (LDPM) simulates concrete on the meso-scale level, approximately the length of the aggregate pieces within the concrete. It provides a detailed representation of the heterogeneous infrastructure of concrete, important to behaviors like crack initiation and propagation, and thus can capture the structural response and failure modes of concrete members.

2.1 Introduction to the LDPM

In this research, LDPM is used to perform quasi-static loading on UHPC shear wall specimens, including the effect of discrete fibers embedded in the concrete matrix, and to obtain information on the structural response and failure mode of the shear wall. The approach represents concrete as a two-phase material: whole aggregate pieces, and the mortar matrix in which they are embedded; which are modeled as discrete elements: particles and lattice elements, respectively. The nature of the construction of the model, with the displacement field defined at a finite number of points which correspond to the center of aggregate particles, lets the capabilities of the approach be realized at a practical computational cost for modeling members at structural component scale (Cusatis et al. 2011).

The aggregates are sized and randomly distributed to mimic the internal heterogeneity of concrete and capture the failure mechanisms and crack network. The input parameters in the particle generation phase correspond to a sieve curve give the size and distribution of the aggregate pieces, defined to be spherical in shape, within the matrix. A lattice is formed by a three-dimensional Delaunay tetrahedralization of the center points of the particles, followed by the formation of additional line segments by a tessellation algorithm, the results of which are shown

in Figure 2.1a. These two processes form triangular facets that surround the aggregate pieces creating polyhedral cells that each contain an aggregate piece, visualized in Figure 2.1b. Stresses and strains are defined at each facet, giving a refined stress resolution in the mesostructure and a detailed representation of cracking distribution and localization (Cusatis et al. 2011).

The tessellation process is formulated to prevent intersections of the spherical aggregate pieces, shown in Figure 2.2a, and the polyhedral cells, maintaining a realistic representation of particle and matrix. This is important because the mechanical interaction between adjacent particles in actual concrete occurs through the mortar. The intersection of the polyhedral cells, or the facets, are potential crack surfaces in the LDPM. Simulated cracks propagate through the model's representation of the mortar and not through aggregate pieces, in agreement with actual concrete behavior, where aggregate pieces are more likely to remain mainly intact and undamaged throughout loading compared to the mortar. Due to the way the model is constructed, an additional algorithm is needed to form the external surfaces of members, upon which loading and restraint conditions can be applied. This is achieved using zero-diameter particles, or nodes, distributed

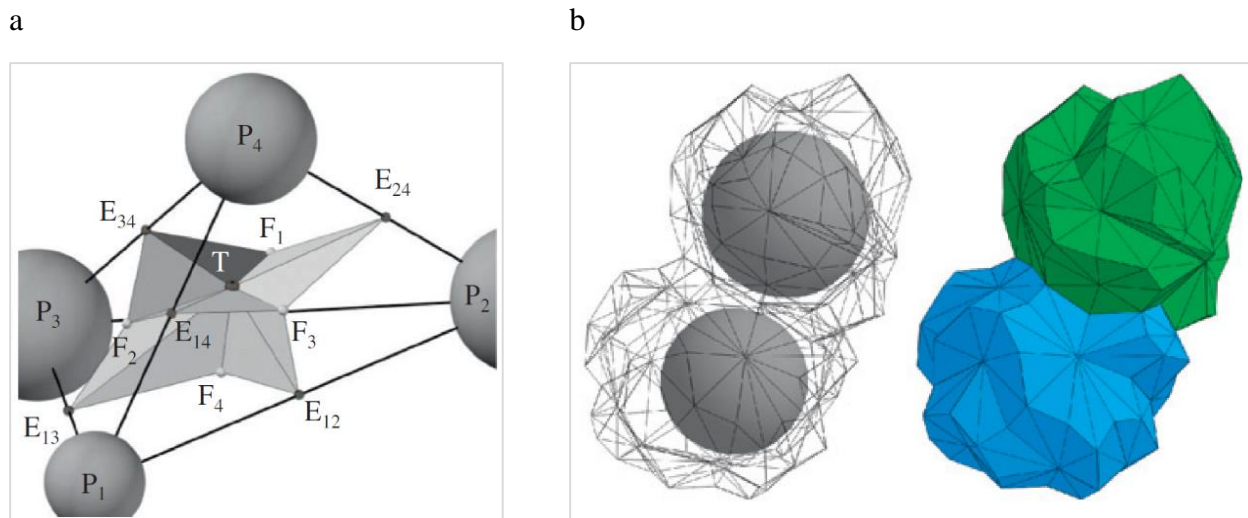


Figure 2.1: a) Tetrahedral between particle centers formed by the LDPM tessellation algorithm, b) Polyhedral cells containing two adjacent particles (Cusatis et al. 2011)

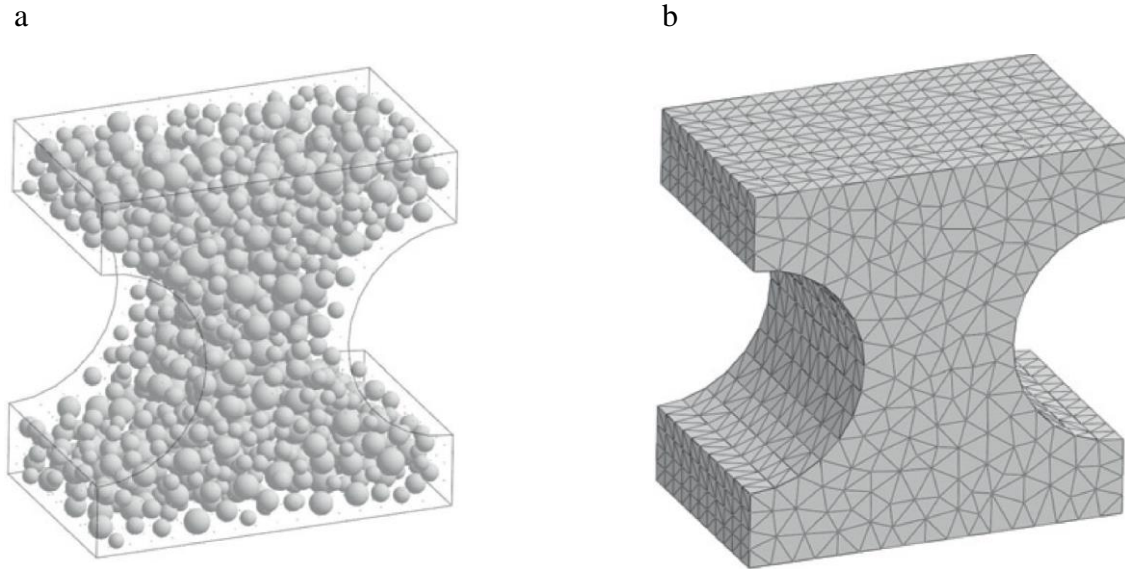


Figure 2.2: a) Distribution of particles within a specimen, b) Fully-constructed LDPM specimen showing external surface facets (Cusatis et al. 2011)

across the user-defined external surfaces, the product of which is shown in Figure 2.2b. The completed concrete mesostructure geometry gives the number, size, and position of, and connections between particles, and the facets through which forces are transmitted between adjacent particles (Cusatis et al. 2011).

The LDPM meso-scale constitutive equations, derived using rigid-body kinematics, define the simulated concrete behavior including the effects of tensile fracturing with strain-softening, cohesive and frictional shearing, and non-linear compressive behavior with strain hardening due to pore collapse. The LDPM, considering these abilities, can simulate all concrete behavior under quasi-static loading on the macroscale, including tensile and compressive response, confinement effects, size effect, and biaxial and triaxial compression effects (Cusatis et al. 2011).

The LDPM has been extended to include the effects of dispersed fibers in fiber-reinforced cementitious composites like UHPC. Fiber reinforcement conveys many advantages to the material properties and design of members: reduced steel bar reinforcement, improving constructability; reduced crack widths during loading and shrinkage throughout the design

lifetime, which enhances concrete durability and longevity; moderate increase in compressive strength; and post-peak load capacity or ductility of the composite itself, and energy absorption during cracking (Schauffert and Cusatis, 2012). These attributes are all important to the structural efficiency and performance of shear walls in tall buildings, discussed in the following chapters. The enhanced model with the ability to simulate dispersed fibers is referred to as the LDPM-F; for simplicity, it will continue to be referred to as the LDPM in this paper.

Within the framework of the model, fibers are represented similarly to aggregate pieces as described above – they are simulated as discrete entities which are dispersed randomly throughout the matrix with a total amount corresponding to a given volume fraction. Fibers are assumed to be straight at the onset of loading and have a circular cross-section. Their behavior and contribution to the stresses and strains at the mesoscale level are defined at the locations where the fibers intersect the polyhedral facets. On the level of a single fiber, its response depends on the magnitude of the mesoscale crack opening that is bridged by the fiber. Embedment length of the fiber is also considered when characterizing the fiber pullout, seen in Figure 2.3a. Appropriately, if a compressive strain is present, the contribution of the fiber to the forces at the intersecting facets is zero (Schauffert and Cusatis, 2012).

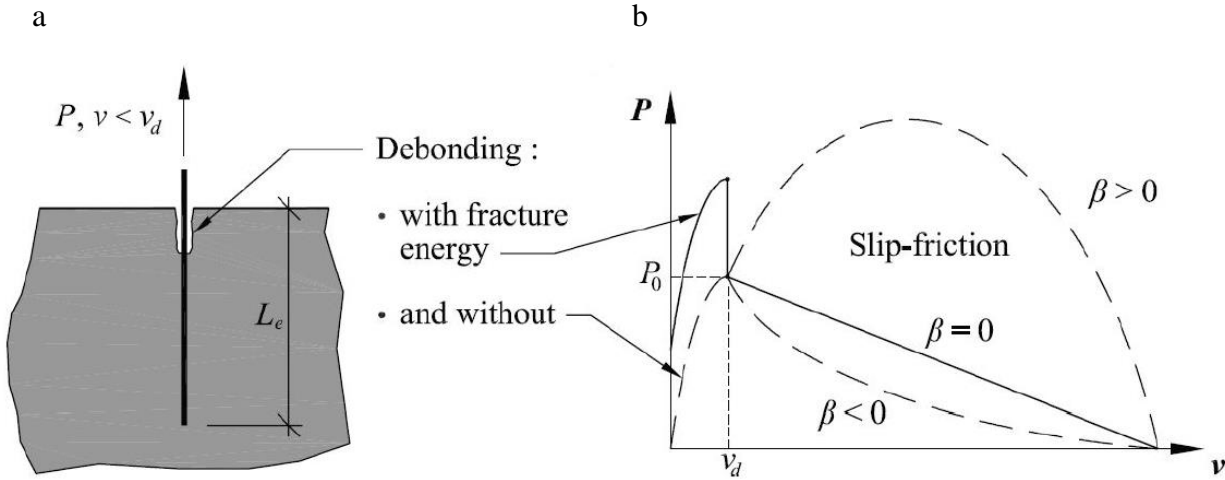


Figure 2.3: a) Debonding of a steel fiber with embedment length L_e and load P , b) load-slip curve showing the portions the fiber response corresponding to fracture energy, and slip-friction, with slip hardening-softening parameter β (Schauffert and Cusatis et al. 2012)

A load-slip curve governs the pullout response of the fibers within the matrix during loading, shown in Figure 2.3b. This curve is comprised of two stages, debonding and frictional slip. The first stage represents the debonding of the fiber from the surrounding matrix and is characterized by the bond fracture energy G_d . The second stage represents the slippage of the fiber following debonding with the effects of interfacial friction between the fiber and the matrix and is characterized by the frictional stress value τ_0 . In the following section, the parameters which govern the particle-matrix interaction are described in more detail.

2.2 LDPM Material Parameters

For a given material, the LDPM is calibrated with experimental data via the determination of appropriate values for a set of LDPM parameters, then validated with additional, separate experimental data to ensure that the model is predictive. Parameters including cement content c , water-to-cement ratio w/c , aggregate to cement ratio a/c , maximum aggregate size d_a , minimum aggregate size d_0 , and Fuller coefficient n_F (which defines the aggregate sieve curve), characterize

the constituents and geometry of the concrete matrix. The model resolution is manifested in the number and size of the particles simulated in a specimen, controlled by the minimum aggregate size d_0 .

Additional parameters, such as normal elastic modulus E_0 , shear-normal coupling parameter (ratio between shear and normal elastic stiffening) α , and tensile fracture energy G_t , govern the physical response of the model on the mesoscale and, when incorporated into the LDPM constitutive equations, define the material's linear and non-linear behaviors. All parameters are calibrated via the mix design information and hydrostatic compression, unconfined compression, fracture, and triaxial compression experiments with both low and high confinement pressures. The LDPM can then simulate all aspects of concrete behavior under any quasi-static loading regime (Cusatis et al. 2011).

The fiber contribution to the concrete matrix is captured through a number of parameters. The bond fracture energy G_d , frictional stress τ_0 , and slip hardening-softening parameter β characterize the load-slip curve of the fibers. The model also takes into account spalling of the matrix during fiber pullout via the spalling parameter k_{sp} , and snubbing, or bending of fibers at the crack surface, via the snubbing parameter k_{sn} , as well as the potential for plastic deformation of fibers following yield, γ_p . A full list of the LDPM concrete parameters and fiber-matrix interface parameters is given in Table 2.1 (Schauffert and Cusatis 2012).

Table 2.1: LDPM Parameters

	Parameter	Description
Concrete	E_0 (GPa)	Normal elastic modulus
	α	Shear-normal coupling parameter
	σ_t (MPa)	Tensile strength
	l_t (mm)	Characteristic length
	G_t (N/m)	Tensile fracture energy
	σ_s/σ_t	Ratio of shear strength to tensile strength
	n_t	Softening exponent
	σ_{c0} (MPa)	Yielding compressive stress
	H_{c0}/E_0	Ratio of initial hardening modulus to normal elastic modulus
	κ_{c0}	Transitional strain ratio
	κ_{c1}	Deviatoric strain threshold ratio
	κ_{c2}	Deviatoric damage parameter
	μ_0	Initial internal friction coefficient
	μ_∞	Asymptotic internal friction coefficient
	σ_{N0} (MPa)	Transitional stress
	d_a (mm)	Maximum aggregate diameter
	d_0 (mm)	Minimum aggregate diameter
	c (kg/m ³)	Cement content
	w/c	Water to cement ratio
	n_F	Fuller coefficient
Fibers	G_d (N/m)	Bond fracture energy
	τ_0 (MPa)	Bond frictional stress
	β	Slip hardening-softening parameter
	k_{sp}	Spalling parameter
	k_{sn}	Snubbing parameter
	σ_{uf} (MPa)	Fiber tensile strength
	k_{rup}	Fiber strength decay parameter
	E_f (GPa)	Fiber elastic modulus
	γ_p	Plastic deformation parameter

2.3 MARS

The LDPM is embedded within a commercial software platform, Modeling and Analysis of the Response of Structures (MARS), available from Engineering and Software System Solutions, Inc. (ES3). MARS is used in this research to define specimen geometry, perform simulations, and obtain results. The user interfaces with the software using written code, following a number of steps to fully define all required inputs.

First, the mix design is inputted via the cement content c , water-to-cement ratio w/c , minimum aggregate size d_0 , maximum aggregate size d_a , and Fuller coefficient n_F . Then, the geometry is entered using MARS commands, or via importing information from SIMULIA Abaqus FEA, a continuum finite element analysis software suite. Following this, the remaining LDPM parameters are defined as well as connections between components of the simulated member, support conditions, and loading conditions of the structural member of interest. The formulation of a LDPM simulation in MARS is explained in much further detail later in this chapter.

MARS provides an output file with different results depending on what was requested by the user. A separate freely-available program, Paraview, is used for visualizing the simulation throughout the test. Together, MARS and Paraview allow the visualization of features of the simulation like crack opening, stresses, the distribution of particles, and the distribution and orientation of fibers in the matrix; and allow these figures to be overlaid with control over transparency. This powerful aspect may be used for analysis of the test to determine failure modes, critical components, and structural performance.

This research utilizes MARS and the LDPM to perform quasi-static loading on concrete specimens. It is important to note that the model is not limited to simulating only this type of

testing; cyclic loading, and dynamic effects like blast loading are also included as capabilities. Expanding upon the results detailed here, future research endeavors may explore these types of effects on UHPC shear walls in tall buildings, and other UHPC structural members.

2.4 Benefits of the LDPM and MARS

The LDPM employs a novel approach to modeling concrete which gives the unique ability to accurately represent crack initiation and propagation through the matrix and simulate the effects of discrete embedded fibers. The use of the LDPM for testing relatively new materials like UHPC accelerates the process of developing design guidelines. Experimental programs are lengthy, costly, and often difficult; a validated simulation platform is advantageous in time savings and reducing complexity.

With the aid of supercomputing resources, the aforementioned LDPM capabilities can be applied even to large-scale structural members at reasonable computational cost. MARS and the LDPM are installed at the Virginia Tech Advanced Research Computing (ARC) supercomputing cluster called NewRiver. The marriage of model, software, and computing resources such as these make research efforts like this possible, and advance the field toward its eventual destination of simulation-based design.

2.5 LDPM Simulation Procedure with Example

Though the development of structural simulations in MARS is intuitive, there is a learning curve to be mastered before a user can efficiently work with the model. The following describes an example of the files necessary to define and run a simulation of a UHPC shear wall, 3000mm long, 4000mm in height, and 600mm thick, using Cor-Tuf concrete (Roth 2010), for the aid of future users to reduce the time to become acclimated with the procedures. The full files for this example and the other structural simulations discussed in this work are included in Appendix A at

the end of the document. MARS code is written in the C++ language, so associated syntax like the escape character “//” for commenting apply here. Additionally, the example detailed here refers to the latest software build as of November 2015; subsequent builds may introduce changes in syntax.

In general, the procedure to define a simulation is organized into three files, referred to here as the “Gen” file, the “Run” file, and the “Submission” file. The “Gen” file involves determining the mix design, LDPM component geometry, and meshing of the LDPM components. The “Run” file involves all other aspects including other material definition (for example, elastic steel), fiber material definition, additional component geometry (for example, steel reinforcing bars), LDPM parameters, constraints, loading, and output formatting. Finally, an additional file is generated by the user in order to submit a job to use supercomputing resources, to run the simulation defined by the “Gen” and “Run” file. This file will be referred to as the “Submission” file.

2.5.1 “Gen” File: *GenUhpWall.mrs*

The header must provide a name; in this case, “UHPC Shear Wall 55 story bldg”, but the user’s choice of nomenclature is not important. Then, a choice of measurement system is made.

```
//-----  
Particle generation:UHPC Shear Wall 55 story bldg  
//-----  
ControlParameters {  
    Units SI  
}  
//-----
```

Next, the parameters relating to the mix design are defined. In the line “Material CONC LDPM {“, *Material* instructs MARS to define a material with name *CONC*. *LDPM* is a MARS command for material definition of concrete. The parameters in *MixDesign* { must all be defined,

with attention to units where appropriate. Those parameters which require units must have units defined as shown here; further information regarding formatting may be found in the manual provided by ES3 (Pelessone 2015).

```
//-----  
Material CONC LDPM {  
  MixDesign {  
    CementContent 794.4 kg/m3  
    WaterToCementRatio 0.2082  
    AggregateToCementRatio 1.6332  
    MinAggregate 2 mm  
    MaxAggregate 4 mm  
    FullerCoefficient 0.5  
  }  
}  
//-----
```

Next, the LDPM component geometry is defined. *HexSolidList* initiates a hexahedral finite element mesh which in this case describes the external surfaces of the LDPM component. The *generate { block {* command generates a rectangular prism with given dimensions in the x, y, and z directions, with a corner at the origin, (0,0,0). *Make ParticleList PRTC* generates the LDPM random particle distribution, with the number following *seed* used for the random number generation.

```
//-----  
HexSolidList MODL Geometry {  
  Material CONC  
  generate {  
    block {  
      dimensions 3000 mm 4000 mm 600 mm  
      elements 1 1 1  
    }  
  }  
  Make qfL MODL  
  Make tfL MODL  
  Make ParticleList PRTC { seed 11011112 , plotSieveCurve }  
}
```

```
//-----
```

Alternatively, an ABAQUS input file may be used for more complex shapes (those other than rectangular prisms, spheres, or cylinders), a selection from a separate example of a file is given below.

```
//-----
```

```
HexSolidList WALL Geometry {  
  ReadAbaqusMesh {  
    FileName UHPC_Full_45Wall.inp // Abaqus file  
    Part UHPC_Wall // Match part name given in Abaqus  
    LengthUnits mm // Keep units consistent  
  }  
}
```

```
//-----
```

The final portion of the “gen” file involves the writing of the “mesh” file, *MeshUhpcWall.mrs* in this case, which provides the finite element mesh for the simulation. Overall, the advantage of grouping these steps in the “gen” file is that subsequent simulations using identical geometry and mix design do not need to repeat the computational work of the “gen” file – the outputted “mesh” file *MeshUhpcWall.mrs* may be reused. For subsequent simulations, the “gen” file may be skipped; only the “run” file needs to be used. The resulting LDPM specimen from this file is shown in Figure 2.4.

```
//-----
```

```
TetSolidList PRTC LDPM {  
  Write PartMeshDataFile MeshUhpcWall.mrs  
  Make tfl EXTN // generation of the TriangularFaceList EXTN  
}
```

```
//-----
```

```
EOF
```

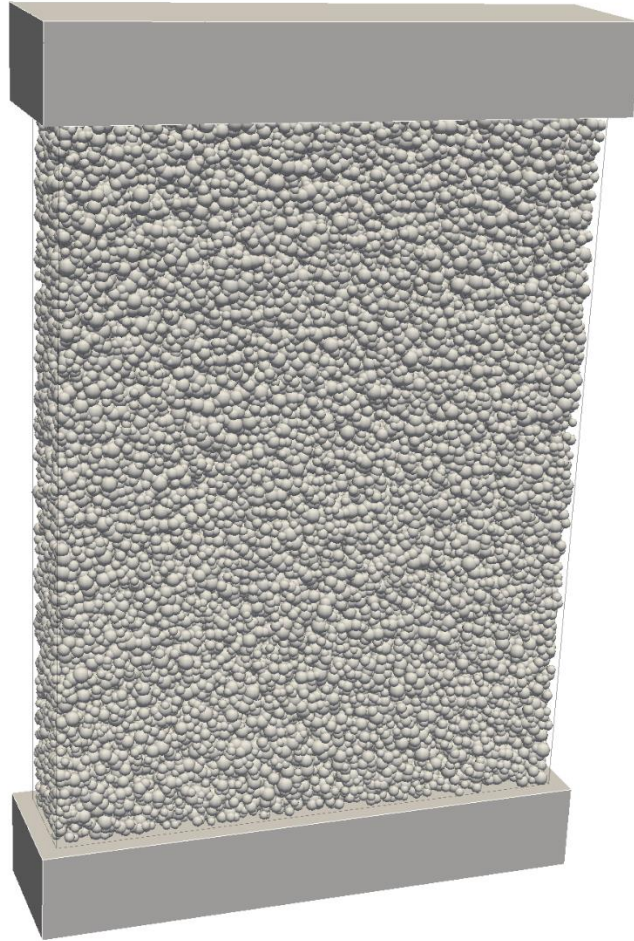


Figure 2.4: Distribution of particles in a shear wall specimen, 2 mm to 4 mm aggregate size, scaled 5x

2.5.2 “Run” File: *RunUhpcWall.mrs*

Again, a header must be used but the nomenclature is not important nor is it used at any point in the simulation. *ControlParameters* defines the units to be used, the termination time of the simulation (simulation time, not real time), the maximum time step during the simulation, and the frequency of output of results to the command window (in this case, every 10 steps).

```
//-----  
SHEAR UHPC CORTUF WALL WITH FIBERS  
//-----  
// GENERAL CONTROL PARAMETERS  
//-----
```

```

ControlParameters {
  Units SI
  TerminationTime 1000.1 ms
  MaximumTimeStep 0.00025 ms
  Monitor Frequency 10
  tsf 0.7 // safe coefficient of the MaximumTimeStep
  Flush every 0.02 ms
}
//-----

```

The following section involves the definition of materials for use in the model. The LDPM concrete material has already been defined in the “gen” file. Elastic materials may be defined to represent uncracked concrete, elastic steel, and so on. If an elastic material is defined to represent the uncracked portion of concrete, consideration should be applied to the choice of parameters so the appropriate material behavior is obtained. Plastic materials may be defined to represent materials like steel, with the option of including a hardening modulus value.

```

//-----
// MATERIAL
//-----
Material ECON elastic {
  Density 2400 kg/m3 // Reminder - must include units if
                    // appropriate
  YoungModulus 58000 MPa
  PoissonsRatio 0.2
}
//-----

```

The material definitions shown here, from a different MARS file which uses rebar, give details to clarify the nomenclature involved with plastic materials in MARS.

```

//-----
// Elastic + plastic steel with strain hardening
Material PSTEEL_Y Plastic {
  Density 7.8 g/cm3
  YoungsModulus 200000 MPa
  PoissonsRatio 0.3
  YieldStrength 400 MPa
  IsotropicHardening
}

```

```

// Alternative: KinematicHardening
// Alternative: Beta 0.5 // Beta=0 isotropic, =1 kinematic
HardeningModulus 520 MPa
}
//-----

```

If fibers are desired to be included in the matrix, a *LDPM-F* material is defined, with values given for the LDPM parameters relating to the fibers, described in Table 2.1. These particular parameter values are calibrated for Cor-Tuf UHPC (Smith et al. 2014).

```

//-----
Material FIBRM LDPM-F {
    ElasticModulus      210 GPa    // ymf, elastic modulus
    SpallingParameter   150 MPa    // sps, spalling parameter
    FiberStrength        1200 MPa  // sfu, fiber strength
    FiberStrengthDecay  0.4        // fsd, fiber strength decay
                                // parameter
    SnubbingParameter   0.05       // fsn, snubbing parameter
    BondStrength         11.5 MPa  // tau, bond strength
    VolumeStiffnessRatio 0.0       // eta
    DebondingFractureEnergy 0 N/m  // gdm, debonding fracture
                                // energy
    PullOutHardening    0.0        // poa, pull-out hardening
                                // coefficient
    PlasticParameter     0.5       // mai maggiore di 1
    CookGordonParameter 2.0       // cgp, Cook-Gordon effect
}
//-----

```

If steel reinforcing bars are included in the simulation, coordinate reference systems must be defined to align the rebar in the correct directions. It is important to note that MARS will not allow the generation of rebar if any bar is aligned with the *FirstDirection* or *SecondDirection* of the preliminary reference system. In this example, the directions of the *ReferenceSystem* “NOORTHO” are chosen so neither is aligned with any rebar in the model. An example of how these reference systems are used to align rebar is included later in this section.

```

//-----
// Reference Systems for Rebar

```

```

//-----
ReferenceSystem RXY cartesian {
  FirstDirection 1. 0. 0.
  SecondDirection 0. 1. 0.
}
ReferenceSystem RYX cartesian {
  FirstDirection 0. 1. 0.
  SecondDirection 1. 0. 0.
}
ReferenceSystem RYZ cartesian {
  FirstDirection 0. 1. 0.
  SecondDirection 0. 0. 1.
}
ReferenceSystem RXZ cartesian {
  FirstDirection 1. 0. 0.
  SecondDirection 0. 0. 1.
}
ReferenceSystem NOORTHO cartesian {
  FirstDirection 1. 1. 1.
  SecondDirection -1. -1. 1.
} // MARS will not generate rebars if any rebar is aligned with
// the FirstDirection or SecondDirection of the preliminary
// reference system
//-----

```

In this section, the LDPM parameters from Table 2.1 are entered into the model. Additionally, the length, cross-sectional area, and volume fraction of fibers are defined, and the random distribution of fibers is performed with the option of including a preferential direction for the fibers (commented out / not used in this case), shown in Figure 2.5.

```

//-----
// LDPM ELEMENT
//-----
TetSolidList PRTC LDPM {
  ReadFile MeshUhpcWall.mrs
  EditNodeList {
    Rename PRTC
  }
  EditMaterial {
    StaticParameters {
      NormalModulus 67000 MPa // nmo

```

```

DensificationRatio 2.5 // drt
Alpha 0.484 // alpha
TensileStrength 4 MPa // ftm
CompressiveStrength 500 MPa // fcm
ShearStrengthRatio 17 // fsm
TensileCharacteristicLength 150 mm // tcl
SofteningExponent 0.2 // ncm
InitialHardeningModulusRatio 0.36 // hmr
TransitionalStrainRatio 2 // hts
InitialFriction 0.5 // mu0
AsymptoticFriction 0 // mu1
TransitionalStress 300 MPa // fts
VolumetricDeviatoricCoupling 0 // beta
DeviatoricStrainThresholdRatio 2 // dk1
DeviatoricDamageParameter 1 // dk2
}
}
EmbeddedFibers {
  FiberConcreteInteraction FIBRM
  GenerateFibers {
    Seed 9995 // seed for random number generator
    FiberLength 3.0 cm // length of fiber
    EdgesPerFiber 1
    FiberSectionArea 0.785 mm2 // cross sectional area
    Tortuosity 0.0 // usually 0
    VolumeFraction 0.20
    //PreferentialDirection 1 0 0 10.
  }
}
Make tfL EXTN
Plotting enabled
MassScaling
}
//-----

```

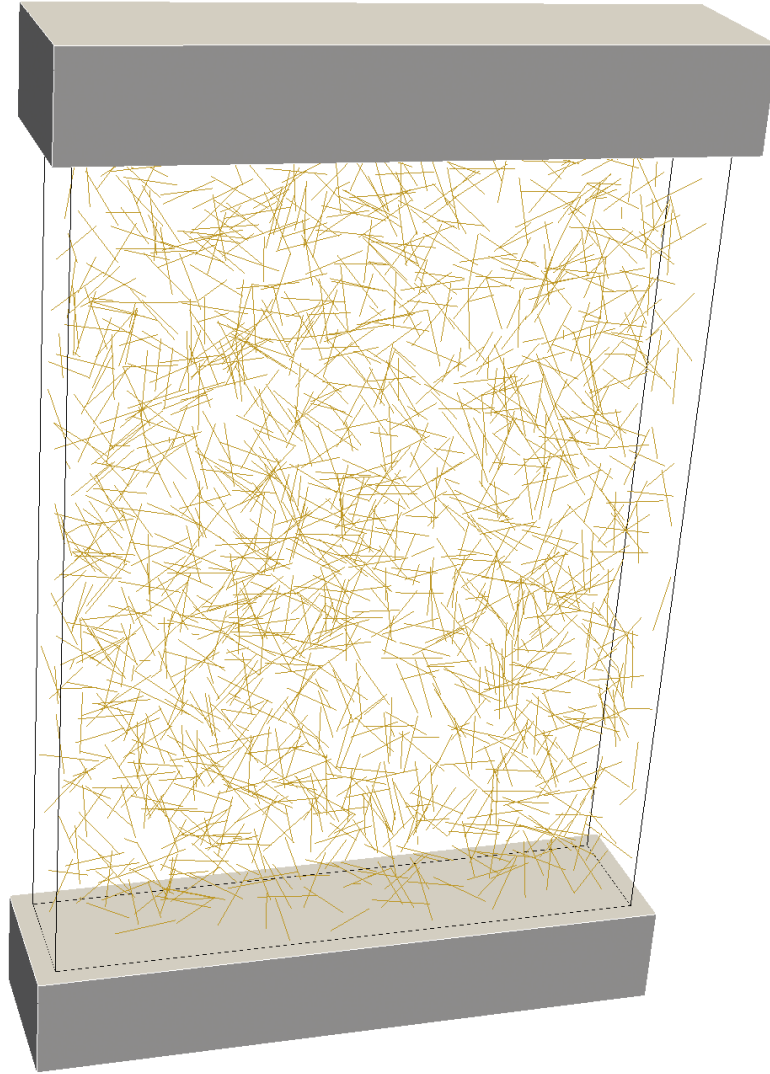


Figure 2.5: Distribution of fibers in the concrete matrix with random orientation and $V_f = 2\%$ (1/4 of the fibers are shown)

Using elastic components for parts of the simulation where failure is not expected reduces the computational cost of the simulation. Elastic concrete blocks are generated, located at the top and bottom of the shear wall. The top block is used to apply the lateral load and axial load to the shear wall, and the bottom block is used to apply the fixed boundary conditions at the bottom. Shapes in MARS are defined with a corner at (0,0,0), so the elastic concrete blocks must be moved to the appropriate location using the *NodeList { Move* command. Note that both blocks use the material *ECON* which was created earlier in the “Run” file.

```

//-----
//          HEXAHEDRAL SOLID ELEMENT
//-----
HexSolidList TOPCON 8IP {
  Material ECON
  Generate {
    Block {
      dimensions 3020 mm 200 mm 620 mm
      elements 200 20 60
    }
  }
  NodeList {
    Move -10 mm 4000 mm -10 mm
  }
  Make tfl TOPCON
}
HexSolidList BTMCON 8IP {
  Material ECON
  Generate {
    Block {
      dimensions 3020 mm 200 mm 620 mm
      elements 200 20 60
    }
  }
  NodeList {
    Move -10 mm -200 mm -10 mm
  }
  Make tfl BTMCON
  Plotting enabled
}
//-----

```

The size, position, and length of the rebar is given with the *Rebar* command. The preliminary reference system, in this case “NOORTHO”, is entered and has no effect on the actual orientation of the bars. The reference system detailing the actual bar orientation is placed within the *Generate { Rebars {* command, with the convention of the first direction being aligned with the bar, and the second direction the axis along which multiples of the bar are placed if desired. In this case, a number of multiples, and spacing of the rebar is given from bar center to bar center.

To create hoops or bent bars, the *Generate { BentRebars {* command is used along with a list of coordinates for the shape of the bars. The simulated reinforcement for a high-strength concrete specimen with edge elements is shown in Figure 2.6.

```
//-----
// STEEL BAR REINFORCEMENT
//-----
// Vertical web bars
EdgeList VWEBBAR Rebar {
  sec o m PSTEEL_Y d 6 mm i 5 p 12 // p is for paraview
    // graphics. i controls subdivision of x-section into sub
    // areas
  ReferenceSystem NOORTHO
  Generate {
    Rebars {
      ReferenceSystem RYX
      LengthUnits mm // required
      Translate 140 0 165 // in global reference system
      RebarLength 1100
      MaxElementSize 5
      NumberOfRebars 7
      RebarSpacing 100
    }
  }
}
//-----
// Edge horizontal hoop reinforcement
EdgeList HOOPS Rebar {
  sec o m PSTEEL_Y d 6 mm i 5 p 12 // p is for paraview
    // graphics. i controls subdivision of x-section into sub
    // areas
  ReferenceSystem NOORTHO
  Generate {
    BentRebars {
      ReferenceSystem RYX
      LengthUnits mm // required
      MaxElementSize 5.
      Translate 15. 19. 15. // global reference system
      Point 0. 0.
      Point 60. 0.
      Point 60. -345.
      Point 0. -345.
    }
  }
}
```

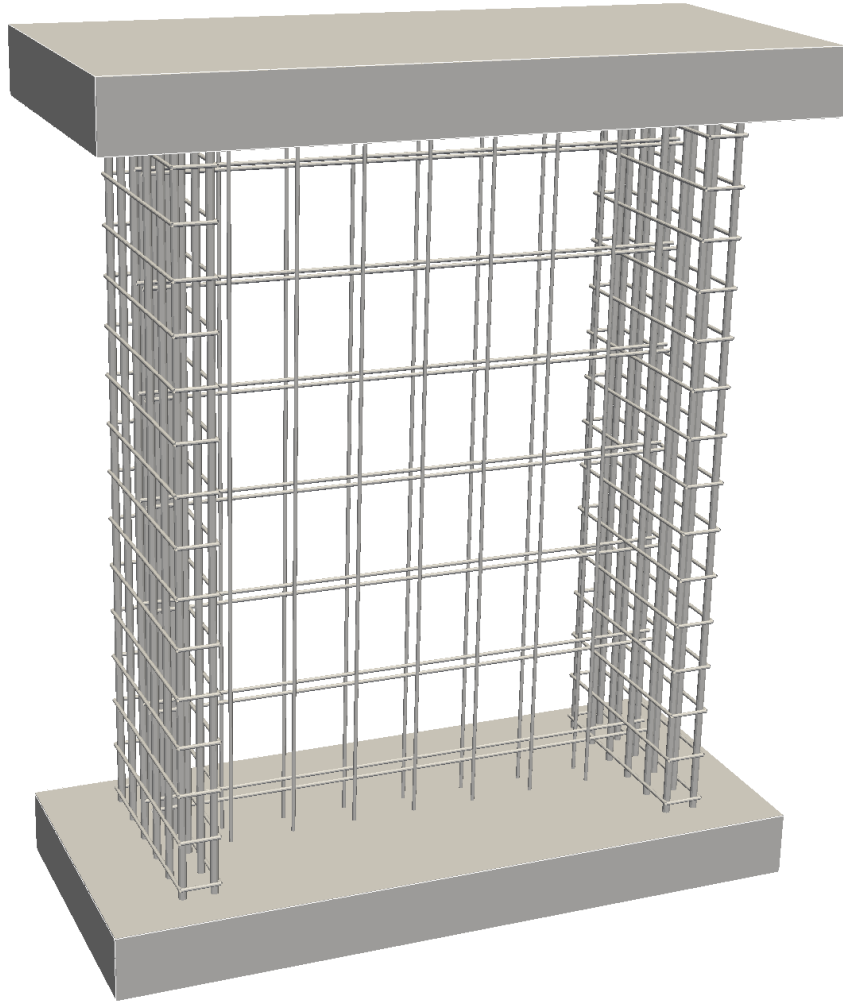


Figure 2.6: Simulated reinforcing bars for a shear wall specimen

```
Point 0. 0.  
Duplicate 15 @ 75.  
}  
}  
}  
//-----
```

The top and bottom elastic concrete blocks were created, but at this point there is nothing that connects them to the LDPM concrete. Now, a *penalty constraint* is added between the

components to connect them together. MARS determines the points at which each component is in contact with one another and should have the penalty constraint applied.

```
//-----  
// LDPM-HEX Constraints  
//-----  
NodeHexConstraintList BONDTOP Penalty {  
  NodeList PRTC  
  HexList TOPCON  
  StiffnessBasedOnTimeStep 0.001 ms  
}  
NodeHexConstraintList BONDBTTM Penalty {  
  NodeList PRTC  
  HexList BTTMCON  
  StiffnessBasedOnTimeStep 0.001 ms  
}  
//-----
```

If reinforcing bars are included in the simulation, they must also be somehow connected to the LDPM concrete. One possibility, used in this research, is to tie the rebar to the concrete in the same way the elastic concrete blocks are connected, using a penalty constraint. The spacing of the constraints is set by the length of the finite elements which comprise the reinforcing bars.

```
//-----  
// Constraints  
//-----  
// Rebar Ties  
NodeTetConstraintList HWEBTIES Penalty {  
  NodeList HWEBBAR  
  TetList PRTC  
  StiffnessBasedOnTimeStep 0.0005 ms  
}  
NodeTetConstraintList HOOPTIES Penalty {  
  NodeList HOOPS  
  TetList PRTC  
  StiffnessBasedOnTimeStep 0.0005 ms  
}  
//-----
```

An alternative is to use the *RebarConcreteInteraction* function to model the connection between rebar and concrete. Using this function, the spacing of the constraints is not limited to the element size of the reinforcing bars as above; the forces transmitted between rebar and concrete are formulated in a smoother way. Additionally, the formulation permits the modeling of rebar slippage in the axial direction.

```
//-----
// Constraints
//-----
// Rebar Ties
BeamParticlesConstraintList HWEBTIES RebarConcreteInteraction {
  BeamList HWEBBAR
  ParticleList PRTC
  RebarConcreteInteraction HWEBBAR_PRTC
  NumberOfCircumferentialConstraintsPerBeamElement 6
  NumberOfAxialConstraintsPerBeamElement 3
  RebarRadius 3 mm
  UpdateInterval 0.001 ms
  MaximumDistance 1.2 mm
  ParticlesFullyOutsideBeam
}
//-----
```

The *Select* and *Reselect* commands are used to choose specific portions of the node lists defined in the generation of the material components of the simulation. New node lists are created for the purpose of applying loads, support conditions, and for the output of results at the chosen locations. Here, the top of the top elastic concrete block is restrained against translations and rotations about the z-axis, and the bottom of the bottom elastic concrete block is fixed against translations and rotations about all axes.

```
//-----
// NODE LIST DEFINITIONS AND BOUNDARY CONDITIONS
//-----
NodeList PRTC {
  Select all
  Reselect cy < 0.1 mm
}
```

```

    Make ndL BTMML
    Select all
    Reselect cy > 3999.9 mm
    Make ndL TOPL
    Select all
}
NodeList TOPCON {
    Select all
    Reselect cy > 4199.9 mm
    Make ndL TOPE
    Set Translations OOX
    Set Rotations OOX
    Select all
        Reselect cy > 3999.9
    Reselect cx < -9.9 mm
    Make ndL SIDEE
    Select all
}
NodeList BTMCON {
    Select all
    Reselect cy < -199.9 mm
    Make ndL BTME
    Set Translations XXX
    Set Rotations XXX
}
//-----

```

In the previous step, the appropriate locations for the application of loads, or for displacement-controlled tests the application of displacements, were defined with node lists. Now, the loads and displacements themselves are described and applied. A *LoadCurve* is defined for the axial load which corresponds to the axial force from gravity loads carried by the shear wall. The coordinate list is necessary to describe the loading curve, so that the loads are not applied instantaneously. This limits the dynamic effects experienced in the simulation, the effectiveness of which can be discerned by plotting the forces within the shear wall. If an unacceptable degree of oscillation is present due to dynamic effects, the load curve must be changed to apply the loads in a more gradual manner.

The *NodalLoadList* command is used to apply the loading curve to the appropriate node list and to choose the direction of the force. The last two lines of this section are critical – *Distribute* tells the model to distribute the load over the nodes, and *All* distributes the load over all the nodes in the node list. Without this portion, the load will be applied at each node in the node list.

Next, another load curve is created but this time describes an applied velocity instead of an applied load. This corresponds to the applied displacements over the course of the simulation in the lateral direction. The steps are very similar to those above, with *PrescribedVelocityList* used instead.

```
//-----
// APPLIED LOADS
//-----
LoadCurve ALoad {
  X-units time ms
  Y-units force N
  ReadPairs 5
  0      0
  1.0    4000
  2.0    15000
  3.0    19800
  5000.1 19800
}
NodalLoadList Load {
  NodeList TOPE
  LoadCurve ALoad
  Direction 0. -1. 0.
  Distribute
  All
}
LoadCurve VELO {
  X-units time ms
  Y-units velocity mm/s
  ReadPairs 5
  0      0
  3.5    0
  4.0    175
}
```

```

100      175
1000.1  175
}
PrescribedVelocityList VELO {
  DisregardMultipleConstraints
  LoadCurve VELO
  Direction 1 0 0
  ndL SIDEE
  All
}
//-----

```

At this point, every requirement to run a simulation has been met. The remaining portion of the “Run” file relates to the generation of results. This section allows the user to choose what to output into the text file produced during the simulation. The variable dt is the frequency at which the results will be outputted. An important metric is ke , the kinetic energy of the specimen. The kinetic energy should be very small throughout the test because it is meant to be quasi-static. A large ke likely means a constraint condition has been incorrectly applied, or the load or velocity used is too high, or the specimen has fractured.

```

//-----
// Output
//-----
TimeHistoryList ResultsUhpcWall {
  dt 0.05 ms
  ndL-TOPE cy D S 1000
  ndL-SIDEE cx D S 1000
  ndL-TOPL cx D S 1000
  ndL-TOPL cy D S 1000
  ndL-BTTML cx D S 1000
  ndL-BTTML cy D S 1000
  ndL-TOPE fy S 1
  ndL-SIDEE fx S 1
  nhL-BONDTOP fx S 1
  nhL-BONDTOP fy S 1
  nhL-BONDBTTM fx S 1
  nhL-BONDBTTM fy S 1
  ndL-BTTME fx S 1
  ndL-BTTME fy S 1
}

```

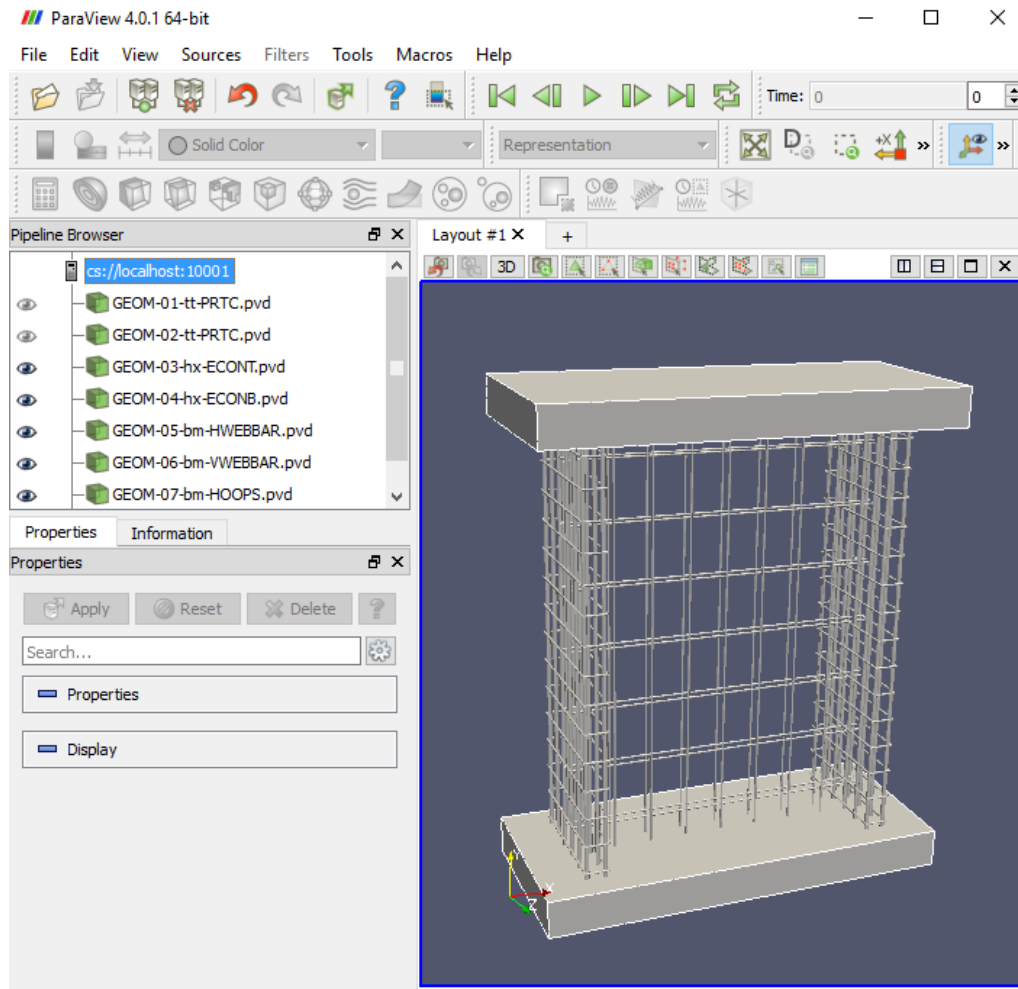


Figure 2.7: Paraview software interface

```

// Energy
ke // kinetic energy, to compare with iw internal work
iw S -1 // internal work, to compare with ke kinetic energy
ew // external work
eb // energy balance, should be =ke+iw
ie // internal energy, defined like elastic energy stored
}
//-----

```

This section results in the generation of files to view the simulation results in Paraview, a freely-available software. Multiple variables and components are possible to be outputted. Generally, the LDPM concrete, crack opening of the LDPM concrete, fibers, elastic concrete blocks, and rebar are included in this process. Variables within these components are generated

to be viewed as necessary, like the stress tensor of the concrete, and axial and shear stresses within the rebar. An example of the Paraview interface for a simulation incorporating rebar is shown in Figure 2.7.

```
//-----
PlotList CRACK Paraview { // opening of the crack
  DeleteAllFiles
  dt 10 ms
  ttl PRTC { }
  //ttl PRTC { Particles }
  //ttl PRTC { Cells }
  //ttl PRTC { Fibers }
  //ttl PRTC { StressTensor }
  ttl PRTC {
    FacetVariable 15
    RangeMinValue 0.0001 mm
    RangeMaxValue 0.03 mm
    DisplayAboveMax
    Scale 1000
  }
  hxL TOPCON { }
  hxL BTMCON { }
}
//-----
```

The final step in the “Run” file is to allow the use of parallel processing in running the simulation. Using parallel processing is critical to obtain reasonable computational time requirements for large simulations. Chapter 18 of the ES3 MARS manual describes the parallelization of MARS in more detail (Pelessone 2015).

```
//-----
// MPI
//-----
MpiDomainList {
  RecursiveBisection ttL-PRTC
}
EOF
//-----
```

2.5.3 “Submission” file: *Nrun.sh*

The “Gen” and “Run” files have been fully defined and describe all necessary parts of the simulation. The “Submission” file is used to create a job on the supercomputing resources to carry out the simulation. *Nodes* refers to the number of nodes on a supercomputer that will be used, and *ppn* indicates the processors per node that will be used. These numbers are varied to match the required computational power needed, depending on the size of the simulation. The maximum values depend on the computational resources accessible by the user. *Walltime* is the limit in real time for which the simulation will run. The syntax used here is compatible with Virginia Tech Advanced Research Computing, and may vary between institutions.

```
//-----  
#!/bin/bash  
#PBS -l nodes=4:ppn=16  
#PBS -l walltime=16:00:00  
#PBS -q normal_q  
#PBS -A UHPC  
#PBS -W group_list=newriver  
  
##PBS -M tdacanay@vt.edu  
##PBS -m bea  
  
export OMP_NUM_THREADS=1  
cd $PBS_O_WORKDIR  
  
marsO -B GenUhpcWall.mrs  
mpirun marsM -B RunUhpcWall.mrs  
  
exit;  
//-----
```

Upon completion of the “Gen”, “Run”, and “Submission” files, the user may choose to directly run the “Gen” and “Run” files via a command line interface with the computing resources. This is called running in *bash mode*. From this process, the user may discern if the components of the simulation have been correctly defined, as a check before submitting a job which may require waiting in a queue before running and the attainment of any results. This is done by

entering `marsO -B GenUhpcWall.mrs` and then `marsO -B RunUhpcWall.mrs` into the command line in this case. The “Run” file runs the actual simulation, so it should only be allowed to run for a short time in bash mode (ceased using `Ctrl+c`), just long enough to ascertain if it is running correctly and to check the geometry and location of components.

After these checks have been completed, the job is ready to be sent to the supercomputer. On the command line, `qsub -o output.txt Nrun.sh` is entered, and the simulation begins to be calculated.

The next chapter discusses the results of the simulations of UHPC shear walls performed via the procedure described above.

CHAPTER 3. Ultra-High Performance Concrete Shear Wall Parameter Study

In this chapter, the results of LDPM shear wall simulations are analyzed to determine the structural benefits of using UHPC in tall buildings. Certain parameters were varied in this study to determine their impact on structural response, including axial stress, the presence of fiber reinforcement, the presence of edge flexural reinforcement, and wall thickness. Two types of cementitious-based composite were chosen for the simulations, both of which have been calibrated and validated for use in MARS. The first type is Cor-Tuf UHPC, which has a compressive strength of $f'_c = 170\text{-}240$ MPa, with an average experimental value (cylinder with fibers) of $f'_c = 193.5$ MPa (Roth et al. 2010). The second type, an HPC mix labeled as “Section 9” in Cusatis et al. (2011), has a compressive strength given as $f'_c = 51.4$ MPa. In this study, the simulated compressive strength of Cor-Tuf UHPC is $f'_c = 231$ MPa, and that of “Section 9” HPC is $f'_c = 51.7$ MPa. Properties of the two concrete types are given in Tables 3.1 through 3.3.

Table 3.1 Cor-Tuf material proportion by weight (Smith et al. 2014)

Material	Proportion by Weight
Cement	1
Sand	0.967
Silica flour	0.277
Silica fume	0.389
Superplasticizer	0.0171
Water (tap)	0.208
Steel fibers (as required)	0.31

Table 3.2 Cor-Tuf material composition (Smith et al. 2014)

Property	Value
Cement content, c (kg/m^3)	794
Measured wet density, ρ (kg/m^3)	2442.5
Water-to-binder ratio, w/b	0.15
Aggregate-to-binder ratio, a/b	1.03

Table 3.3 “Section 9” HPC material composition (Cusatis et al. 2011)

Property	Value
Cement content, c (kg/m ³)	686
Water-to-cement ratio, w/c	0.5
Aggregate-to-cement ratio, a/c	2
Density, ρ (kg/m ³)	2400

The simulated specimen represents a typical shear wall section of a tall building, with an aspect ratio (wall height over wall length) of 1.33 and an initial slenderness ratio (wall height over wall thickness) of 6.67 when thickness $t = 60$ mm. The scale of the shear wall section is approximately one-tenth that of an actual tall building shear wall due to current computing constraints, discussed at a later point in this chapter. Figure 3.1 shows the basic form of the specimen, with the shear wall section, modeled with the LDPM, outlined in black. The top and bottom blocks are outlined in red and blue, respectively, and are modeled as restricted to the elastic regime to reduce computational cost. Dimensions of the simulated shear wall section can be seen in Figure 3.2 and the elastic concrete blocks in Figure 3.3. Note that the wall thickness is denoted by the variable “ t ” as the thickness varies for the specific simulations. Figure 3.4 provides a visualization of the constraint and loading conditions applied to the shear wall sections. The bottom face of the bottom elastic concrete block (blue) is fixed against translation in any direction and rotation about any axis, and is labeled as “ c ” in the figure. All other surfaces are free to move and rotate in any direction. The lateral loading of the specimen is achieved using a set velocity curve applied to the side face of the top elastic concrete block, labeled as “ a ” in Figure 3.4. Lastly, a constant axial load is applied to the specimen during lateral loading to represent realistic conditions in tall building shear walls. This load is distributed evenly across the top surface of the top elastic concrete block, labeled as “ b ” in Figure 3.4.

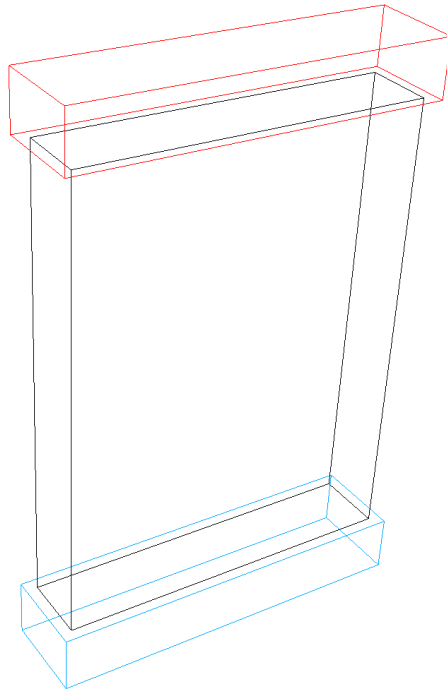


Figure 3.1: Simulated shear wall specimen

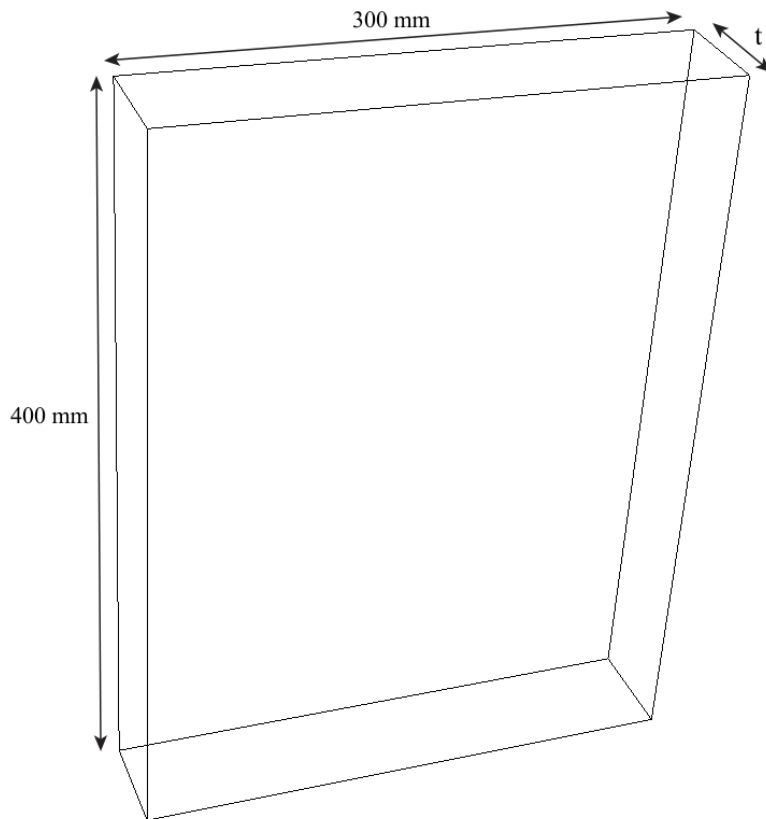


Figure 3.2: LDPM-simulated component dimensions

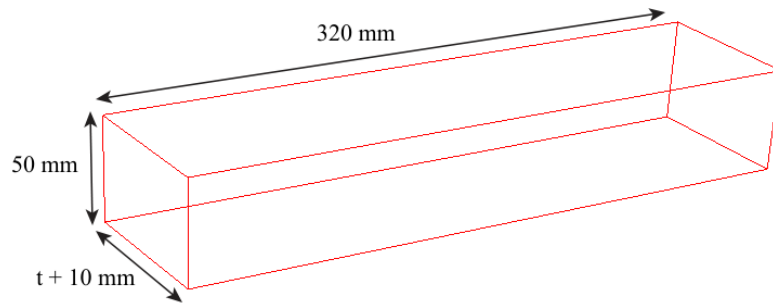


Figure 3.3: Top and bottom elastic concrete block dimensions

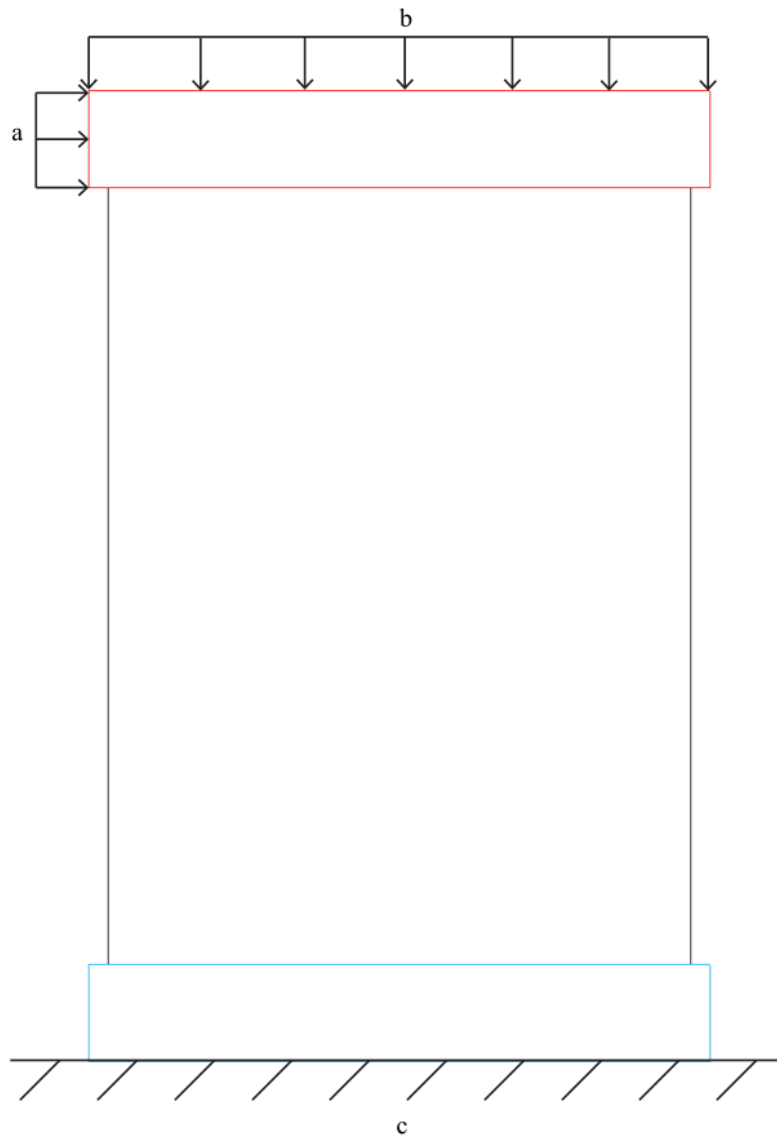


Figure 3.4: Elevation view of the simulated specimen, showing a) the applied location of the velocity curve on the side of the top elastic concrete block; b) the distributed axial load on the top surface of the top elastic concrete block; and c) the fixed displacement and rotation conditions applied to the bottom face of the bottom elastic concrete block

The LDPM parameters for each type of cementitious-based composite used in the simulations are given in Table 3.4. A technique known as *coarse graining* is used to achieve a reasonable computational cost for modeling concrete members using the LDPM. This technique results in larger aggregate sizes while maintaining accurate simulation of material properties and response. More detail regarding the coarse graining process and theory is given by Smith et al. (2014). This process is manifested in the minimum and maximum aggregate sizes of 2 mm and 4 mm, respectively, compared to the actual Cor-Tuf maximum aggregate size of 0.6 mm (Smith et al. 2014). Current software and hardware limitations resulted in the need to coarse grain further, to a minimum and maximum aggregate size of 8 mm and 16 mm, respectively. Simulations were performed to ensure this process minimally affected the results; this information may be viewed in Appendix B. On Virginia Tech's NewRiver system, the current limit for number of particles simulated in this study was determined anecdotally to be approximately 100,000 particles, limited by computational power and required wall time. Hardware specifications of the NewRiver cluster can be obtained via Virginia Tech's Advanced Research Computing (ARC) website. As modeling techniques, software, and hardware improve, full-scale modeling will become more feasible for future studies.

It should be noted that no full-scale validation was performed due to the lack of available shear wall experimental tests with sufficient material characterization data. As will be discussed in the future work section, work furthering this research may include validating the LDPM for simulating actual shear wall behavior.

Table 3.4: LDPM parameters for shear wall simulations

	Parameter	Cor-Tuf (Smith et al. 2014)	Cor-Tuf (further coarse graining)	“Section 9” HPC (Cusatis et al. 2011)
Concrete	E_0 (MPa)	67000	71000	55610
	α	0.484	Unchanged (-)	0.25
	σ_t (MPa)	4	-	4.65
	l_t (mm)	150	100	100
	σ_s/σ_t	17	15.7	2.75
	n_t	0.2	0.25	0.1
	σ_{c0} (MPa)	500	-	150
	H_{c0}/E_0	0.36	-	0.40
	κ_{c0}	2	-	4
	κ_{c1}	2	-	1
	κ_{c2}	1	-	5
	μ_0	0.5	-	0.4
	μ_∞	0	-	0
	σ_{N0} (MPa)	300	-	600
	d_a (mm)	4	16	5
	d_0 (mm)	2	8	2
	c (kg/m ³)	794.4	-	686
	w/c	0.2082	-	0.5
	n_F	0.5	-	0.5
Fibers	G_d (N/m)	0	-	No fibers (*)
	τ_0 (MPa)	11.5	-	*
	k_{sp}	150	-	*
	k_{sn}	0.05	-	*
	σ_{uf} (MPa)	1200	-	*
	k_{rup}	0.4	-	*
	E_f (GPa)	210	-	*
	γ_p	0.5	-	*
Fiber length (mm)	30	-	*	
Volume fraction	0.02	-	*	
Fiber area (mm ²)	0.785	-	*	

Figures detailing the simulation results are presented as base shear versus drift ratio. Given the dimensions shown in Figure 3.2, 1% drift ratio corresponds to a lateral displacement of 4 mm at the top of the shear wall section.

3.1 Varied Axial Stress

The compressive axial stress on the simulated shear wall specimens was varied to capture the resulting effects on the response. These specimens have a thickness of 60 mm, slenderness ratio of 6.67, contain 2% fiber reinforcement by volume, and use Cor-Tuf LDPM parameters with additional coarse graining (aggregate size from 8 to 16 mm). The stresses tested were 20, 25, 30, 40, 50, 75, 100, 125, and 150 MPa, and remain constant throughout each simulation. The base shear-drift ratio curves for each axial stress value tested are shown in Figure 3.5. There are two failure modes evident in these simulations; one is a horizontal crack opening at the bottom of the wall due to the flexural effects which result from the overturning moment. This is seen in Figure 3.6, which shows the progression of the simulation of the 20 MPa axial stress specimen. The second failure mode is diagonal cracking from the top corner of the wall section, where the lateral loading regimen is applied, to the bottom opposite corner. This is seen in Figure 3.7, which shows the progression of the simulation of the 100 MPa axial stress specimen. This cracking may be attributed to tensile splitting effects with the development of the compression strut, or a combination of these effects and compressive cracking at the bottom opposite corner.

At lower levels of axial stress, the dominant failure mode is the opening of the flexural crack at the bottom of the wall. Simulations meeting this statement include those with 20, 25, and 30 MPa axial stress. At higher levels of axial stress, the dominant failure mode is the opening of the diagonal crack. Simulations meeting this statement include those with 100, 125, and 150 MPa axial stress. In all specimens, the flexural crack at the bottom of the wall is present.

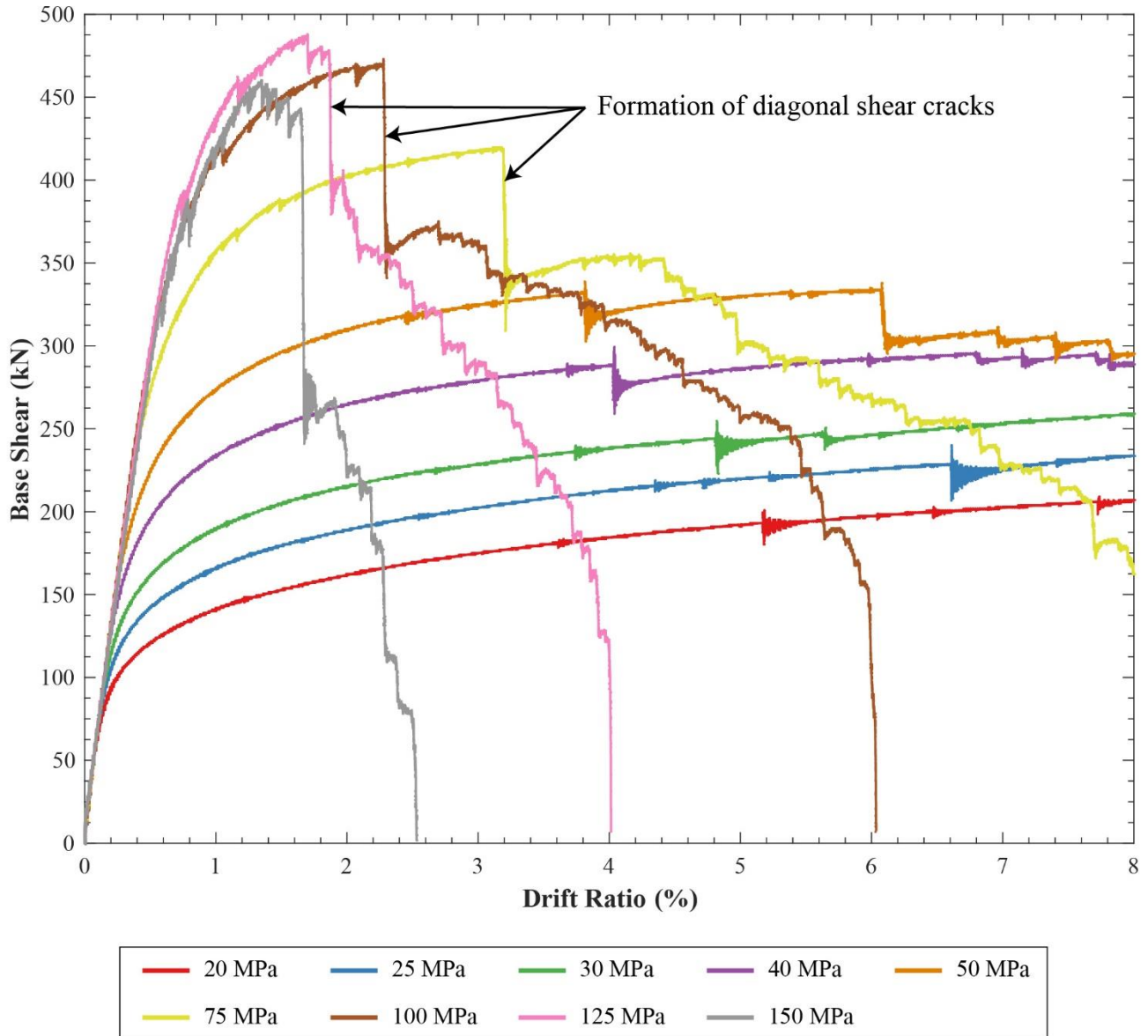


Figure 3.5: Base shear vs. drift ratio for Cor-Tuf UHPC with $t = 60$ mm, with different applied axial stresses

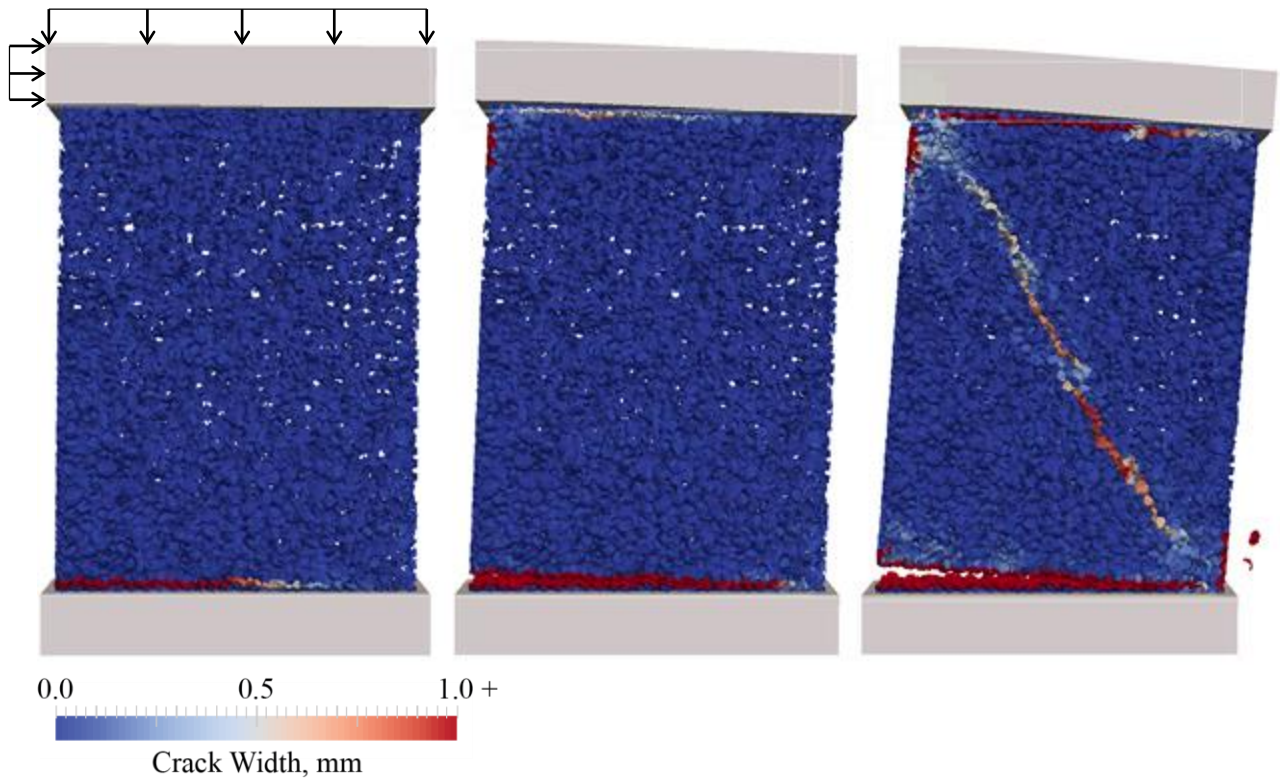


Figure 3.6: Crack widths at 1.2%, 4.4%, and 8.0% drift for Cor-Tuf UHPC specimen with $t = 60$ mm and 20 MPa axial stress

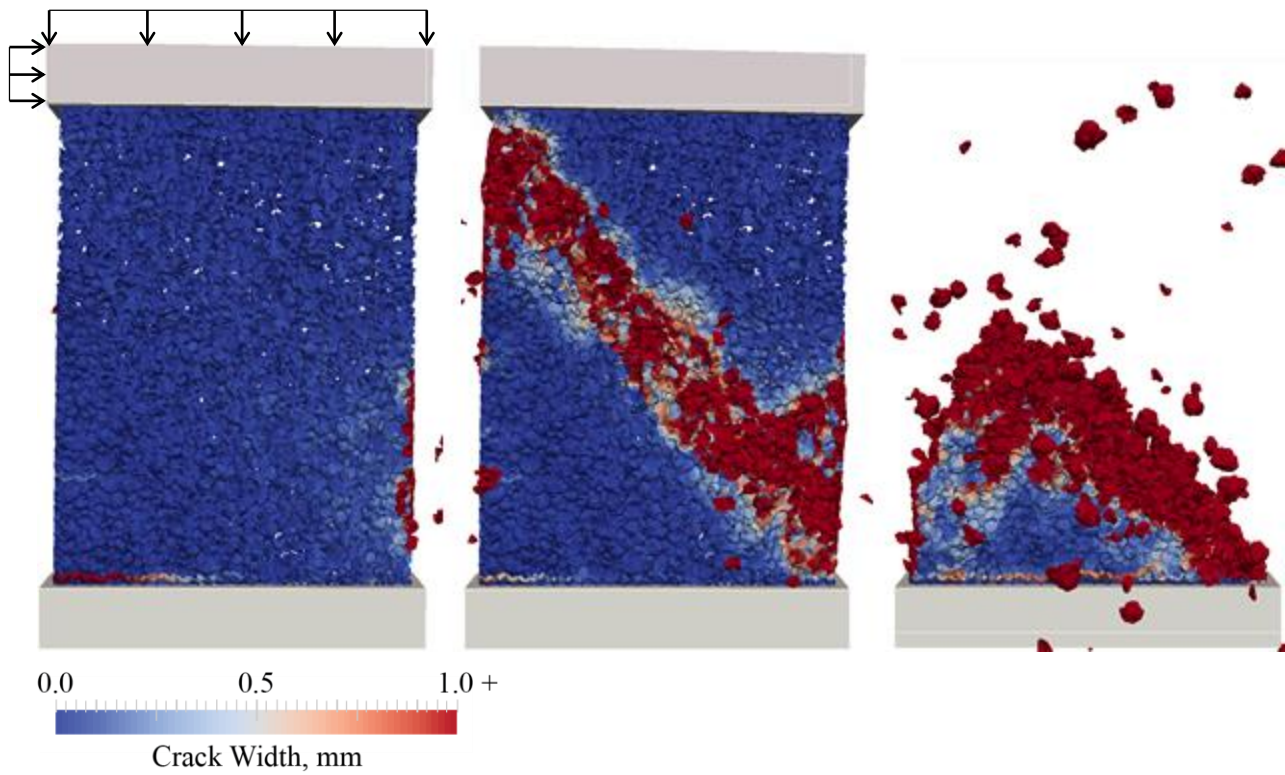


Figure 3.7: Crack widths at 1.2% drift, 4.4% drift, and post-failure for Cor-Tuf UHPC specimen with $t = 60$ mm and 100 MPa axial stress

3.2 Edge Vertical Reinforcing Bars

Vertical steel bar reinforcement was added at the edges of the shear wall section to control the crack opening at the bottom of the wall, visible in Figure 3.6, and to allow the specimens to reach the diagonal shear cracking failure mode. Six reinforcing bars on each side were used, each with a diameter of 12.5 mm, as shown in Figure 3.8 and Figure 3.9, and have a perfect bond to the concrete – no bond-slip law is applied in this research. The required MARS parameters for the simulated rebar include the following: density of 7800 kg/m³, Young's modulus of 200 GPa, Poisson's ratio of 0.3, yield strength of 345 MPa, and hardening modulus of 3600 MPa. The reinforcing bars were sized empirically, as they are simply meant to control the flexural crack opening at the bottom of the wall and have minimal effect on the response related to the opening of the diagonal crack. This statement was examined by simulating a wall with larger rebar (diameter of 15 mm) and ensuring minimal differences in response; the results of this simulation are shown in Appendix C.

The wall specimens tested in this section again have a thickness of 60 mm and corresponding slenderness ratio of 6.67, contain 2% fiber reinforcement by volume, and use Cor-Tuf LDPM parameters with additional coarse graining (aggregate size from 8 to 16 mm). Three different values of axial stress were used: 20, 50, and 100 MPa. Curves showing base shear versus drift ratio for this section are given in Figure 3.10. Figure 3.11 shows the progression of the simulation of the 20 MPa axial stress specimen; Figure 3.12 shows that of the 100 MPa axial stress specimen.

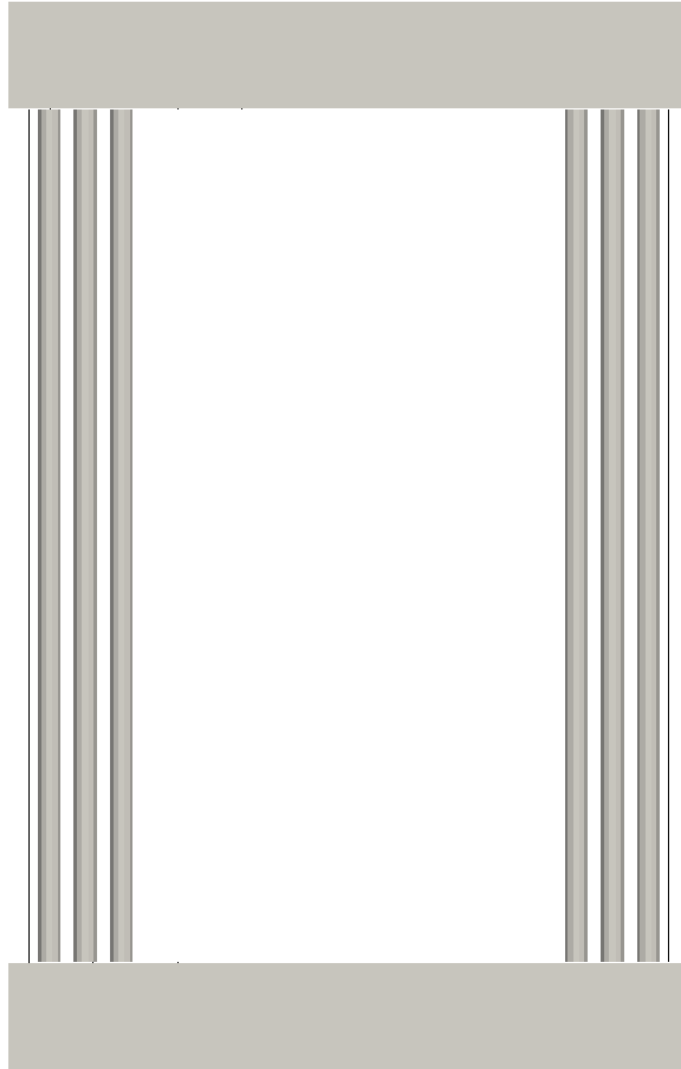


Figure 3.8: Elevation view of wall specimen with 12.5 mm diameter steel reinforcing bars



Figure 3.9: Cross-sectional view of shear wall, showing the layout of the 12.5 mm diameter steel reinforcing bars

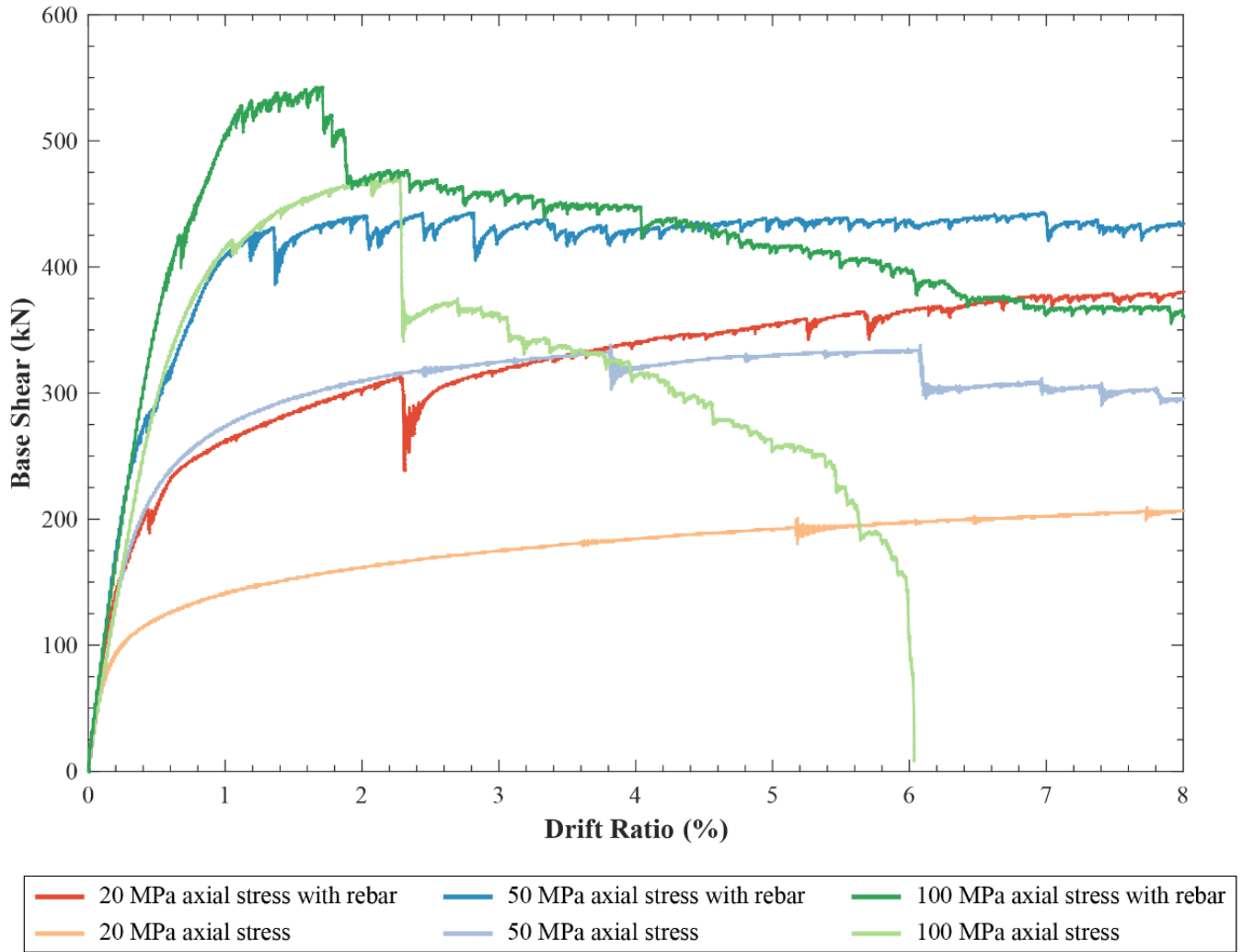


Figure 3.10: Base shear vs. drift ratio for Cor-Tuf UHPC with $t = 60$ mm, with and without rebar at wall edges

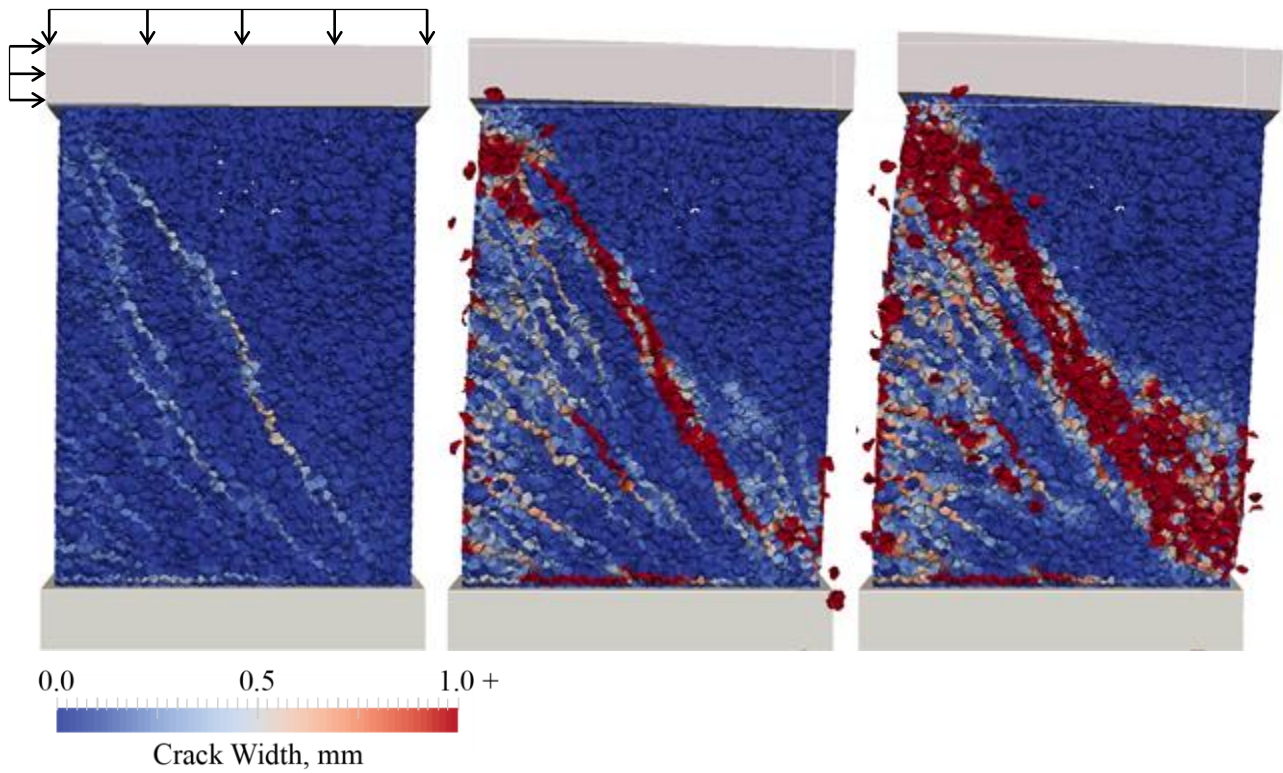


Figure 3.11: Crack widths at 1.2%, 4.4%, and 8.0% drift for Cor-Tuf UHPC specimen with $t = 60$ mm, vertical reinforcing bars at the wall edges and 20 MPa axial stress

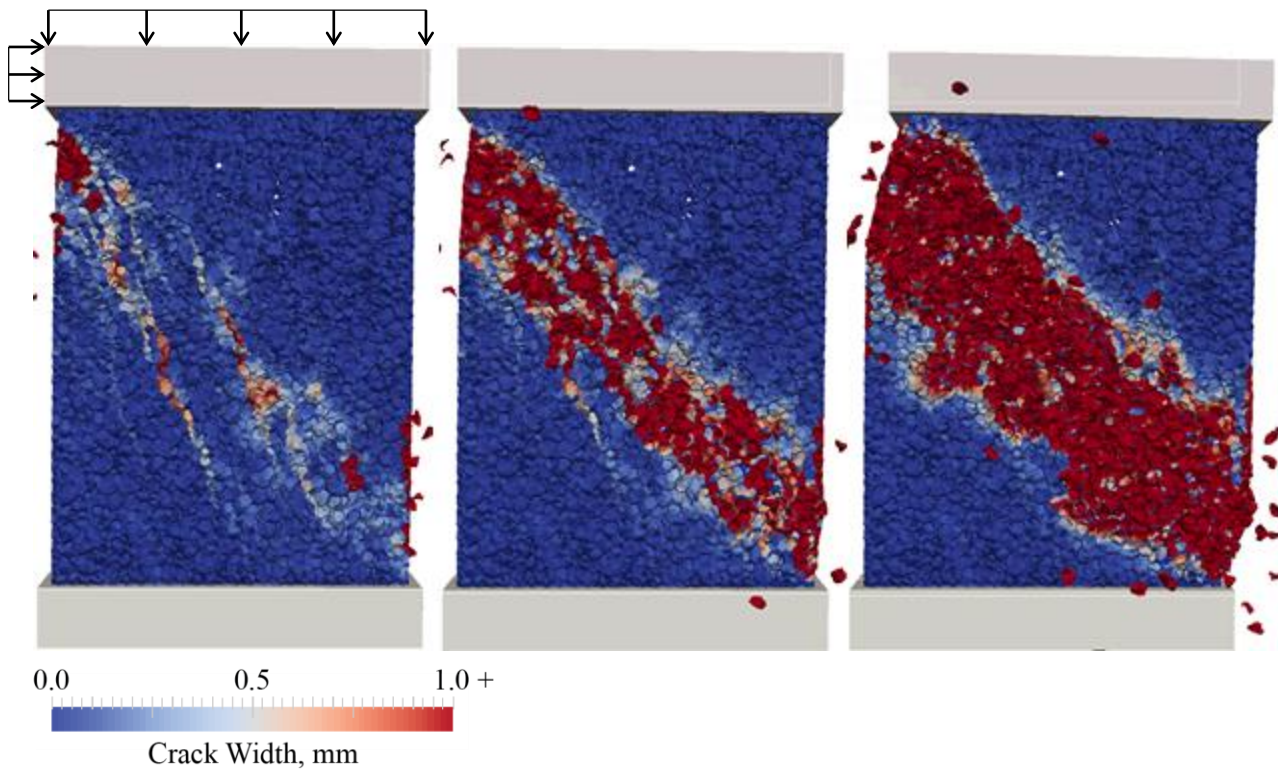


Figure 3.12: Crack widths at 1.2%, 4.4%, and 8.0% drift for Cor-Tuf UHPC specimen with $t = 60$ mm, vertical reinforcing bars at the wall edges, and 100 MPa axial stress

3.3 Fiber Reinforcement

Next, the effect of the inclusion of micro steel fiber reinforcement was determined. The properties of the fiber reinforcement may be seen in Table 3.4. The wall specimens tested in this section have a thickness of 60 mm and corresponding slenderness ratio of 6.67, have the same reinforcing bar diameter and layout as in the previous section, and use Cor-Tuf LDPM parameters with additional coarse graining (aggregate size from 8 to 16 mm). Three different values of axial stress were used: 20, 50, and 100 MPa. Curves showing base shear versus drift ratio for this section are given in Figure 3.13. Figure 3.14 shows the progression of the simulation of the 50 MPa axial stress specimen without fiber reinforcement; Figure 3.15 shows that of the 50 MPa axial stress specimen with fiber reinforcement. The distributed fibers within the concrete matrix may be viewed in Figure 2.5.

As expected, the inclusion of fiber reinforcement has no effect on the uncracked stiffness of the shear wall section, but improves the post cracking capacity. The dissipated energy for each case to 2% drift (8 mm), and the percentage increase in dissipated energy due to the addition of fibers is given in Table 3.5. Energy dissipation is found by calculating the area under the base shear-lateral displacement curve. It is hypothesized that energy dissipation increases with increasing axial loads because the principal stress planes become more inclined. With this increased inclination, the cracks that form are more diagonal as opposed to horizontal and thus have greater length, increasing energy dissipation from crack propagation. In this study, the effect of fiber reinforcement is likely to be underrepresented because the effects of confinement are not yet included in the simulations. Confining pressures increase the work during fiber pullout, which occurs during crack opening.

Table 3.5: Energy dissipation with and without fiber reinforcement from 0 to 2% drift

Axial Stress (MPa)	% Fibers by Volume	Energy dissipated (kN-mm or MJ)	Percentage increase in dissipated energy with fibers
20	0%	1.71	9.5%
	2%	1.87	
50	0%	2.47	12.9%
	2%	2.78	
100	0%	2.79	19.8%
	2%	3.34	

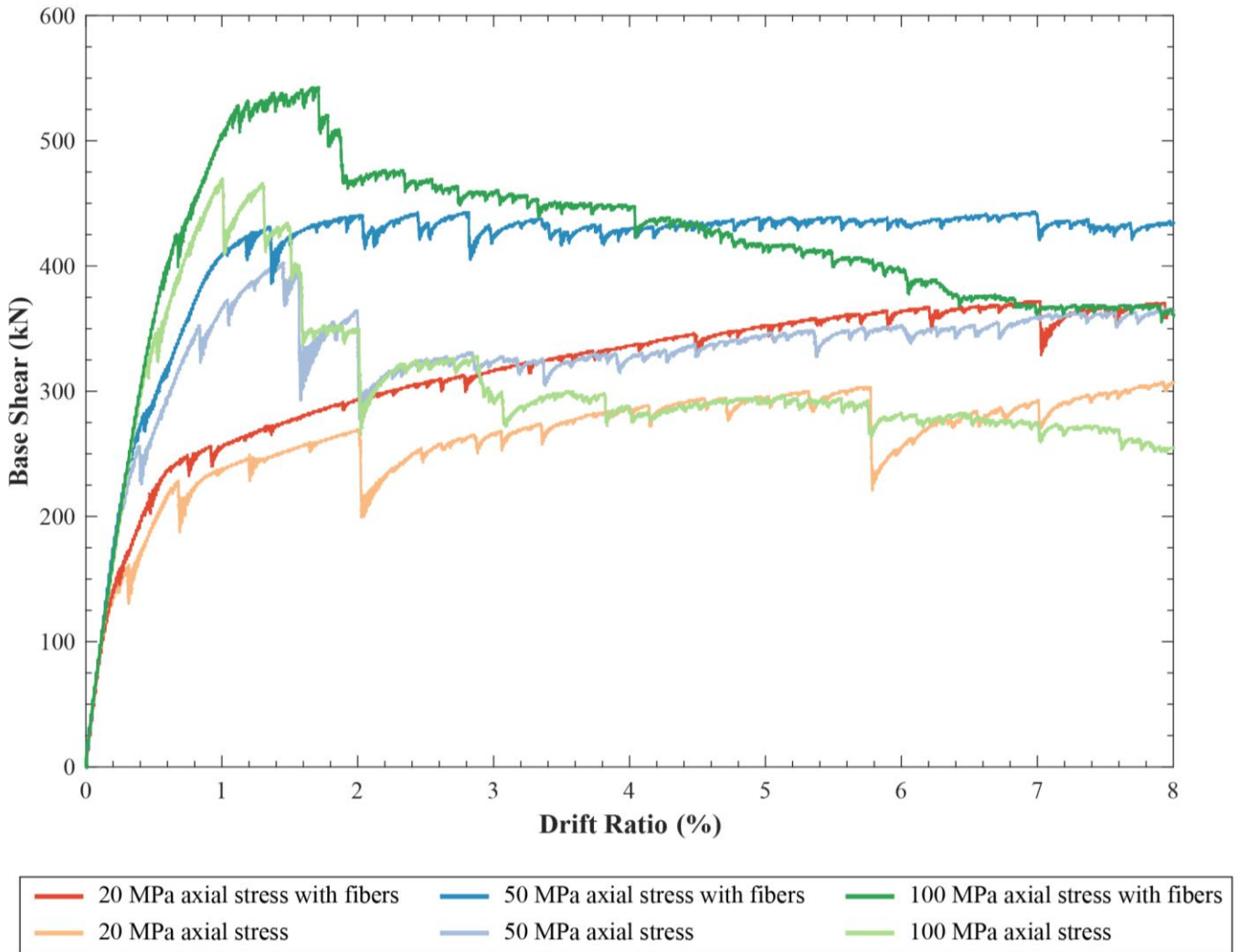


Figure 3.13: Base shear vs. drift ratio for Cor-Tuf UHPC with $t = 60$ mm, with and without fibers

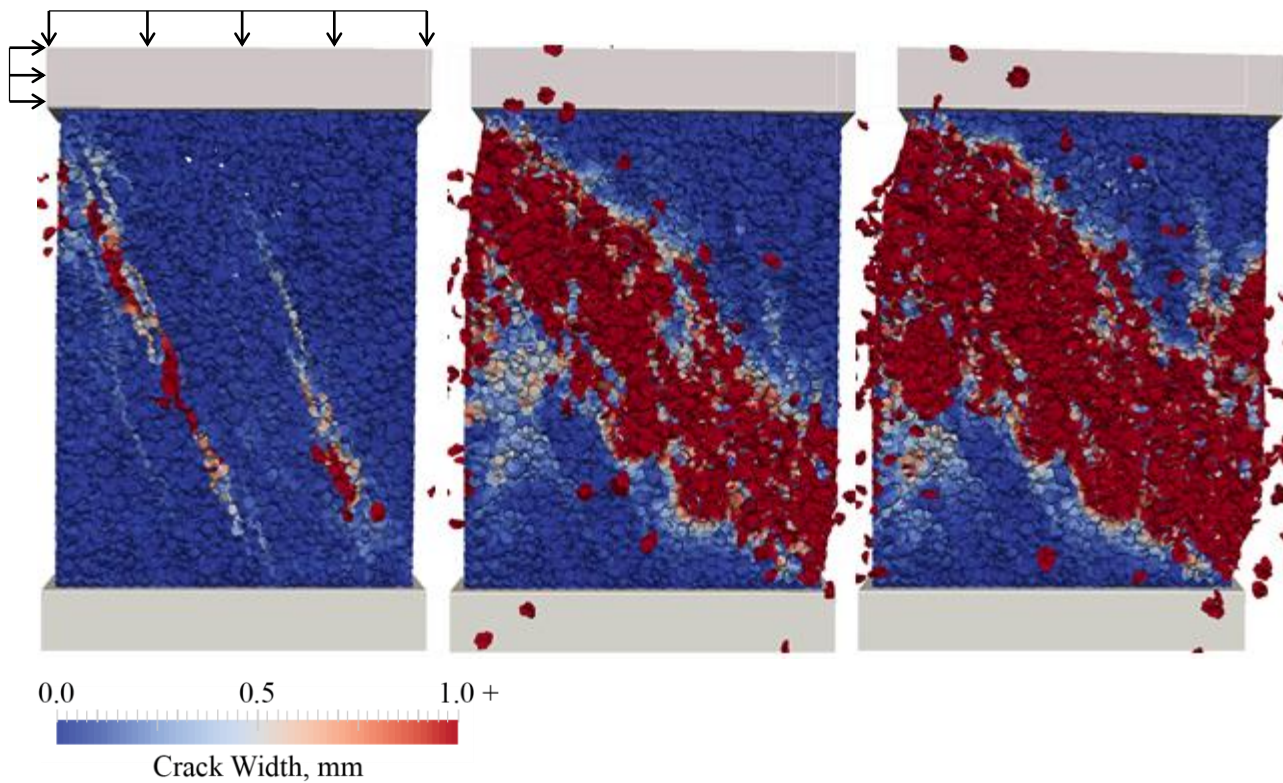


Figure 3.14: Crack widths at 1.2%, 4.4%, and 8.0% drift for Cor-Tuf UHPC specimen with $t = 60$ mm, without fiber reinforcement, and with 50 MPa axial stress

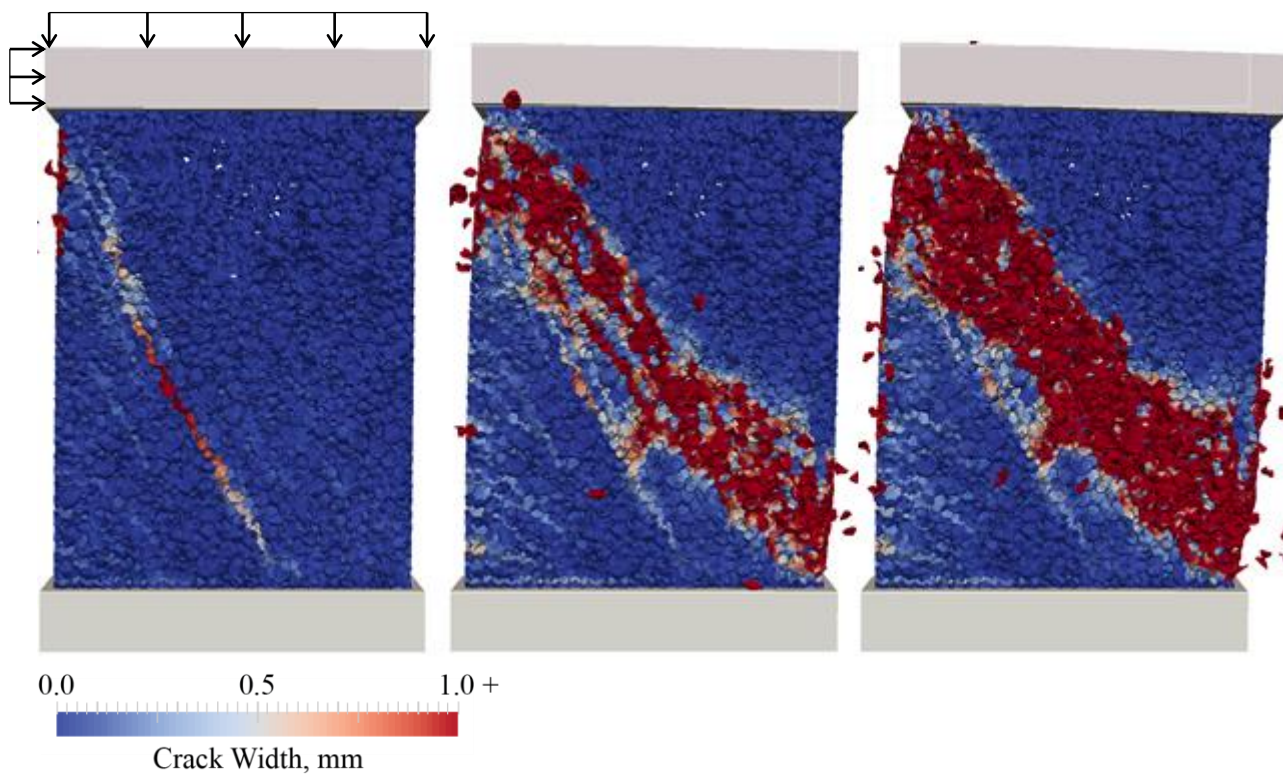


Figure 3.15: Crack widths at 1.2%, 4.4%, and 8.0% drift for Cor-Tuf UHPC specimen with $t = 60$ mm, fiber reinforcement, and 50 MPa axial stress

3.4 Comparison of the Shear Response of Cement-Based Composites

The structural response in shear of Cor-Tuf UHPC ($f'_c = 231$ MPa) was compared to that of “Section 9” HPC ($f'_c = 51.7$ MPa), with all parameters equal aside from those associated with the materials. The wall specimens tested in this section have a thickness of 60 mm and corresponding slenderness ratio of 6.67, have the same reinforcing bar diameter and layout as detailed in section 3.2, and the Cor-Tuf wall uses LDPM parameters with additional coarse graining (aggregate size from 8 to 16 mm). Two different values of axial stress were used: 11 and 20 MPa, and results for Cor-Tuf with and without fiber reinforcement were generated. Curves showing base shear versus drift ratio for “Section 9” HPC at each axial stress value are shown in Figure 3.16; for HPC and UHPC at 11 MPa axial stress in Figure 3.17; and for HPC and UHPC at 20 MPa axial stress in Figure 3.18. Figure 3.19 shows the progression of the simulation of the HPC 11 MPa axial stress specimen; Figure 3.20 shows that of the UHPC 11 MPa axial stress specimen without fiber reinforcement; and Figure 3.21 shows that of the UHPC 11 MPa axial stress specimen with fiber reinforcement.

The uncracked stiffness of the HPC shear wall section is calculated to be 146.0 kN/mm, while that of the UHPC shear wall section is calculated to be 214.4 kN/mm. The UHPC shear wall section, therefore, has an uncracked stiffness 147% of the HPC shear wall section.

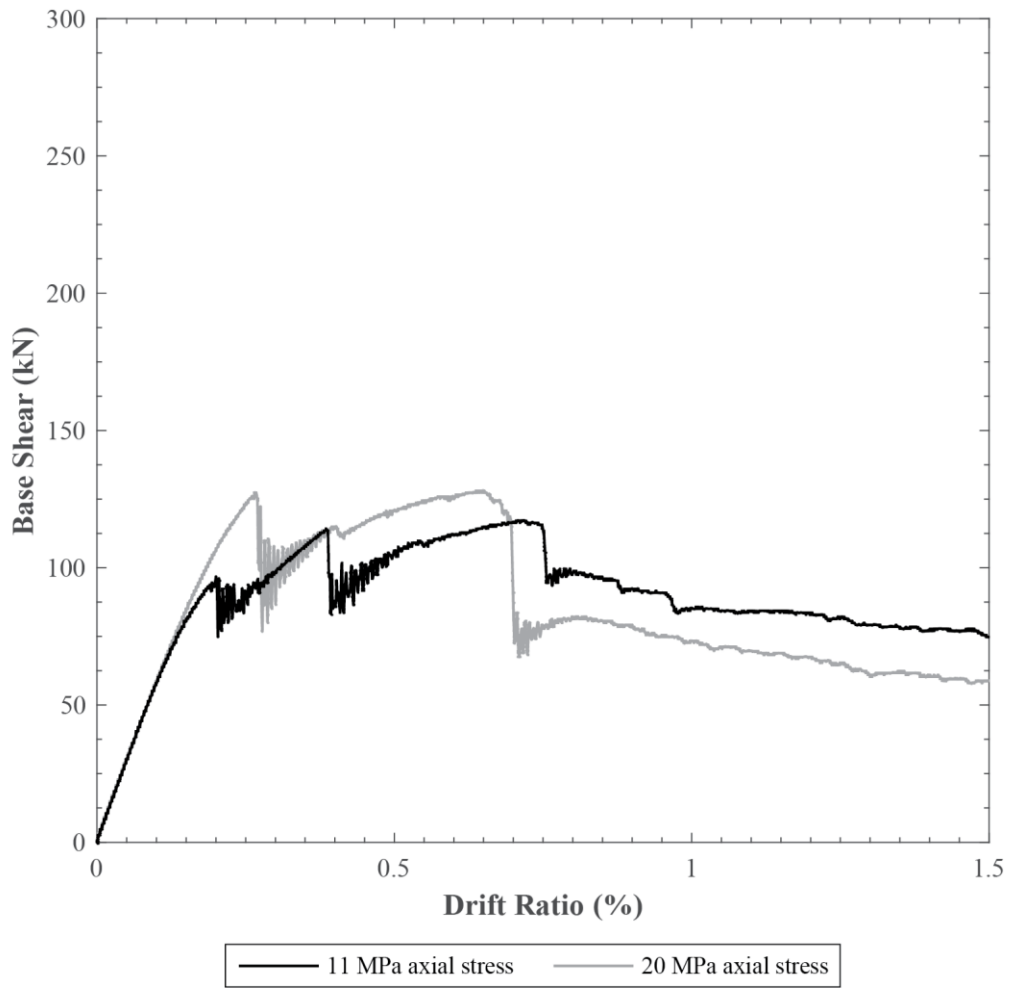


Figure 3.16: Base shear vs. drift ratio for “Section 9” HPC with $t = 60$ mm

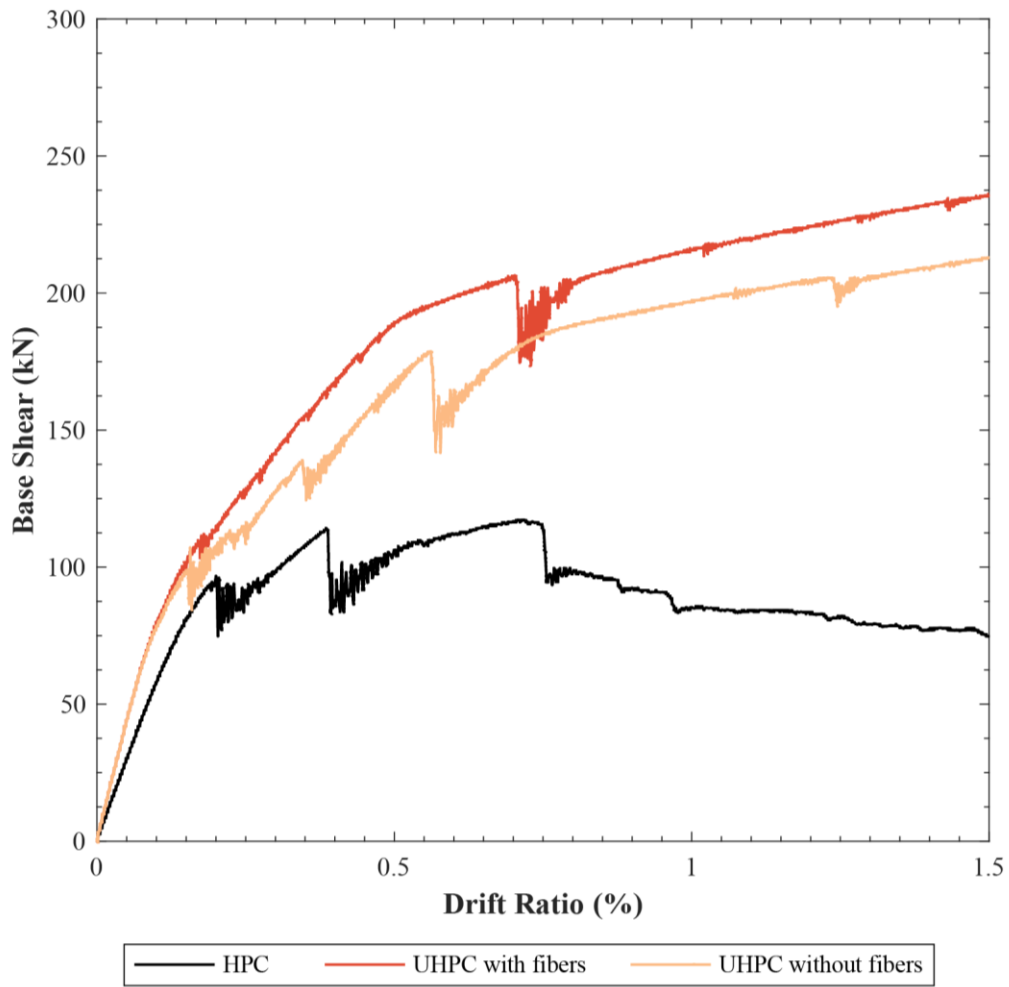


Figure 3.17: Base shear vs. drift ratio for “Section 9” HPC and Cor-Tuf UHPC with $t = 60$ mm and 11 MPa axial stress

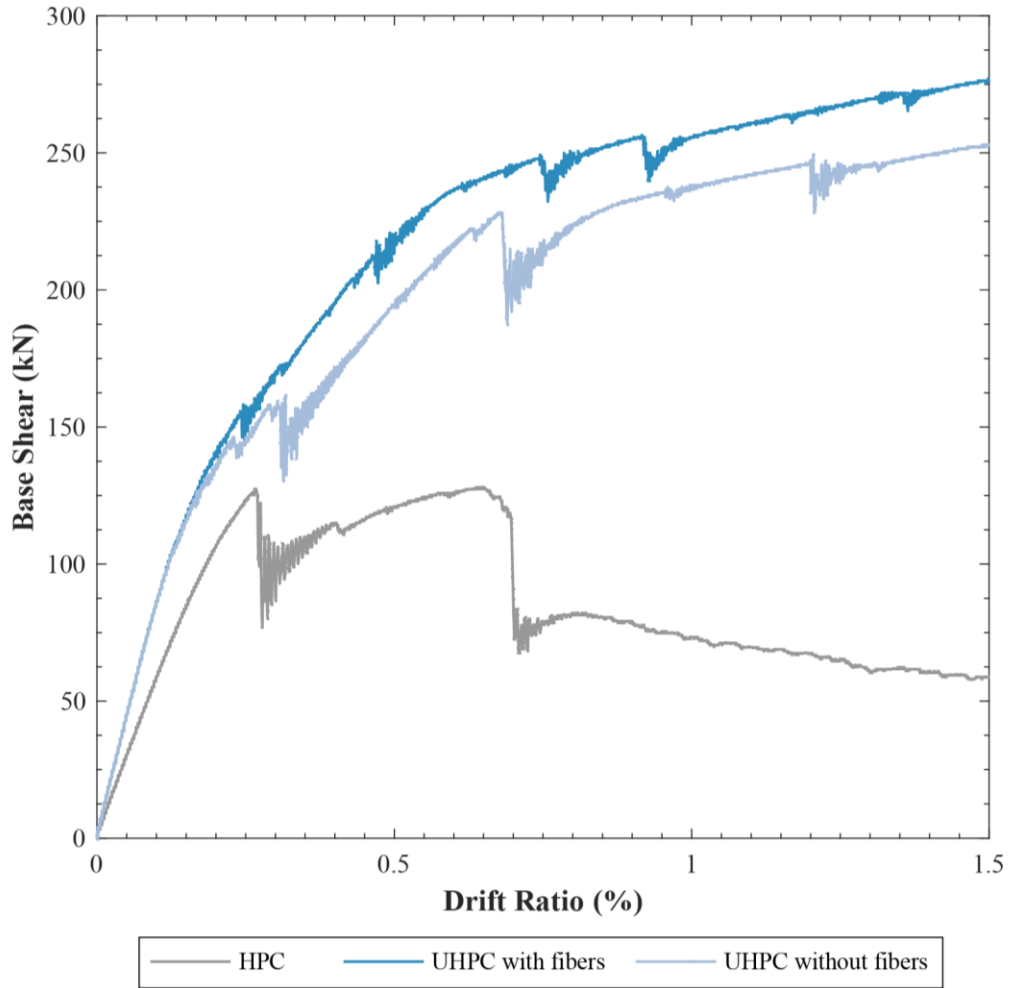


Figure 3.18: Base shear vs. drift ratio for “Section 9” HPC and Cor-Tuf UHPC with $t = 60$ mm and 20 MPa axial stress

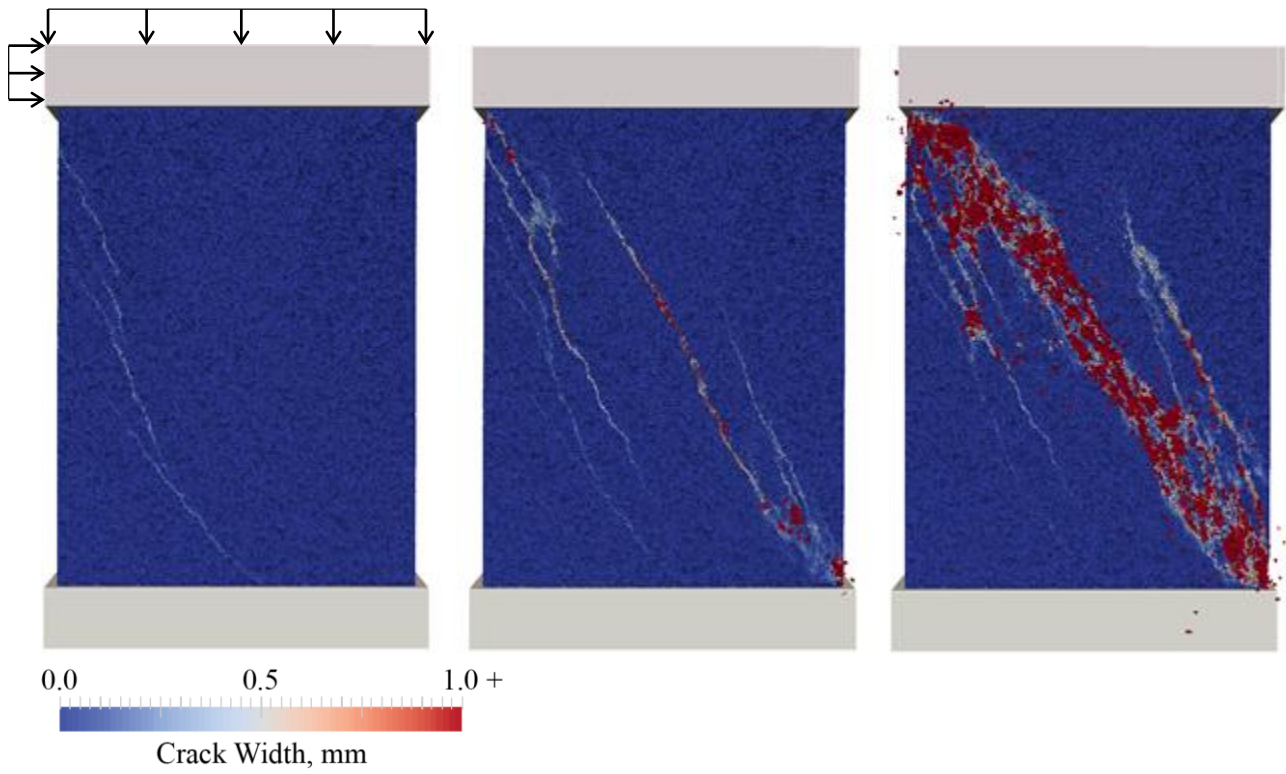


Figure 3.19: Crack widths at 0.4%, 0.8%, and 1.5% drift for “Section 9” HPC specimen with 11 MPa axial stress

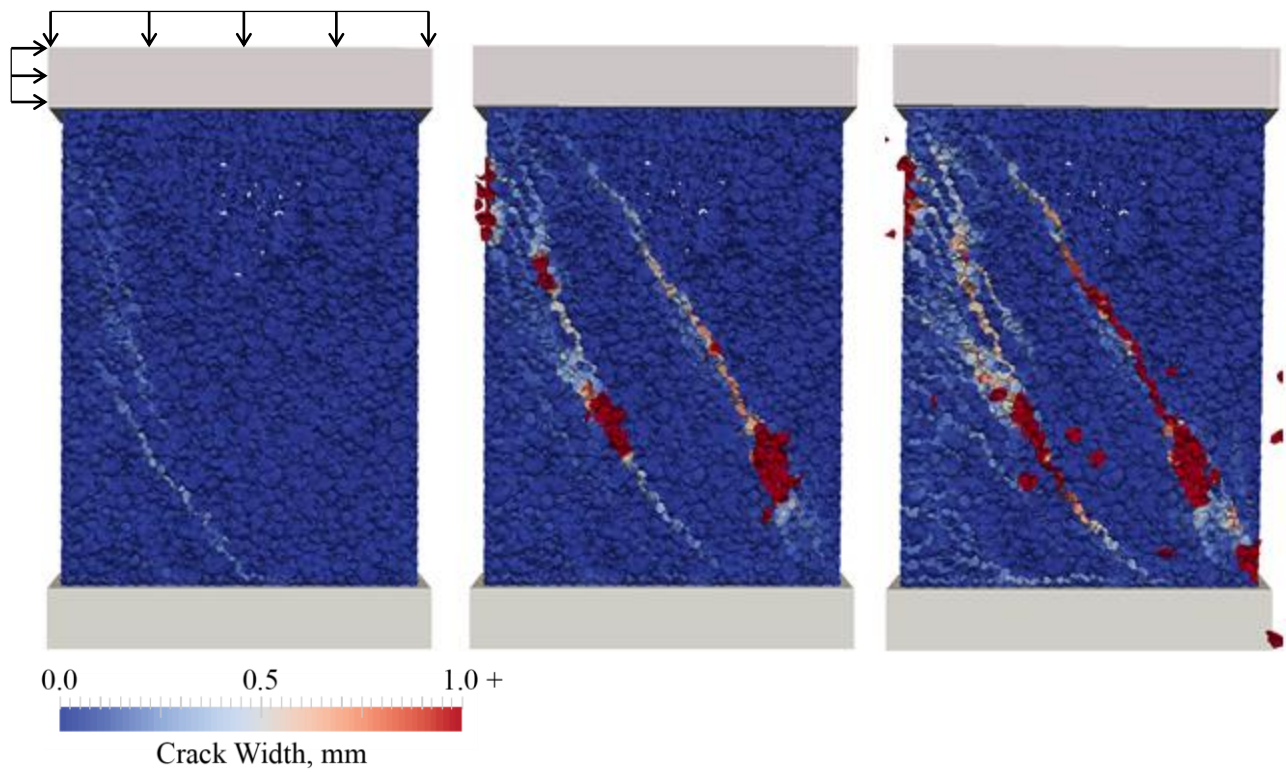


Figure 3.20: Crack widths at 0.4%, 0.8%, and 1.5% drift for Cor-Tuf UHPC specimen with 11 MPa axial stress and without fiber reinforcement

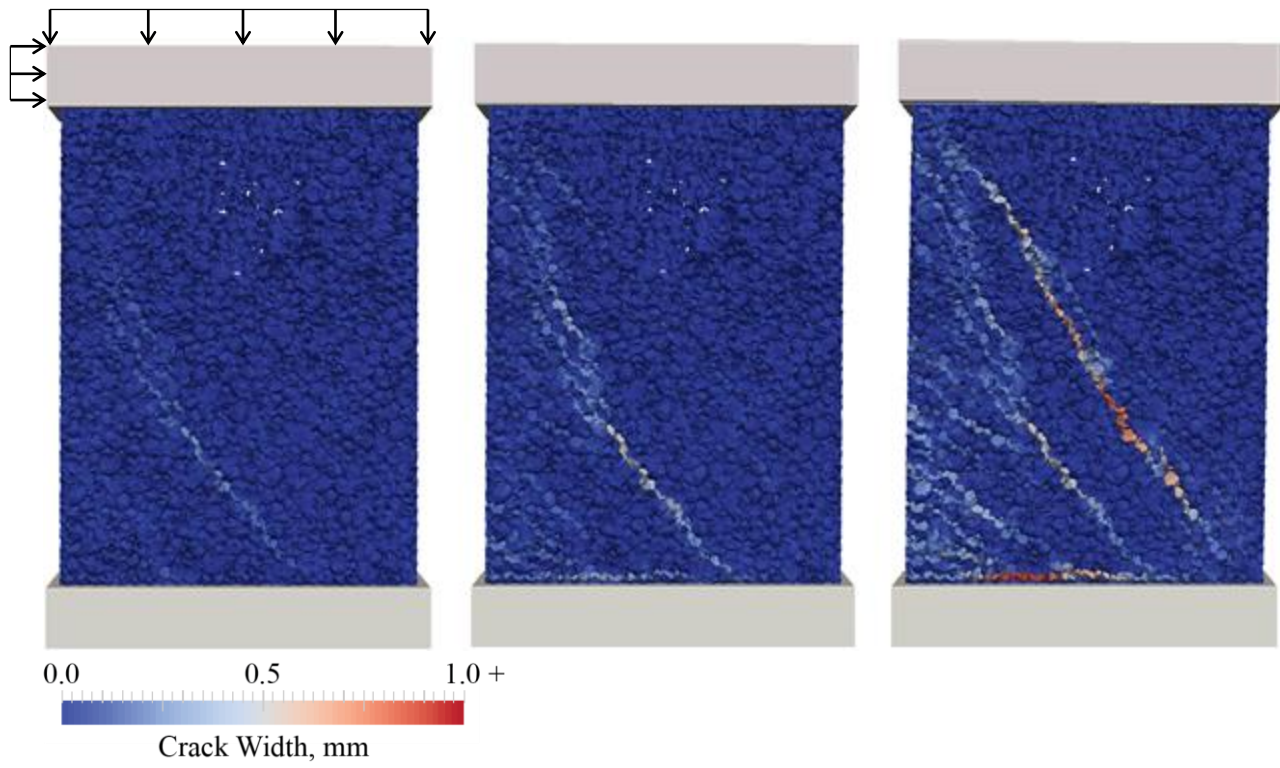


Figure 3.21: Crack widths at 0.4%, 0.8%, and 1.5% drift for Cor-Tuf UHPC specimen with 11 MPa axial stress and with fiber reinforcement

3.5 UHPC Shear Wall Thickness Study Without Transverse Reinforcement

The thickness of the Cor-Tuf UHPC ($f'_c = 231$ MPa) shear wall was decreased to the value at which the structural response in shear was equal or superior to that of the “Section 9” HPC ($f'_c = 51.7$ MPa) specimen with unchanged thickness. The wall specimens tested in this section have the same reinforcing bar diameter and layout as detailed in section 3.2, with transverse location adjusted for specimens with decreased thickness, and the Cor-Tuf wall uses LDPM parameters from Smith et al. (2014) (aggregate size from 2 to 4 mm). The specimens do not have transverse reinforcement and thus, these simulations do not represent the behavior of an actual shear wall specimen with realistic reinforcing layout and reinforcing ratio. The results described here are meant to describe the response of wall sections made of concrete and containing no steel bar reinforcement.

Iterations of UHPC shear wall thicknesses were performed, culminating in the determination of equal uncracked stiffness (146.0 kN/mm, found in the previous section) and superior post-cracking response at a thickness of $t = 35$ mm and corresponding slenderness ratio of 11.4, or 58% of the HPC shear wall thickness and a 71% increase in slenderness ratio. Considering the unit weights given in Tables 3.2 and 3.3 of 2442.5 kg/m³ for UHPC and 2400 kg/m³ for HPC, the weight of the UHPC shear wall is 59% of the HPC shear wall weight. Because in this study thickness was the independent variable, different values of axial load were used to allow direct comparison of the wall response.

Figure 3.22 shows the results of UHPC wall simulations compared to HPC with a 198 kN axial load and thickness $t = 60$ mm, corresponding to an axial stress of 11 MPa. UHPC shear wall response at thickness $t = 35$ mm with and without fiber reinforcement is shown for axial loads of 198, 360, and 900 kN in the figure.

Figure 3.23 shows the results of UHPC wall simulations compared to HPC with a 360 kN axial load and thickness $t = 60$ mm, corresponding to an axial stress of 20 MPa. UHPC shear wall response at thickness $t = 35$ mm with and without fiber reinforcement is shown for axial loads of 360 and 900 kN in the figure.

Figure 3.24 shows the progression of the simulation of the HPC 198 kN axial load specimen; Figure 3.25 shows that of the UHPC 198 kN axial load specimen without fiber reinforcement; and Figure 3.26 shows that of the UHPC 198 kN axial load specimen with fiber reinforcement.

Figure 3.27 shows the progression of the simulation of the HPC 360 kN axial load specimen; Figure 3.28 shows that of the UHPC 360 kN axial load specimen without fiber reinforcement; and Figure 3.29 shows that of the UHPC 360 kN axial load specimen with fiber reinforcement.

The dissipated energy for each case to 1% drift (4 mm), and the percentage increase in dissipated energy of the UHPC specimens with and without fiber reinforcement compared to that of the HPC specimens at equal axial load is given in Table 3.6. As in Table 3.5, energy dissipation is found by calculating the area under the base shear-lateral displacement curve.

Table 3.6: Energy dissipation of HPC, $t = 60$ mm and UHPC, $t = 35$ mm from 0 to 1% drift

Axial Load (kN)	Wall Specimen	Energy dissipated (N-mm or kJ)	Percentage increase in dissipated energy compared to HPC
198	HPC, $t = 60$ mm	345	-
	UHPC, 0% fibers, $t = 35$ mm	468	35.7%
	UHPC, 2% fibers, $t = 35$ mm	526	52.6%
360	HPC, $t = 60$ mm	353	-
	UHPC, 0% fibers, $t = 35$ mm	542	53.4%
	UHPC, 2% fibers, $t = 35$ mm	599	69.4%

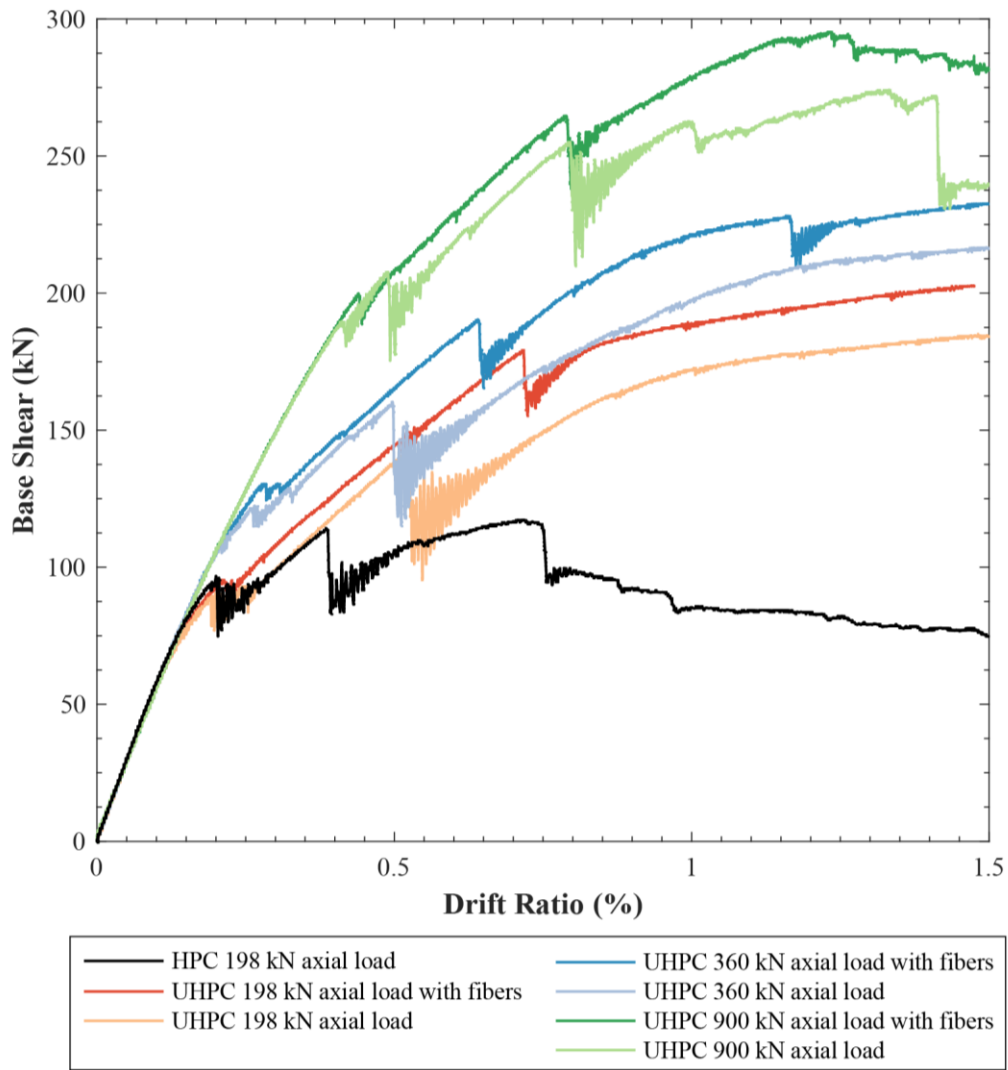


Figure 3.22: Base shear vs. drift ratio for “Section 9” HPC with $t = 60$ mm and 198 kN axial load, and Cor-Tuf UHPC with $t = 35$ mm

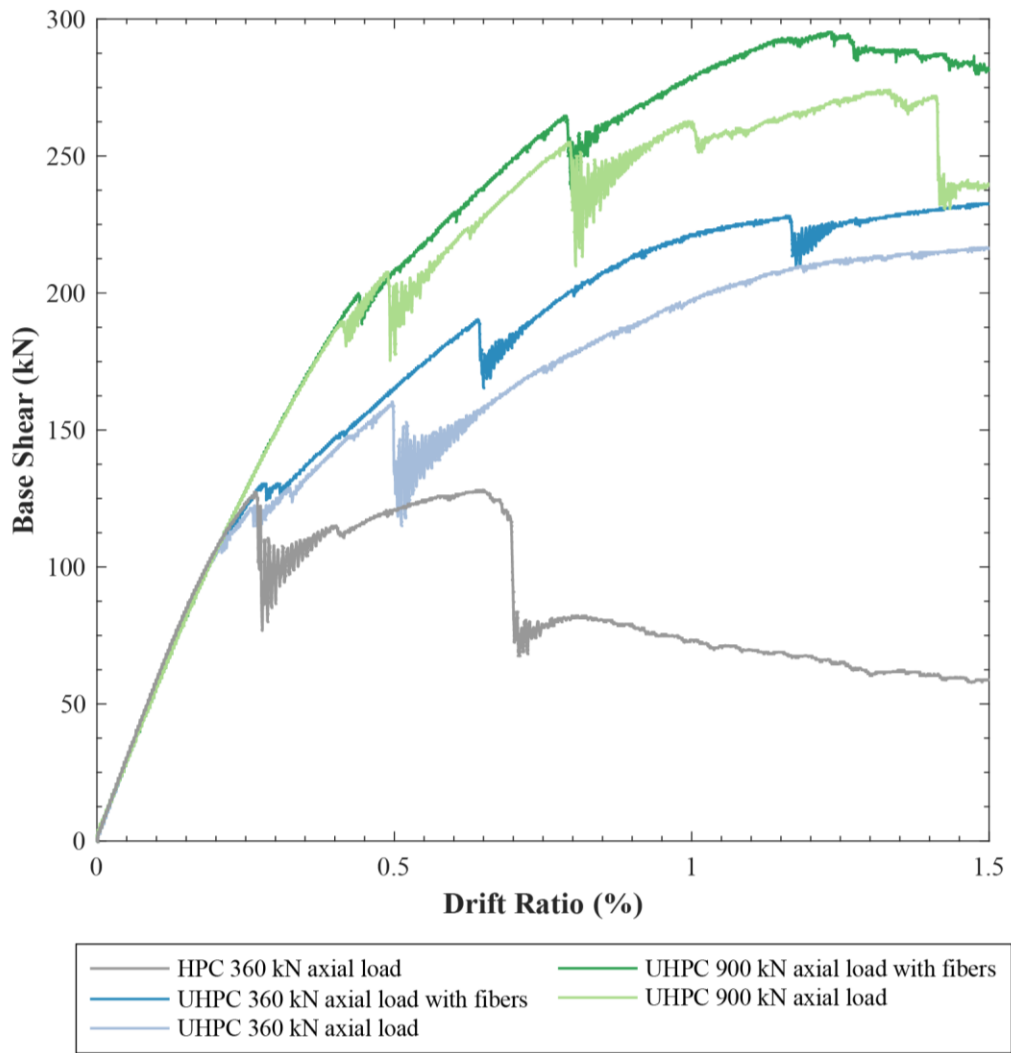


Figure 3.23: Base shear vs. drift ratio for “Section 9” HPC with $t = 60$ mm and 360 kN axial load, and Cor-Tuf UHPC with $t = 35$ mm

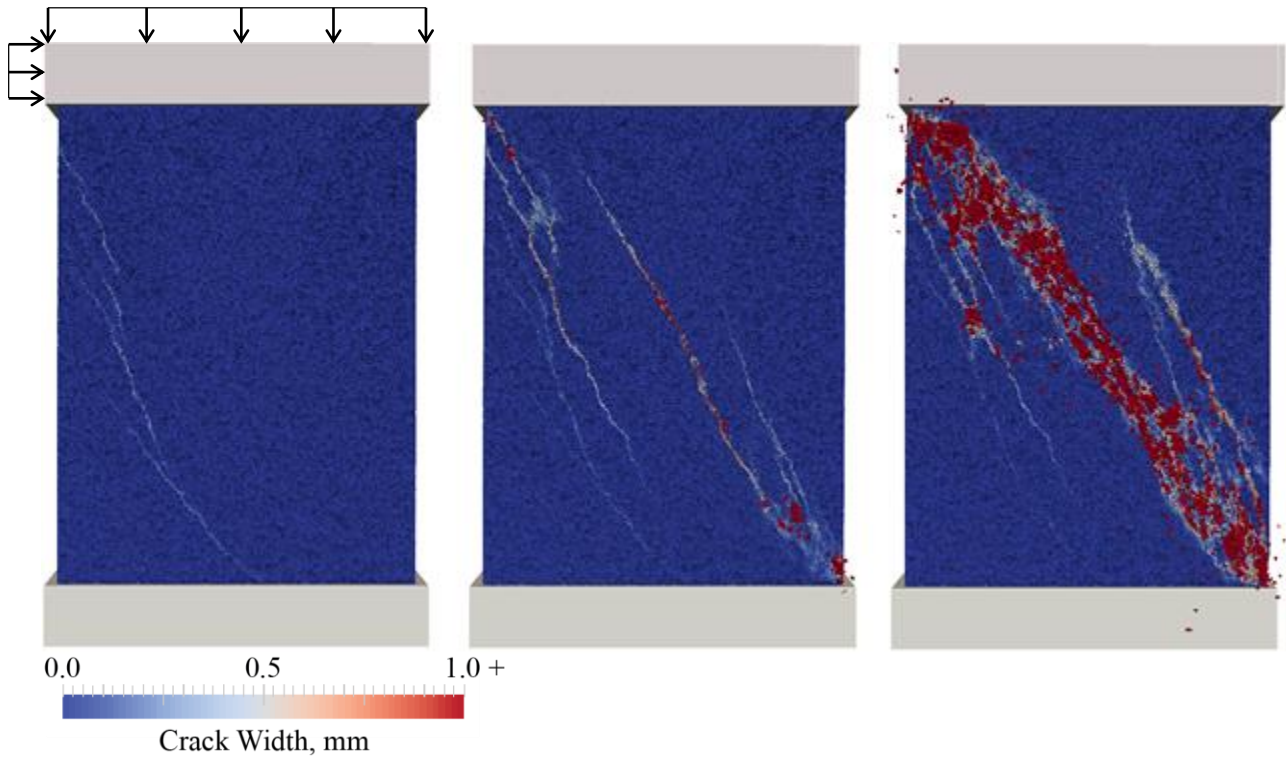


Figure 3.24: Crack widths at 0.4%, 0.8%, and 1.5% drift for “Section 9” HPC specimen with $t = 60$ mm and 198 kN axial load

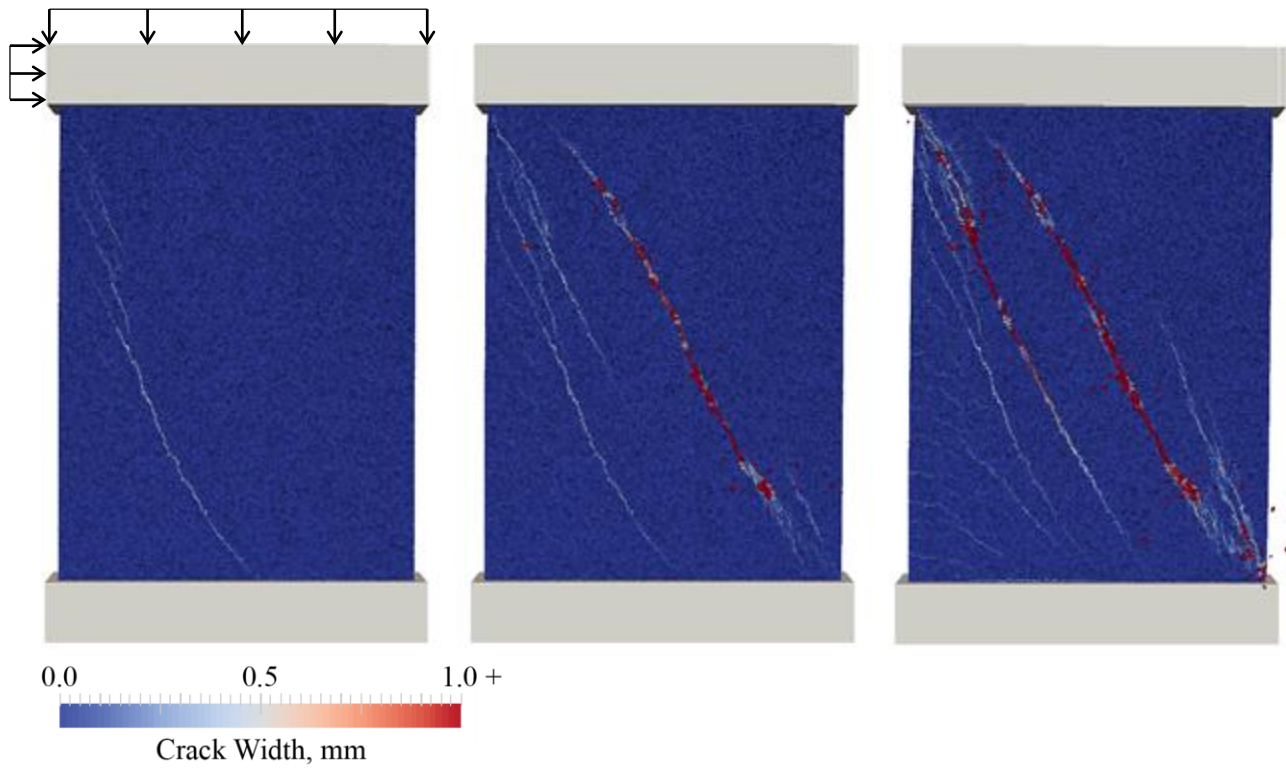


Figure 3.25: Crack widths at 0.4%, 0.8%, and 1.5% drift for Cor-Tuf UHPC specimen with $t = 35$ mm, 198 kN axial load, and without fiber reinforcement

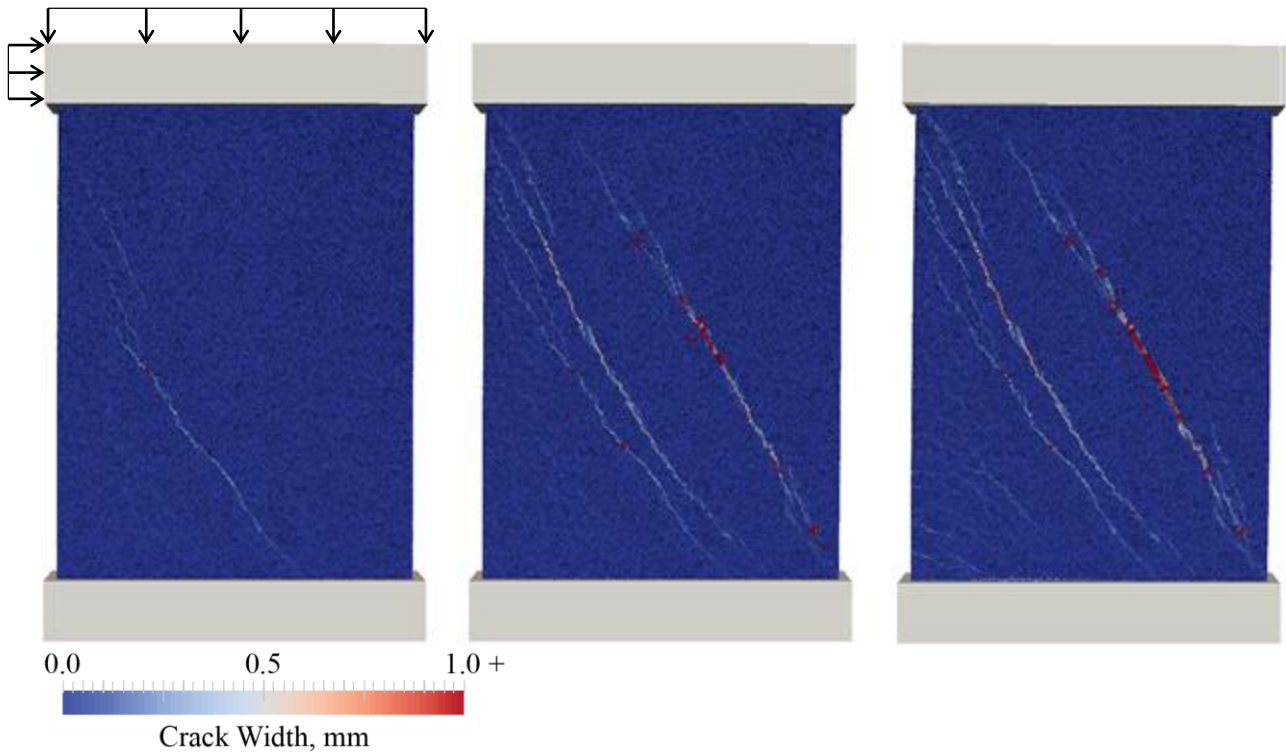


Figure 3.26: Crack widths at 0.4%, 0.8%, and 1.5% drift for Cor-Tuf UHPC specimen with $t = 35$ mm, 198 kN axial load, and fiber reinforcement

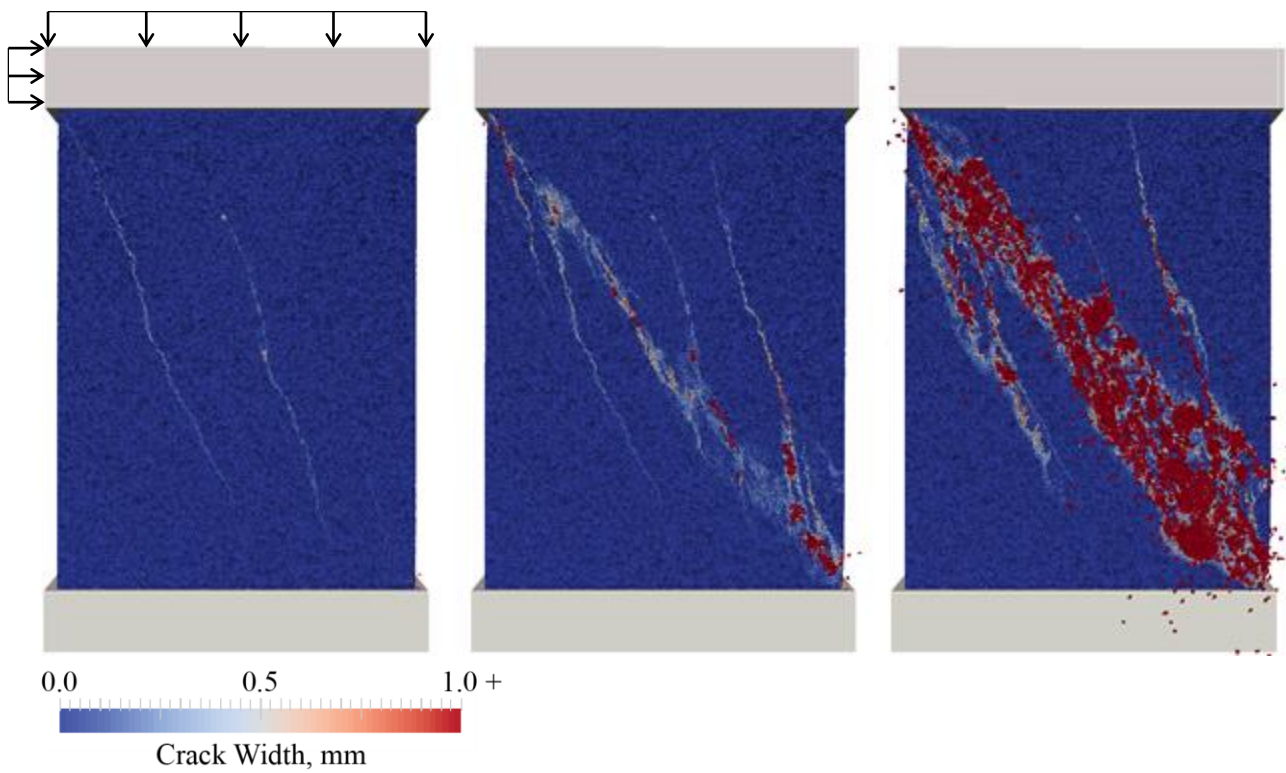


Figure 3.27: Crack widths at 0.4%, 0.8%, and 1.5% drift for "Section 9" HPC specimen with $t = 60$ mm and 360 kN axial load

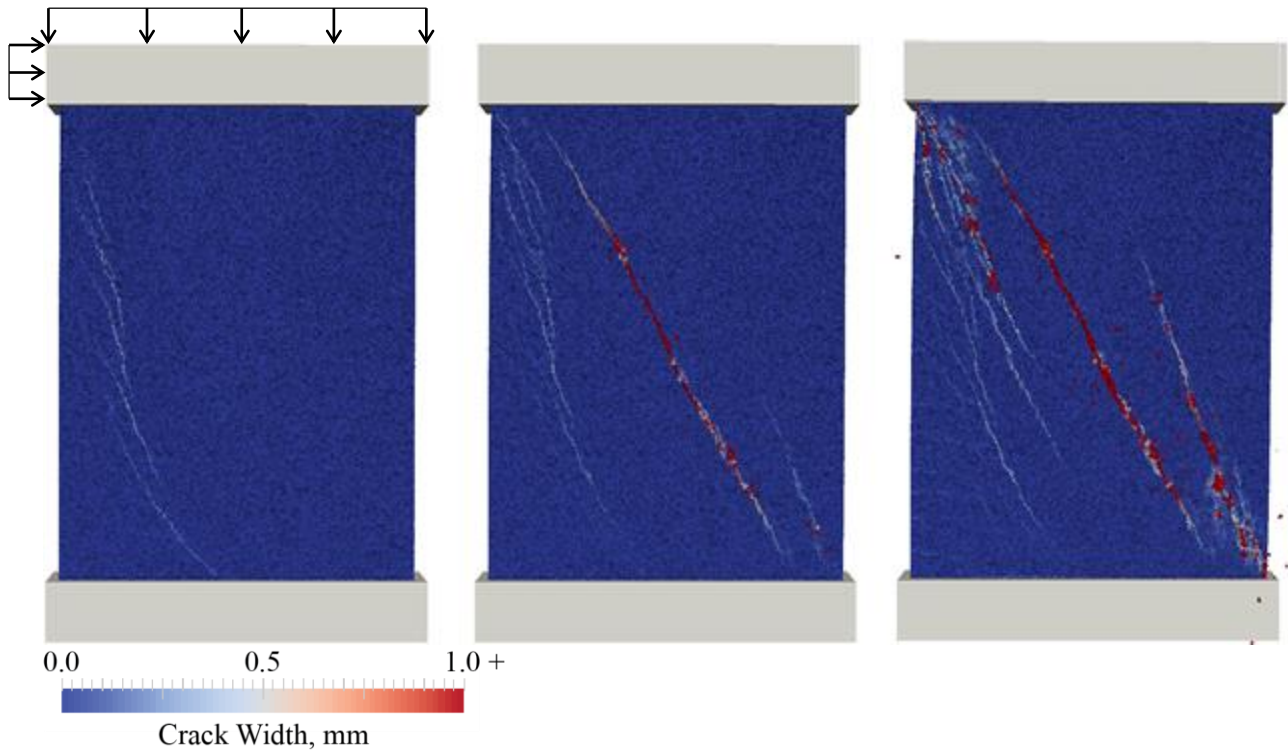


Figure 3.28: Crack widths at 0.4%, 0.8%, and 1.5% drift for Cor-Tuf UHPC specimen with $t = 35$ mm, 360 kN axial load, and without fiber reinforcement

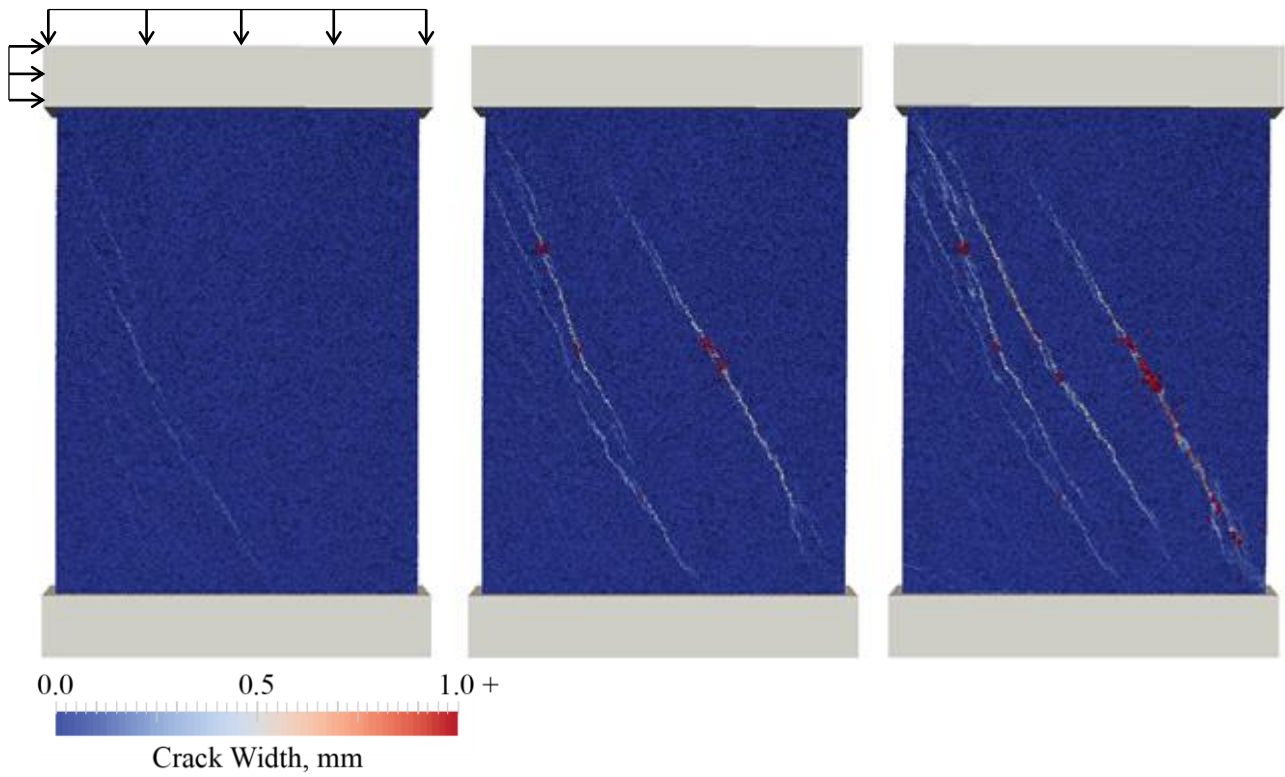


Figure 3.29: Crack widths at 0.4%, 0.8%, and 1.5% drift for Cor-Tuf UHPC specimen with $t = 35$ mm, 360 kN axial load, and fiber reinforcement

CHAPTER 4. SimaPro and Life-Cycle Assessment

The construction industry accounts for a significant portion of the environmental impact of the activities of society each year, and concrete is in turn a significant contributor. This impact is comprised of greenhouse gases, pollutants, waste, and use of resources, from the manufacture of cement, acquisition and processing of aggregate, and manufacture of steel for reinforcement. As the world's population has grown, eclipsing 7 billion in late 2011, so too has the use of building materials like concrete to support the needs of society.

Manufacturing Portland cement is energy-intensive and results in a large amount of greenhouse gas emissions (Mehta 2001). The cement industry is undertaking carbon dioxide reduction efforts to mitigate environmental impact, with more fuel-efficient kilns and substitution of other supplementary cementitious materials in finished product, among other methods. Production is rapidly increasing, however, from less than 2 billion tons per year in the early 2000s to 4.18 billion tons in 2014 (Oss 2015), meaning despite efforts to lessen impact per volume of material, the effect on the environment of the industry as a whole is still growing.

There are other ways to explore how to solve these problems; discussed here are those postulated by Mehta (2001). One, discussed above, is reducing the use of cement in products by using other cementitious or pozzolanic materials in concrete mixes. Related is the use of superplasticizer or high-range water reducer to shorten the set time of mixes incorporating supplementary cementitious materials, and in the process lessening the large freshwater requirements of the manufacture of cement. Another is improving the durability of concrete. Most modern reinforced concrete structures are built with a design life of 50 years, and some deteriorate in much less time if exposed to harsh conditions, such as those in coastal regions. Using less

permeable concrete that is not as prone to degradation may lead to longer service life and therefore less material used since structures would need to be replaced or repaired less often.

Ultra-high performance concrete has the potential to incorporate all of the above factors to reduce the environmental impact of construction in the future. Its advanced material properties allow for reduced cross-sections of structural components, and therefore lighter overall weight to be considered for the subsequent design of other components. However, UHPC has a high proportion of energy-intensive raw materials per unit volume, containing micro steel fibers and a large amount of Portland cement.

For structural components, determining whether using new materials like UHPC versus conventional methods yields improved sustainability requires the gathering and analysis of environmental data for the material constituents. This process is performed using an approach called life-cycle assessment (LCA), which allows quantitative decision-making for the design and construction of structures with sustainability in mind. The procedure for performing an LCA is given in standard ISO 14040 (ISO 2006), outlining the phases and requirements involved. Similar to the approach of Stengel and Schießl (2014), the numerous materials and processes involved with the manufacture of UHPC are modeled with the help of an LCA software, SimaPro (2013), which incorporates a database of environmental information for materials and processes, called Ecoinvent.

4.1 Life-Cycle Assessment with SimaPro

SimaPro affords the user full control over the definition of processes that make up the constituents of the material being studied (for example, the modeling of Portland cement includes processes like extraction of raw material, transport to the factory, and use of electricity at the factory), down to the basic elements of the model which come from the Ecoinvent database. This

gives transparency of how results are obtained, manifested in the ability to analyze every detail of the model. Users can also customize all aspects of the LCA, which proves useful to perform actions like adjusting the processes to reflect manufacture in a specific country or region, or to perform sensitivity analysis to determine potential variability of results.

The construction of an LCA in SimaPro is done by selecting the appropriate processes for the constituents of the material in question, organized into a network the same way the actual materials are made. A figure showing the network may be generated in SimaPro; a portion of this network diagram for a UHPC mix is shown in Figure 4.1. Upon completion of the definition of the network, results and comparisons can be calculated using an LCA method chosen by the user. There are many different LCA methods available, many of which are embedded within the software and available for use. The selected methods for this research are discussed in the following section.

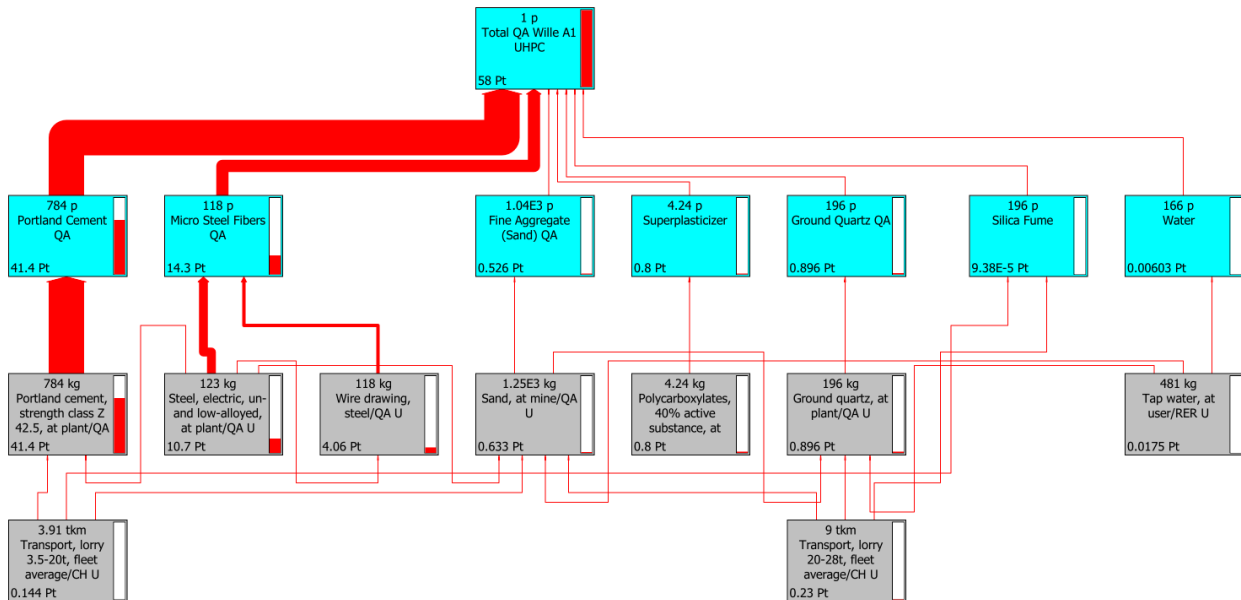


Figure 4.1: Excerpt of a SimaPro network diagram for a UHPC, showing constituents and the top level processes

4.2 Life-Cycle Assessment Methods

A number of LCA methods, also called impact assessment methods, are available in SimaPro. These methods consist of a series of steps to take the inputs for the model, which are the processes defined by the user involved in the manufacturing of the material or product in question (for example, a unit volume of UHPC, or a UHPC shear wall with a small amount of steel bar reinforcement), perform analysis on the associated entries from the Ecoinvent database, and assign factors in order to combine data to form results, which are then outputted to tables or figures.

LCA methods differ from one another in the factors applied to obtain results, but they share the same general procedure. The steps taken in these methods are: *characterization*, *damage assessment*, *normalization*, and *weighting*. Per ISO 14040, only the first step, characterization, is required (ISO 2006), though the remaining steps are commonly included for reasons described later in this section.

4.2.1 Structure of LCA Methods

Characterization, the first step in an impact assessment method, involves assessing a material (for example, a byproduct like ozone) to determine its contribution to an *impact category*. Impact categories differ between methods; examples include climate change, human toxicity, ionizing radiation, and freshwater ecotoxicity. The calculation of a material's contribution to an impact category is performed using a factor that reflects a material's impact relative to others, called a *characterization factor* or a *life cycle impact parameter*. To illustrate this process, using the ReCiPe 2008 method (Goedkoop et al. 2013), for the impact category “climate change”, carbon dioxide has a characterization factor of 1, while methane has a characterization factor of 25. This means that 1 kilogram of methane causes the same amount of climate change as 25 kilograms of carbon dioxide. Characterization factors are determined through scientific research. As

knowledge in the field of environmental impact assessment advances, new methods are created or incumbent ones are updated that reflect the most up-to-date information available (Goedkoop 2010).

The purpose of damage assessment, the second step of LCA methods, is to combine the numerous impact categories like those listed above, also known as *midpoint categories*, into a smaller number of *damage categories*, also called *endpoint categories*. Following this nomenclature, methods that incorporate the optional step of damage assessment are called *endpoint methods*. The combination of midpoint categories into endpoint categories makes it easier to

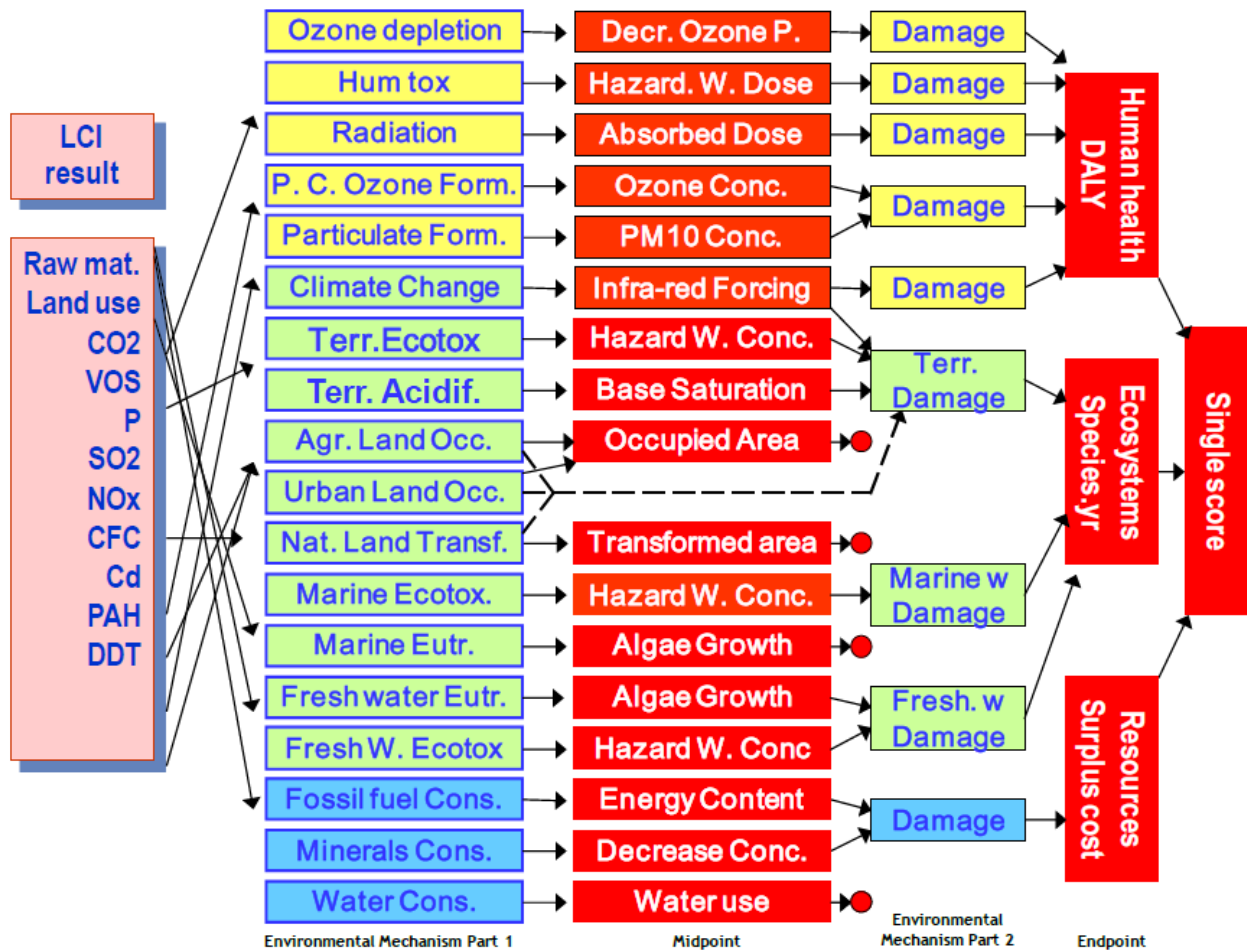


Figure 4.2: Flowchart of ReCiPe 2008 methodology (Goedkoop et al. 2013)

convey and work with data. All midpoint categories within an endpoint category have the same unit, allowing the results to be directly summed together; for example, the ReCiPe 2008 midpoint categories ozone depletion, human toxicity, ionizing radiation, climate change, and others all have a common unit of disability-adjusted life years (DALY) and are added together into an endpoint category, human health, also expressed in DALY (Goedkoop 2010). A flowchart showing how midpoint categories are formed, assessed, and combined into endpoint categories in ReCiPe 2008 is shown in Figure 4.2. It is important to note that even after performing damage assessment, the ReCiPe 2008 midpoint or impact categories are still intact, and data may be viewed at both a midpoint vantage as well as endpoint when analyzing results (Goedkoop et al. 2013).

Next, midpoint or endpoint categories are *normalized*. Normalization is performed so that the categories, which previously held no relation to one another, may be directly compared for their relative amount of environmental impact. Following this process, all categories have the same unit. A commonly-used method, which has been used in this research, is to divide the average yearly environmental load in a country or continent by the number of inhabitants, yielding the average environmental impact of one citizen of that country or continent in one year. This reference may be changed by the user; for example, the environmental load of lighting a 60-watt light bulb for one hour. SimaPro offers multiple sets of normalization factors to be freely chosen by the user. In this way, with a reference that can be easily envisioned, results following normalization are conveyed in a format that is simple to understand. As mentioned above, normalizing categories allows the determination of which categories contribute the most to the overall environmental impact of the material or product being analyzed. An example illustrating this fact, shown here for Cor-Tuf UHPC (Roth et al. 2010), may be examined in Table 4.1.

Table 4.1 SimaPro normalized percentage of total environmental impact for Cor-Tuf UHPC using ReCiPe 2008 midpoint method

Impact Category	Normalized Percentage of Total Environmental Impact
Climate change, human health	43.3%
Fossil depletion	41.3%
Human toxicity	5.9%
Particulate matter formation	5.2%
Climate change, ecosystems	3.8%
Natural land transformation	0.5%
Agricultural land occupation	< 0.1%
Urban land occupation	< 0.1%
Metal depletion	< 0.1%
Ionizing radiation	< 0.1%
Terrestrial ecotoxicity	< 0.1%
Terrestrial acidification	< 0.1%
Ozone depletion	< 0.1%
Photochemical oxidant formation	< 0.1%
Freshwater eutrophication	< 0.1%
Freshwater ecotoxicity	< 0.1%
Marine ecotoxicity	< 0.1%

The final step of an LCA, called *weighting*, multiplies the normalized results for each midpoint or endpoint category by a weighting factor so that they may be added together to create a total or *single score*. Weighting values are assigned based on research and correspond to the importance of the categories to the overall environmental effects. For example, the climate change midpoint category, where the associated environmental effects are well-studied and high-impact, would be given a higher weighting factor than the marine ecotoxicity midpoint category, where the effects are less understood by the scientific community or may have less impact. In many LCA methods, there are multiple sets of weighting factors available. This is one way sensitivity analysis may be performed in SimaPro – sets of factors which give both best-case and worst-case results for environmental impact are available to discern potential variability. After the weighting factors are applied, the single score for environmental impact (expressed in “points” in ReCiPe 2008, as

units are lost in weighting and combining categories) may be found for the material or product being analyzed, and results can be generated (Goedkoop 2010).

4.2.2 ReCiPe 2008

There are many LCA methods available in SimaPro which may be used and switched at will after defining the process network for a material or product. Two methods were chosen for this research, ReCiPe 2008 and Cumulative Energy Demand. The first, ReCiPe 2008, takes a multi-issue approach, meaning it utilizes multiple impact assessment categories as described in the previous section. It updates and integrates two earlier models, CML 2001 and Ecoindicator 99, both of which were widely used in the scientific community (Goedkoop et al. 2013).

ReCiPe 2008 combines the “problem-oriented approach” of CML 2001 and the “damage-oriented approach” of Ecoindicator 99. The CML 2001 “problem-oriented approach” refers to the definition of impact categories at a midpoint vantage. When analyzing results at this level, direct comparisons between materials or products is difficult due to the number of categories in which the results are presented. However, at the midpoint level, scientific knowledge is relatively strong and there is less uncertainty in the results. The Ecoindicator 99 “damage-oriented approach” refers to the definition of impact categories at an endpoint vantage. When analyzing results at this level, comparisons between materials or products may be more readily and conclusively performed due to the small number (three in the case of Ecoindicator 99) of categories. At the same time, because this method combines many areas of environmental impact together, there is more uncertainty regarding the results of the LCA. ReCiPe 2008 is formulated to express the advantages of both approaches while also updating the older methods with newer knowledge and more accurate factors. The midpoint categories of ReCiPe 2008 may be seen in both Figure 4.2 and Table 4.1; the endpoint categories are given in Figure 4.2 (Goedkoop et al. 2013).

The major benefit of using ReCiPe 2008 to perform life cycle assessment is its ability to obtain a single score of environmental impact for a material or product, and thus directly compare products' sustainability. This method also allows the user to analyze results further – determining environmental impact by constituent, discerning the nature of the environmental impacts (which categories constitute the biggest impact), and performing sensitivity analysis.

4.2.3 Cumulative Energy Demand

The second LCA method used in this research is Cumulative Energy Demand. Cumulative Energy Demand is a single issue method, meaning it calculates results for one metric only, in this case the method's namesake. It has a long history of development, having been in use since the early 1970s. Like ReCiPe 2008, this method may be used to directly compare the sustainability of materials or products. Cumulative Energy Demand has been criticized, however, as it focuses only on energy, and more in-depth analysis is not available aside from its division of energy resources into five impact categories: non-renewable fossil, non-renewable nuclear, renewable biomass, renewable wind/solar/geothermal, and renewable water (Goedkoop 2010).

The advantage of the methodology lies in its simplicity. In this research, Cumulative Energy Demand is used not only for obtaining results, but also to check against the validity of the results from ReCiPe 2008, a more complex method. Compared to other LCA methods, it boasts the longest scientific history as well as the lowest data uncertainty in its calculations. Using this method as a check of results is possible due to the fact that Cumulative Energy Demand has been proven to correlate with other methods (Huijbregts et al. 2010). The final results, which express the cumulative energy demand in the manufacture of a material or product, are conveyed in units of energy.

The following chapter describes the results of the sustainability study of shear walls in tall buildings using SimaPro. A comparison of currently-used materials and UHPC is performed for the metric of environmental impact. At the conclusion of the results presented in the next chapter, improvements in both structural efficiency and sustainability from using UHPC for shear walls have been quantitatively defined.

CHAPTER 5. Sustainability of Ultra-High Performance Concrete Shear Walls

This chapter presents the life-cycle assessment (LCA) results using SimaPro for ultra-high performance concrete shear walls. Two LCA methods were used: ReCiPe 2008 and Cumulative Energy Demand. LCA results for the cementitious-based composite constituents were determined for both the United States and Qatar by using each country’s energy mix profile as appropriate, shown in Table 5.1. The analysis was performed based on a cradle-to-gate perspective, meaning the results reflect all processes from extraction of raw material (“cradle”) through finished product, ready to be used in construction (“at the factory gate”). Results detailed in Chapter 3 were used to determine the amount of material in each shear wall to input into the sustainability model, and to perform a comparison of embodied energy versus dissipated energy in the simulations.

Table 5.1 Electricity mixes for the United States and Qatar

Type	Electricity Mix, United States (%) (Itten et al. 2012)	Electricity Mix, Qatar (%) (EIA 2015)
Hard coal	46.26	0
Nuclear	19.37	0
Natural gas	20.64	100
Hydropower, run-of-river and reservoir	6.25	0
Lignite	1.97	0
Wind	1.37	0
Oil	1.32	0
Wood	0.94	0
Waste	0.68	0
Hydropower, pumped storage	0.62	0
Geothermal	0.40	0
Industrial gas	0.09	0
Solar	0.06	0
Biogas	0.02	0
Other	0.02	0

5.1 LCA Results by Constituent

To enable the SimaPro model to easily incorporate different mix designs of cementitious-based composites, the processes involved in the production of a unit weight of the constituents of the materials were defined. This gives LCA results for each constituent; in this study, the constituents included Portland cement, superplasticizer, silica fume, ground quartz, water, coarse aggregate, fine aggregate, and micro steel fibers, shown in Table 5.2. Silica fume is taken as a byproduct of other processes, and thus the only impact from the material results from transportation processes (Stengel and Schießl 2014). Not enough information was available for superplasticizer and water to determine the effect of location of manufacture (Qatar vs. United States) on sustainability.

Table 5.2 Constituent single score results per kg of material

	ReCiPe 2008, (Points × 10³)	Cumulative Energy Demand (MJ)
Coarse Aggregate (Gravel) QA	1.19	0.15
Coarse Aggregate (Gravel) US	1.20	0.16
Fine Aggregate (Sand) QA	0.51	0.06
Fine Aggregate (Sand) US	0.51	0.07
Ground Quartz QA	4.57	0.61
Ground Quartz US	4.59	0.63
Micro Steel Fibers QA	121.75	12.38
Micro Steel Fibers US	122.68	13.18
Portland Cement QA	52.80	3.93
Portland Cement US	52.93	4.04
Silica Fume	0.00	0.00
Superplasticizer	188.60	29.57
Water	0.04	0.01

5.2 LCA Results for Cementitious-Based Composites

Chapter 3 provided the results of simulations for Cor-Tuf UHPC, with simulated $f'_c = 231$ MPa, and “Section 9” HPC, with simulated $f'_c = 51.7$ MPa. Cor-Tuf UHPC requires the use of heat treatment to achieve its specified compressive strength. The effect of this heat treatment on environmental impact is not known and could result in inaccuracy of the SimaPro model. Thus, a UHPC which does not require the use of heat treatment was used instead. The mix, detailed in Wille et al. (2012) and labeled as “Type C”, has a similar compressive strength range, given as $f'_c = 220 - 240$ MPa at 28 days. The density of “Type C” UHPC was assumed to be 2500 kg/m^3 .

Information regarding the mix design of “Section 9” HPC was not available. Therefore, an HPC mix with similar compressive strength that had constituent information available was used. The mix, detailed in Einsfeld and Velasco (2006) and labeled as “HP2”, has a listed compressive strength of $f'_c = 49$ MPa and a density of 2466 kg/m^3 . The mix design information for both “Type C” UHPC and “HP2” HPC is shown in Table 5.3.

Table 5.3 Constituent amount per m^3 for “Type C” UHPC and “HP2” HPC

	“Type C” UHPC, 0% fibers by volume (kg)	“Type C” UHPC, 2% fibers by volume (kg)	“HP2” HPC (kg)
Portland cement	915	880	456
Fine aggregate (sand)	943	885	820
Coarse aggregate	0	0	992
Ground quartz	229	220	0
Silica fume	229	220	50
Superplasticizer	9.9	9.5	9.0
Water	174	167	152
Micro steel fibers	0	158	0

LCA results for each cementitious-based composite are shown in Tables 5.4 and 5.5, broken down by each constituent. The results shown in the last row of each table indicate that the

environmental impact of 1 m³ of “Type C” UHPC with 0% fibers is approximately 1.8 to 1.9 times that of “HP2” HPC, and the impact of 1 m³ of “Type C” UHPC with 2% fibers is approximately 2.5 to 2.7 times that of “HP2” HPC.

Table 5.4 Single score per m³ for “Type C” UHPC and “HP2” HPC, ReCiPe 2008

	“Type C” UHPC, 0% fibers (Points × 10 ⁶)		“Type C” UHPC, 2% fibers (Points × 10 ⁶)		“HP2” HPC, (Points × 10 ⁶)	
	Qatar	United States	Qatar	United States	Qatar	United States
Portland cement	48.3	48.5	46.5	46.6	24.1	24.1
Fine aggregate (sand)	0.48	0.48	0.45	0.45	0.42	0.42
Coarse aggregate	-	-	-	-	1.18	1.19
Ground quartz	1.05	1.05	1.01	1.01	-	-
Silica fume	0.00	0.00	0.00	0.00	0.00	0.00
Superplasticizer	1.87	1.87	1.79	1.79	1.70	1.70
Water	0.01	0.01	0.01	0.01	0.01	0.01
Micro steel fibers	-	-	19.3	19.4	-	-
TOTAL	51.7	51.9	69.1	69.3	27.4	27.4
Normalized to Qatar “HP2” HPC	<i>1.89</i>	<i>1.89</i>	<i>2.52</i>	<i>2.53</i>	1.00	<i>1.00</i>

**Table 5.5 Single score per m³ for “Type C” UHPC and “HP2” HPC,
Cumulative Energy Demand**

	“Type C” UHPC, 0% fibers (MJ)		“Type C” UHPC, 2% fibers (MJ)		“HP2” HPC (MJ)	
	Qatar	United States	Qatar	United States	Qatar	United States
Portland cement	3593.7	3695.5	3454.6	3552.4	1790.0	1840.7
Fine aggregate (sand)	58.4	61.9	54.8	58.1	50.8	53.8
Coarse aggregate	-	-	-	-	150.1	162.3
Ground quartz	140.3	145.1	134.8	139.5	-	-
Silica fume	0.0	0.0	0.0	0.0	0.0	0.0
Superplasticizer	292.5	292.5	281.0	281.0	266.2	266.2
Water	1.1	1.1	1.0	1.0	0.9	0.9
Micro steel fibers	-	-	1961.8	2087.5	-	-
TOTAL	4086	4196	5888	6120	2258	2324
Normalized to Qatar “HP2” HPC	<i>1.81</i>	<i>1.86</i>	<i>2.61</i>	<i>2.71</i>	1.00	<i>1.03</i>

5.3 LCA Results for Shear Walls

In this section, the environmental impact of UHPC and HPC shear walls are compared, with the dimensions of the walls, and therefore the volume of material used, determined using the results detailed in Chapter 3. Simulations of the structural response of shear wall sections were carried out, and showed that Cor-Tuf UHPC shear walls with thickness $t = 35$ mm have equal stiffness and superior post-cracking response to “Section 9” HPC shear walls with thickness $t = 60$ mm. Both types of shear walls have a length of 300 mm and a height of 400 mm, resulting in a volume of UHPC of $4.2 \times 10^{-3} \text{ m}^3$ and a volume of HPC of $7.2 \times 10^{-3} \text{ m}^3$. The LCA results are detailed in Table 5.6, calculated using these volumes and the LCA results per unit volume for “Type C” UHPC and “HP2” HPC. The results indicate that the UHPC shear wall with 0% fibers by volume has an environmental impact approximately 6-10% greater than the HPC shear wall, and the UHPC shear wall with 2% fibers by volume has an environmental impact approximately 47-58% greater than the HPC shear wall. Table 5.7 shows a comparison of structural dissipated energy and embodied energy for these UHPC and HPC sections.

Important aspects not studied or included in this research would affect the quantitative results described here. First, UHPC structural members may have a longer lifespan due to improved durability (if subjected to deteriorating effects/conditions) or seismic performance. Next, using UHPC in shear walls may allow the reduction or elimination of some or all horizontal and vertical bar reinforcement, lowering steel use and improving constructability. Finally, in a related fashion, formwork requirements and construction efforts may be lessened through using UHPC. Future research may aim to determine the results of these effects and others on the sustainability of UHPC.

Table 5.6 LCA results for UHPC and HPC shear wall specimens

	UHPC, 0% fibers		UHPC, 2% fibers		HPC	
	Qatar	United States	Qatar	United States	Qatar	United States
Wall volume ($\text{m}^3 \times 10^{-3}$)	4.2		4.2		7.2	
Single score, ReCiPe 2008 (Points)	217	218	290	291	197	197
Single score, ReCiPe 2008, normalized to Qatar HPC	1.10	1.10	1.47	1.48	1.00	1.00
Cumulative Energy Demand (MJ)	17.2	17.6	24.7	25.7	16.3	16.7
Cumulative Energy Demand, normalized to Qatar HPC	1.06	1.08	1.52	1.58	1.00	1.03

Table 5.7 Comparison of Dissipated Energy and Embodied Energy

	UHPC, 0% fibers	UHPC, 2% fibers	HPC
Dissipated Energy (MJ)	0.47	0.53	0.35
Embodied Energy (MJ)	17.2	24.7	16.3
$\frac{\text{Dissipated Energy}}{\text{Embodied Energy}}$ (%)	2.7%	2.1%	2.1%

CHAPTER 6. Conclusions

6.1 Summary of Conclusions

For the types of cementitious-based composites, shear wall dimensions simulated herein, and without steel bar reinforcement in the web of the shear walls, a UHPC shear wall has equal uncracked stiffness and superior post-cracking capacity at a thickness 58% that of an HPC shear wall and at a weight 59% that of an HPC shear wall. With the same conditions, a UHPC shear wall with 0% fiber reinforcement by volume has an environmental impact 6% to 10% greater than that of an HPC shear wall, and a UHPC shear wall with 2% fiber reinforcement by volume has an environmental impact 47% to 58% greater than that of an HPC shear wall. Aspects not studied in this research may affect these results, including potential increase in life span with UHPC, reduction or elimination of steel bar reinforcement and corresponding improvement in constructability, and reduction in formwork required for construction.

A UHPC shear wall with 0% fiber reinforcement by volume dissipates significantly more energy during lateral loading after cracking than an HPC shear wall. A UHPC shear wall with 2% fiber reinforcement by volume in turn dissipates significantly more energy during lateral loading after cracking than a UHPC shear wall with 0% fiber reinforcement by volume. The degree to which the dissipated energy is greater depends on the drift ratio reached by the specimen during lateral loading as well as the amount of axial load on the specimen.

6.2 Future Work

The nature of the presented sustainability results, which convey the environmental impact per unit weight of cementitious-based composite components, such as Portland cement and ground

quartz, will allow future studies to easily quantify the sustainability of structural members or materials.

Advancements in modeling techniques, computing power, and software will allow future studies to perform simulations of UHPC structural members at larger scales or at full scale. These future studies, as well as the work described in this paper, could be incorporated into design guidelines that allow the industry to better take advantage of UHPC material properties and structural response in design.

Future work may involve comparing simulations to actual experimental efforts. A shear wall experimental program using concrete with adequate material characterization information would be useful for validation of the LDPM shear wall simulation capabilities. Further simulation efforts, using the results developed herein, may include realistic reinforcing bar layouts and reinforcing ratios to compare true shear wall simulations using different materials. Additionally, analysis of the results developed in this research may determine the actual failure modes of the wall sections, as well as compare the quantitative LDPM results to those predicted by ACI equations.

One way UHPC properties may be advantageously used is through the incorporation of topology optimization into design. Input parameters from this research may include embodied energy per unit volume of concrete, concrete material properties and response, and energy dissipation per unit volume of material. Though the use of UHPC has potential ramifications due to its higher cost and environmental impact per unit volume as compared to conventional concrete, topology optimization can aid in determining ways in which UHPC can be used in tandem with other materials to achieve superior solutions in terms of structural efficiency and environmental sustainability.

REFERENCES

- Ali, M. M. (2001). Evolution of concrete skyscrapers: From Ingalls to Jin mao. *Electronic Journal of Structural Engineering*, 1(1), 2-14.
- American Concrete Institute (1997). *State-of-the Art Report on High-Strength Concrete (ACI 363R-92) (Reapproved 1997)*.
- American Concrete Institute (2014). *Building Code Requirements for Structural Concrete (ACI 318-14) and Commentary (ACI 318R-14)*.
- Blanco-Carrasco, M., Hornung, F., & Ortner, N. (2010). "Qatar: Green Concrete Technologies".
- Crow, J. M. (2008). "The concrete conundrum". *Chemistry World*.
- Council on Tall Buildings and Urban Habitat (CTBUH). "The Skyscraper Center: Doha, Qatar." (28 October 2015) <<http://skyscrapercenter.com/city/doha>>
- Cusatis, G., Mencarelli, A., Pelessone, D., and Baylot, J. (2011). "Lattice Discrete Particle Model (LDPM) for failure behavior of concrete. II: Calibration and validation." *Cement and Concrete Composites*, 33, 891-905.
- Cusatis, G., Pelessone, D., and Mencarelli, A. (2011). "Lattice Discrete Particle Model (LDPM) for failure behavior of concrete. I: Theory." *Cement and Concrete Composites*, 33, 881-890.
- Einsfeld, R. A., & Velasco, M. S. (2006). Fracture parameters for high-performance concrete. *Cement and Concrete Research*, 36(3), 576-583.
- Gerometta, R. S. Retrieved from http://www.gettyimages.com/galleries/photographers/roberto_soncin_gerometta.
- Goedkoop, M. (2010). "SimaPro Database Manual: Methods Library v2.8."
- Goedkoop, M. et al. (2013). "ReCiPe 2008: A life cycle impact assessment method which comprises harmonized category indicators at the midpoint and the endpoint level. Report I: Characterisation." Ministerie van Volkshuisvesting, Ruimtelijke Ordening en Milieu.
- Graybeal, B. A. (2006). "Material Property Characterization of Ultra-High Performance Concrete." Tech. Rep. FHWA-HRT-06-103, Federal Highway Administration (August 2006).
- Graybeal, B. A. & Russell, H. G. (2013). *Ultra-high performance concrete: A state-of-the-art report for the bridge community* (No. FHWA-HRT-13-060).
- Huijbregts, M. A., Hellweg, S., Frischknecht, R., Hendriks, H. W., Hungerbühler, K., & Hendriks, A. J. (2010). Cumulative energy demand as predictor for the environmental burden of commodity production. *Environmental science & technology*, 44(6), 2189-2196.

- International Organization for Standardization (ISO). (2006). *ISO 14040:2006 Environmental management – Life cycle assessment – Principles and framework*.
- Itten, R., Frischknecht, R., & Stucki, M. (2012). Life cycle inventories of electricity mixes and grid.
- Kosmatka, S. H., & Panarese, W. C. (2002). “Design and control of concrete mixtures”.
- Mehta, P. K. (2001). Reducing the environmental impact of concrete. *Concrete international*, 23(10), 61-66.
- Oss, H. G. (2015). “Cement”. U.S. Geological Survey, Mineral Commodity Summaries.
- Pelessone, D. (2015). *MARS: Modeling and Analysis of the Response of Structures – User’s Manual* (<http://www.es3inc.com/marssolver/>). ES3, San Diego, California.
- QNRf. (2015). Retrieved from <http://www.qnrf.org/en-us/>.
- Roth, M. J., Rushing, T. S., Flores, O. G., Sham, D. K., & Stevens, J. W. (2010). *Laboratory Investigation of the Characterization of Cor-Tuf Flexural and Splitting Tensile Properties* (No. ERDC/GSL-TR-10-46).
- Schauffert, A. and Cusatis, G. (2012). “Lattice Discrete Particle Model for Fiber-Reinforced Concrete. I: Theory.” *Journal of Engineering Mechanics*, 138(7), 826-833.
- Schauffert, A. and Cusatis, G. (2012). “Lattice Discrete Particle Model for Fiber-Reinforced Concrete. II: Tensile Fracture and Multiaxial Loading Behavior.” *Journal of Engineering Mechanics*, 138(7), 834-841.
- Simapro v7.3.3 [Computer software]. (2013). Retrieved from <<https://www.pre-sustainability.com/simapro>>
- Smith, J., Cusatis, G., Pelessone, D., Landis, E., O'Daniel, J., & Baylot, J. (2014). Discrete modeling of ultra-high-performance concrete with application to projectile penetration. *International Journal of Impact Engineering*, 65, 13-32.
- Stengel, T. and Schiebl, P. (2014). “Life cycle assessment (LCA) of ultra high performance concrete (UHPC) structures.” *Eco-efficient Construction and Building Materials*, (2014) 528 – 564.
- U.S. Energy Information Administration (EIA). (2015). “Qatar international energy data and analysis”.
- Wille, K., Naaman, A. E., El-Tawil, S., & Parra-Montesinos, G. J. (2012). Ultra-high performance concrete and fiber reinforced concrete: achieving strength and ductility without heat curing. *Materials and structures*, 45(3), 309-324.

APPENDIX A. Sample of MARS Files

A.1 GenUhpcWall.mrs

```
Particle generation:UHPC Shear Wall 55 story bldg
//-----
ControlParameters {
  Units SI
}
//-----
Material CONC LDPM {
  MixDesign {
    CementContent 794.4 kg/m3
    WaterToCementRatio 0.2082
    AggregateToCementRatio 1.6332
    MinAggregate 8 mm
    MaxAggregate 16 mm
    FullerCoefficient 0.5
  }
}
//-----
LdpmModelGenerator MODL {
  Material CONC
  Seed 34565
  //DebugPlot
  GeneratePrism {
    Dimensions 3000 mm 4000 mm 180 mm
    ConstantSpacedParticlesOnEdges
    MaximumIterations 40000 // default 10000
  }
  WriteLdpmMeshFile MeshUhpcWall.mrs
}
//-----
EOF
```

A.2 RunUhpcWall.mrs

```
SHEAR UHPC CORTUF WALL
//-----
//GENERAL CONTROL PARAMETERS
//-----
ControlParameters {
  Units SI
  TerminationTime 1000.1 ms
  MaximumTimeStep 0.0001 ms
  // PrintProgressLine Frequency 1
  Monitor Frequency 10
  tsf 0.7 // safe coefficient of the MaximumTimeStep
  Flush every 0.02 ms
  PlottingDefaults {
    X-DisplacementScalingFactor 1 // 0.000000001 // horizontal
amplification
    Y-DisplacementScalingFactor 1 // 0.000000001 // horizontal
amplification
    Z-DisplacementScalingFactor 1 // 0.000000001 // vertical
amplification
  }
  //WritePlotDataFile plot.dat Every 2.25 ms
}
//-----
//          MATERIAL
//-----
Material ECON Elastic {
  Density 2400 kg/m3
  YoungModulus 58000 MPa
  PoissonsRatio 0.2
}
Material FIBRM LDPM-F {
  ElasticModulus                210 GPa // ymf, elastic
modulus
  SpallingParameter             150 MPa // sps, spalling
parameter
  FiberStrength                 1200 MPa // sfu, fiber
strength
  FiberStrengthDecay            0.4 // fsd, fiber
strength decay parameter // 0.3
  SnubbingParameter            0.05 // fsn, snubbing
parameter // 0.5
  BondStrength                 11.5 MPa // tau, bond
strength %circa 3.0
}
```

```

    VolumeStiffnessRatio          0.0    // eta
    DebondingFractureEnergy       0 N/m // gdm, debonding
fracture energy 1-10
    PullOutHardening              0.0    // poa, pull-out
hardening coefficient
    PlasticParameter              0.5    // mai maggiore di
1
    CookGordonParameter          2.0    // cgp, Cook-Gordon
effect
// ElasticAnalysis
}
//-----
//          LDPM ELEMENT
//-----
TetSolidList PRTC LDPM {
  ReadFile MeshUhpcWall.mrs
  EditNodeList {
    Rename PRTC
    Plotting enabled
    PlotAttributes {
      MinRadius 0.3 mm
    }
  }
}
EditMaterial {
  StaticParameters {
    NormalModulus 67000 MPa // nmo
    DensificationRatio 2.5 // drt
    Alpha 0.484
    TensileStrength 4 MPa // 4 MPa // ftm
    CompressiveStrength 500 MPa // fcm
    ShearStrengthRatio 17 // 2.55 // 2.5 // fsm
    TensileCharacteristicLength 150 mm // 400 mm // 350 mm //
300 mm // 270 mm // tcl
    SofteningExponent 0.2 // 0.1 // 0.4 // ncm
    InitialHardeningModulusRatio 0.36 // hmr
    TransitionalStrainRatio 2 // hts
    InitialFriction 0.5 // 0.2 // mu0
    AsymptoticFriction 0 // mui
    TransitionalStress 300 MPa // fts
    VolumetricDeviatoricCoupling 0 // beta
    DeviatoricStrainThresholdRatio 2 // dk1
    DeviatoricDamageParameter 1 // dk2
    //ElasticAnalysis
  }
  // FacetFailure
}
  EmbeddedFibers {

```

```

FiberConcreteInteraction FIBRM
GenerateFibers {
  Seed 9995
  FiberLength 3.0 cm // length of fiber
  //ElementSize 5.01 cm //
  EdgesPerFiber 1
  FiberSectionArea 0.785 mm2 // cross sectional area
  Tortuosity 0.0 // usually 0
  //Chopped // comment this value when concrete is cast
  VolumeFraction 0.02
  //PreferentialDirection 1 0 0 10.
}
}
Make tfl EXTN
Plotting enabled
MassScaling
// CrackOpening 0.001 mm
// WriteCellDataDump Cell.txt
}
//-----
//          HEXAHEDRAL SOLID ELEMENT
//-----
HexSolidList TOPCON 8IP {
  Material ECON
  Color red
  Generate {
    Block {
      dimensions 3020 mm 200 mm 200 mm
      elements 200 20 20
    }
  }
  NodeList {
    Move -10 mm 4000 mm -10 mm
  }
  Make tfl TOPCON
  Plotting enabled
}
HexSolidList BTMCON 8IP {
  Material ECON
  Color red
  Generate {
    Block {
      dimensions 3020 mm 200 mm 200 mm
      elements 200 20 20
    }
  }
  NodeList {

```

```

    Move -10 mm -200 mm -10 mm
  }
  Make tfl BTMCON
  Plotting enabled
}
//-----
//          LDPM-HEX Constraints
//-----
NodeHexConstraintList BONDTOP Penalty {
  NodeList PRTC
  HexList TOPCON
  StiffnessBasedOnTimeStep 0.0001 ms
}
NodeHexConstraintList BONDBTTM Penalty {
  NodeList PRTC
  HexList BTMCON
  StiffnessBasedOnTimeStep 0.0001 ms
}
//-----
//          NODE LIST DEFINITIONS AND BOUNDARY CONDITIONS
//-----
NodeList PRTC {
  Select all
  Reselect cy < 0.1 mm
  Make ndL BTML
  Select all
  Reselect cy > 3999.9 mm
  Make ndL TOPL
  Select all
}
NodeList TOPCON {
  Select all
  Reselect cy > 4199.9 mm
  Make ndL TOPE
  Set Translations 00X
  Set Rotations 000
  Select all
  Reselect cy > 3999.9 mm
  Reselect cx < -9.9 mm
  Make ndL SIDEE
  Select all
}
NodeList BTMCON {
  Select all
  Reselect cy < -199.9 mm
  Make ndL BTME
  Set Translations XXX

```

```

    Set Rotations XXX
}
//-----
// APPLIED LOADS
//-----
LoadCurve ALoad {
  X-units time ms
  Y-units force N
  ReadPairs 5
  0      0
  1.0    4000000
  2.0    15000000
  3.0    19800000
  5000.1 19800000
}
NodalLoadList Load {
  NodeList TOPE
  LoadCurve ALoad
  Direction 0. -1. 0.
  All
  Distribute
}
LoadCurve VELO {
  X-units time ms
  Y-units velocity mm/s
  ReadPairs 5
  0      0
  3.5    0
  4.0    165
  100    165
  1000.1 165
}
PrescribedVelocityList VELO {
  DisregardMultipleConstraints
  LoadCurve VELO
  Direction 1 0 0
  ndL SIDEE
  All
}
//-----
// O u t p u t
//-----
TimeHistoryList ResultsUhpcWall {
  dt 0.01 ms
  ndL-SIDEE cx D S 1000
  //ndL-TOPE cy D S 1000
  ndL-TOPL cx D S 1000
}

```

```

//ndL-TOPL cy D S 1000
ndL-BTTML cx D S 1000
//ndL-BTTML cy D S 1000
ndL-SIDEE fx S 1
//ndL-TOPE fx S 1
//ndL-TOPE fy S 1
//ndL-TOPL fx S 1
//ndL-TOPL fy S 1
//ndL-BTTML fx S 1
//ndL-BTTML fy S 1
ndL-BTTME fx S 1
ndL-BTTME fy S 1
//nhL-BONDTOP fx S 1
//nhL-BONDTOP fy S 1
//nhL-BONDBTTM fx S 1
//nhL-BONDBTTM fy S 1
// Energy
ke // kinetic energy, to compare with iw internal work
iw S -1 // internal work, to compare with ke kinetic energy
ew // external work
eb // energy ballance, should be =ke+iw
ie // internal energy, defined like elastic energy stored
}
//-----
-----
PlotList CRACK Paraview { // opening of the crack
  DeleteAllFiles
  dt 10 ms
  Zip
  ttl PRTC { }
  //ttl PRTC { Particles }
  //ttl PRTC { Cells }
  //ttl PRTC { StressTensor }
  ttl PRTC {
    FacetVariable 15 // in Mars is stv[14]
    Scale 1000
  }
  hxL TOPCON { }
  hxL BTMCON { }
}
//-----
// MPI
//-----
MpiDomainList {
  RecursiveBisection ttL-PRTC
}
EOF

```

A.3 Nrun.sh

```
#!/bin/bash
#PBS -l nodes=16:ppn=16
#PBS -l walltime=96:00:00
#PBS -q normal_q
#PBS -A UHPC
#PBS -W group_list=newriver

##PBS -M relhelou@vt.edu
##PBS -m bea

cd $PBS_O_WORKDIR
export OMP_NUM_THREADS=1

##marsO -B GenUhpcWall.mrs
##marsO -B RunUhpcWall.mrs
mpirun marsM -B RunUhpcWall.mrs

exit;
```

APPENDIX B. Effect of Further Coarse Graining

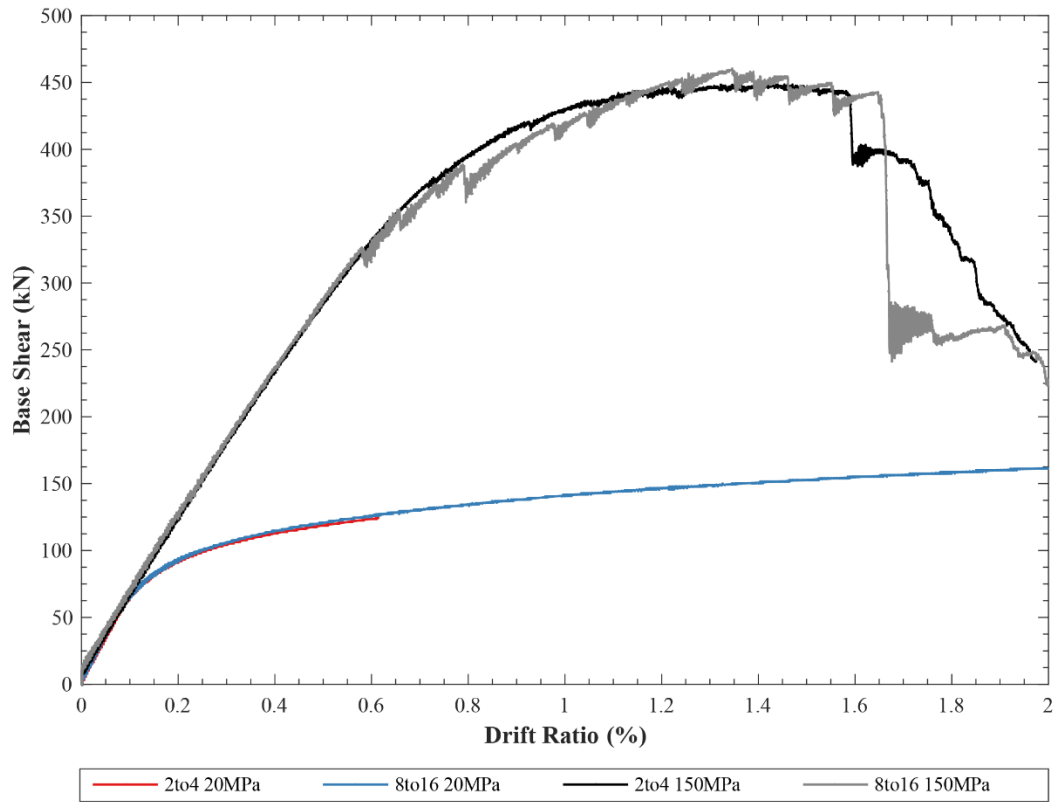


Figure B.1: Base shear vs. drift ratio for aggregate size 2 to 4 mm and 8 to 16 mm

APPENDIX C. Effect of Rebar Size

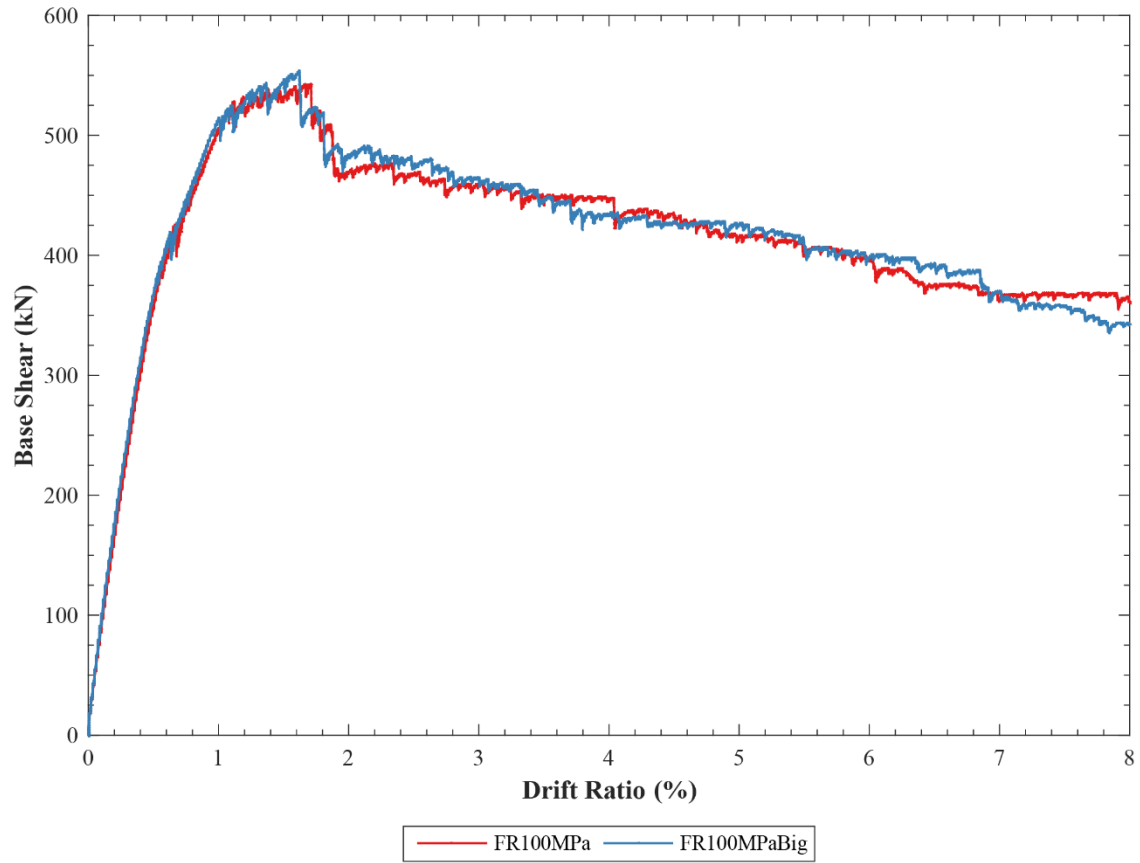


Figure C.1: Base shear vs. drift ratio for Cor-Tuf UHPC shear wall specimen with $d = 12.5$ mm and $d = 15$ mm rebar at wall edges